UNIVERSIDAD AUTÓNOMA DEL ESTADO DE MÉXICO

FACULTAD DE QUÍMICA

Preparación, caracterización y evaluación de dos radiofármacos terapéuticos de liberación controlada basados en nanosistemas poliméricos

TESIS

Que para obtener el grado de

Doctora en Ciencias Químicas

P R E S E N T A

M. en C.Q. Brenda Vianey Gibbens Bandala

Dirigido por:

D. en C.Q. Enrique Morales Avila (UAEMéx)
Dra. en C. Blanca Eli Ocampo García (ININ)
Dra. en C. Guillermina Ferro Flores (ININ)

Toluca, Estado de México, 2020

Este trabajo se realizó de manera conjunta entre la Universidad Autónoma del Estado de México y el Instituto Nacional de Investigaciones Nucleares (ININ), en el Departamento de Materiales Radiactivos, bajo la asesoría del D. en C.Q. Enrique Morales Avila, D. en C. Blanca Eli Ocampo García y D. en C. Guillermina Ferro Flores.

El presente contó con el financiamiento del Consejo Nacional de Ciencia y Tecnología (CONACYT-CB-A1S38087) y de la Agencia Internacional de Energía Atómica (CRP-F22064, contract 18358).

Contenido

a. Índice de Figuras

RESUMEN

Hoy en día, el cáncer es una de las principales causas de muerte a nivel mundial. La urgente necesidad de contar con sistemas que permitan una terapia exitosa, ha promovido al desarrollo de nanosistemas multifuncionales que combinen alternativas terapéuticas farmacológicas dirigidas a sitios específicos y, estrategias de rastreo para el seguimiento de la evolución de la patología.

Las nanoestructuras poliméricas han sido ampliamente descritas como sistemas transportadores de fármacos que, mediante un direccionamiento activo, favorecen la entrega de los antineoplásicos en sitios tumorales y no en tejido sano.

Adicionalmente, la administración de radionúclidos emisores gama, permiten el registro espacio temporal del trascurso de la enfermedad, mediante la obtención de imágenes moleculares en tiempo real de la evolución de la enfermedad. Recientemente se han propuesto nanoestructuras poliméricas conjugadas con agentes quelantes como medios para el anclaje de radiofármacos que cuentan con capacidades teranósticas (terapia y diagnóstico).

Las nanopartículas a base de poli(ácido láctico-co-glicólico) (PLGA) y dendrímeros a base de poli(amidoamina) (PAMAM) han sido ampliamente utilizados debido a sus características de biocompatibilidad y, Paclitaxel se ha incorporado a ellas produciendo un mejor efecto terapéutico; actualmente los trabajos que evalúan el efecto de terapias combinadas quimioterapia/radioterapia es limitado en el presente trabajo, se propone el uso del radionúclido Lutecio-177 utilizando como quelante al ácido 1,4,7,10-tetraazaciclododecano-N,N’,N’’,N’’’-tetraacético (DOTA) y como ligante de direccionamiento un análogo al péptido liberador de gastrina: Bombesina, para que, conjugados a las estructuras poliméricas de nanopartículas de PLGA o dendrímeros PAMAM y cargadas con Paclitaxel, sean una herramienta teranóstica eficaz y específica para cáncer positivo a receptores del péptido liberador de gastrina.

ABSTRACT

Today, cancer is one of the leading causes of death worldwide. The urgent need to have systems that require a successful therapy has promoted the development of multifunctional nanosystems that combine pharmacological therapeutic alternatives aimed at specific sites and, tracking strategies to monitor the evolution of the pathology.

Polymeric nanostructures have been described as drug carrier systems that, through active addressing, favor the delivery of antineoplastic drugs in tumor sites and not in healthy tissue.

In addition, the administration of gamma-emitting radionuclides, allow the registration of the temporal space of the disease course, by obtaining molecular images in real time of the evolution of the disease. Polymeric nanostructures conjugated with chelating agents have been proposed as means for anchoring radiopharmaceuticals that have therapeutic abilities (therapy and diagnosis).

The nanoparticles based on poly (lactic-co-glycolic acid) (PLGA) and dendrimers based on poly (amidoamine) (PAMAM) have been widely used due to their biocompatibility characteristics and, Paclitaxel has been incorporated into them, producing a better therapeutic effect; currently, the works that evaluate the effect of combined chemotherapy/ radiotherapy therapies are limited. So, in the present work, the use of ^{177}Lu radionuclide is proposed. Using as a chelator to acid 1,4,7,10-tetraazacyclododecane-N , N ', N' ', N' " - tetraacetic (DOTA) and as a targeting linker to the gastrin-releasing peptide: Bombesina, so that, conjugated to the polymeric structures of PLGA or PAMAM and loaded with Paclitaxel, they are an effective and specific for cancer positive for gastrin-releasing peptide receptors.

1. MARCO TEÓRICO

Con el desarrollo de la nanomedicina, numerosas investigaciones se han centrado en la obtención de sistemas que permitan la entrega selectiva y controlada de fármacos en sitios específicos para disminuir, en lo posible, la presencia de efectos adversos y con ello, volver más exitosa la terapia oncológica actual (Di Mauro & Borrós, 2014). Del mismo modo, con el desarrollo de éste campo, han surgido varios sensores para imagen molecular como excelentes herramientas no invasivas, que presentan alta sensibilidad y alta resolución a nivel celular y molecular para permitir el diagnóstico de dicho padecimiento (Mukerjee, Ranjan, & Vishwanatha, 2012).

En la terapia farmacológica convencional, el progreso de la enfermedad difícilmente puede ser monitoreado en tiempo real. Ante esta situación, surge una posibilidad de construir sistemas multifuncionales que permitan volver eficiente la actividad terapéutica y combinar la función de obtención de imágenes ópticas en una sola plataforma para monitorear dinámicamente el progreso de las enfermedades y la eficacia terapéutica (Ahmed, Fessi, & Elaissari, 2012).

A la fecha, existen reportes de nanopartículas (NPs) metálicas que incluyen agentes quimioterapéuticos conjugados a su superficie para aplicaciones teranósticas. Sin embargo, las nanoestructuras a base de polímeros son prometedoras herramientas para el transporte y liberación de fármacos y grandes candidatos para radiomarcado (Krasia-Christoforou & Georgiou, 2013; Peng et al., 2015).

1.1. Nanoestructuras a base de polímeros

Debido a la alta biocompatibilidad, biodegradabilidad y versatilidad estructural de fuentes sintéticas o naturales, los materiales poliméricos se han convertido en materiales de interés para aplicaciones teranósticas (terapia y diagnóstico).

Con estos materiales se han construido diversas estructuras como: nanoesferas, nanocápsulas, micelas, liposomas, dendrímeros y conjugados polímero-fármaco (**Figura 1**).

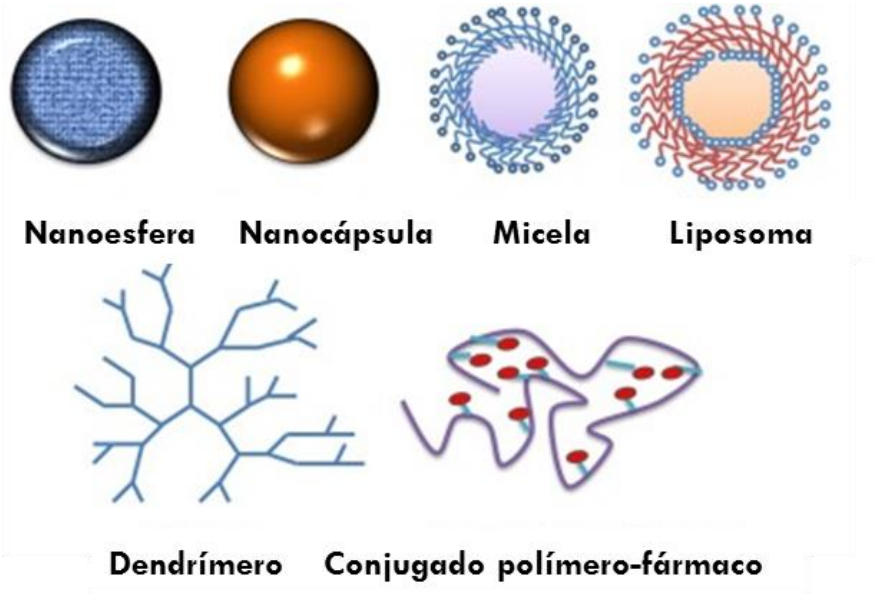

Figura 1. Representación de nanoestructuras orgánicas para el transporte y liberación de fármacos

Dichas estructuras han sido ampliamente reportadas como sistemas de transporte de fármacos, debido a características como: a) mejoran la solubilidad y biodisponibilidad de fármacos poco solubles (Kumari, Yadav, & Yadav, 2010); b) favorecen el paso a través de membranas (Y. Li et al., 2010); c) controlan la liberación del fármaco a través de la modulación de la difusión del fármaco a través y/o la degradación del polímero; d) protegen al fármaco de la rápida degradación en sistemas biológicos (Kumari et al., 2010; Y. Li et al., 2010; Mei et al., 2013); e) incorporan ligandos de direccionamiento sobre la superficie del polímero (Y. Li et al., 2010); f) modifican el perfil farmacocinético de los fármacos incorporados (Heidel & Davis, 2011; S.-D. Li & Huang, 2008); g) Facilitan los regímenes de combinación que se practica en la terapéutica actual (Bertrand, Wu, Xu, Kamaly, & Farokhzad, 2014) y h) ofrecen una plataforma ideal para combinar modalidades como la liberación controlada y dirigida de fármacos con el anclaje a radiofármacos utilizados en técnicas de imagen molecular como la tomografía por emisión de positrones (PET) o la tomografía por emisión de fotón único (SPECT), con la finalidad de identificar la presencia de las nanopartículas en un modelo *in vivo* (Stockhofe, Postema, Schieferstein, & Ross, 2014).

Dentro de los polímeros más utilizados para el diseño de nanosistemas de liberación de fármacos está el poli(ácido láctico) (PLA), poli(ácido láctico-co-gllicólico) (PLGA), poli(etilenglicol) (PEG), poli(metil metracrilato) (PMMA), poli(N-isopropil acrilamida) (PNIPAAm) y poli(amidoamina) (PAMAM) (Jaimes-Aguirre et al., 2016; Liechty, Kryscio, Slaughter, & Peppas, 2010; Srivastava et al., 2016).

Sistemas de poli(ácido láctico-co-glicólico): PLGA

El ácido poli(láctico-co-glicólico) es el copolímero del ácido láctico y el ácido glicólico, perteneciente a la familia de los poliésteres (**Figura 2**). Es un compuesto hidrofóbico, ampliamente requerido en el campo de la medicina debido a su facilidad para formar NPs, su biocompatibilidad, su seguridad clínica establecida y características de degradación favorables (Sadat Tabatabaei Mirakabad et al., 2014; Shen et al., 2013; Ye & Squillante, 2013).

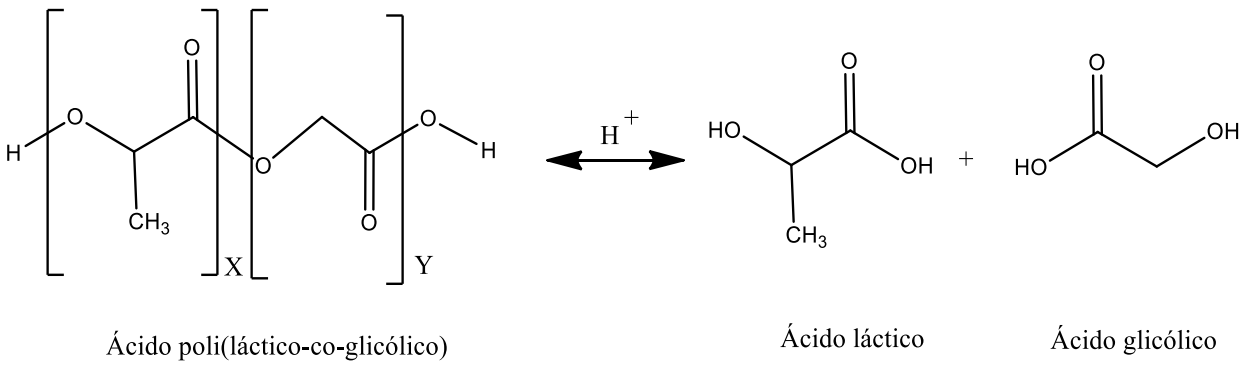

Figura 2. Estructura del PLGA y la formación de sus productos de degradación.

El interés por este sistema como medio de transporte de fármacos puede verse reflejado en la gran cantidad de publicaciones donde es utilizado para el transporte de antineoplásicos, antihipertensivos, inmunomoduladores y hormonas, entre otros (Danhier et al., 2012; Kumari et al., 2010; Sadat Tabatabaei Mirakabad et al., 2014).

Sistemas de poli(amidoamida): PAMAM

Los dendrímeros son estructuras poliméricas hiper-ramificadas, con peso molecular y tamaño bien definido, que varían en su núcleo iniciador, unidades repetitivas, grupos funcionales terminales, carga y perfil de solubilidad. Un fármaco puede ser atrapado dentro de las cavidades internas o ser conjugado a los grupos funcionales externos del dendrímero. Los dendrímeros basados en PAMAM son macromoléculas esféricas compuestas de unidades repetitivas de poli(amidoamina) que son conocidas por tener baja toxicidad biológica, buena compatibilidad y estabilidad in vivo. Su uso ha sido ampliamente reportado el transporte de fármacos (Mendoza-Nava et al., 2016).

Específicamente, los dendrímeros de PAMAM generación 4 (**Figura 3**) son estructuras inferiores a 5 nm, con peso molecular 14,215 g/mol. Su superficie cuenta con 64 grupos aminos primarios y en el interior posee 62 aminos terciarios.

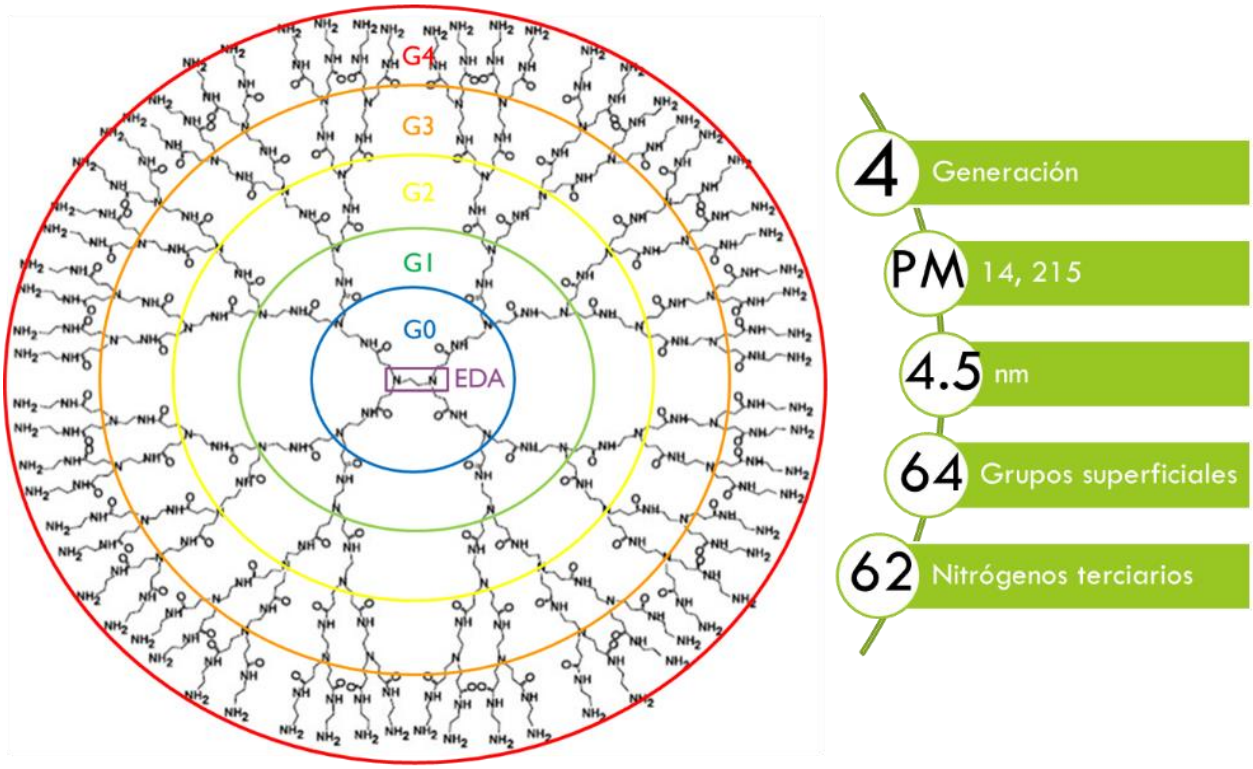

Figura 3. Estructura del dendrímero PAMAM generación 4

1.2. Nanomedicina y el cáncer

El cáncer comienza como una enfermedad localizada, que, posteriormente, se disemina a sitios distantes de donde se originó (metástasis), proceso que involucra una serie de cambios bioquímicos que hace del cáncer un padecimiento muy complejo. Su tratamiento recae en gran medida en la quimioterapia. El mecanismo de acción de la mayoría de los agentes quimioterapéuticos se basa en la interferencia de la proliferación celular para evitar la división celular descontrolada de las células cancerosas. Sin embargo, las células sanas también se encuentran en constante proceso de proliferación (en este caso regulada), por lo que un antineoplásico no discriminará entre una célula sana y una maligna, traduciéndose en efectos adversos muy severos durante el tratamiento.

Sin duda alguna, la nonomedicina se vislumbra como la puerta de entrada a una serie de estrategias de diagnóstico y tratamiento que superan muchos de los obstáculos que enfrentan las terapias convencionales.

Idealmente, después de su administración, el nanoacarreador deberá ser capaz de alcanzar el tejido tumoral librando todas las barreras biológicas presentes y, una vez en el blanco, liberar el fármaco. La llegada de los sistemas nanométricos a su sitio de acción y su posterior permanencia puede ser a través de dos mecanismos.

Acumulación pasiva. Una de las características más importantes que distingue al tejido tumoral es que, para que las células crezcan rápida y descontroladamentes, debe haber una estimulación de la angiogénesis (formación de nuevos vasos sanguíneos), lo cual da lugar a una arquitectura defectuosa con fenestraciones que van de los 10 a los 800 nm. Esta fisiopatología, sumada al deficiente drenaje linfático que acompaña al proceso es conocida como efecto EPR (Enhanced Permeation and Retention). Por lo tanto, por difusión pasiva, los sistemas de tamaño nanométrico llegan al tejido tumoral, se internan a través de las fenestras y permanecen ahí por un tiempo prolongado debido al escaso drenaje linfático. De esta manera, se pueden alcanzar concentraciones del nanosistema hasta 10 veces más altas en el tumor en comparación con el tejido sano (Barua & Mitragotri, 2014; Bertrand et al., 2014; Lammers, Kiessling, Hennink, & Storm, 2012; Rojas-Aguirre, Aguado-Castrejón, & González-Méndez, 2016).

Por otra parte, el *direccionamiento activo*, también conocido como direccionamiento mediado por ligando, involucra que el sistema nanoparticulado cuente con ligandos (anticuerpos, proteínas, péptidos, vitaminas, etc.) en la superficie que permitan la interacción con receptores sobre-expresados en la superficie de la célula diana, con el consecuente incremento en selectividad y eficiencia en la entrega del fármaco (Bertrand et al., 2014; Lammers et al., 2012).

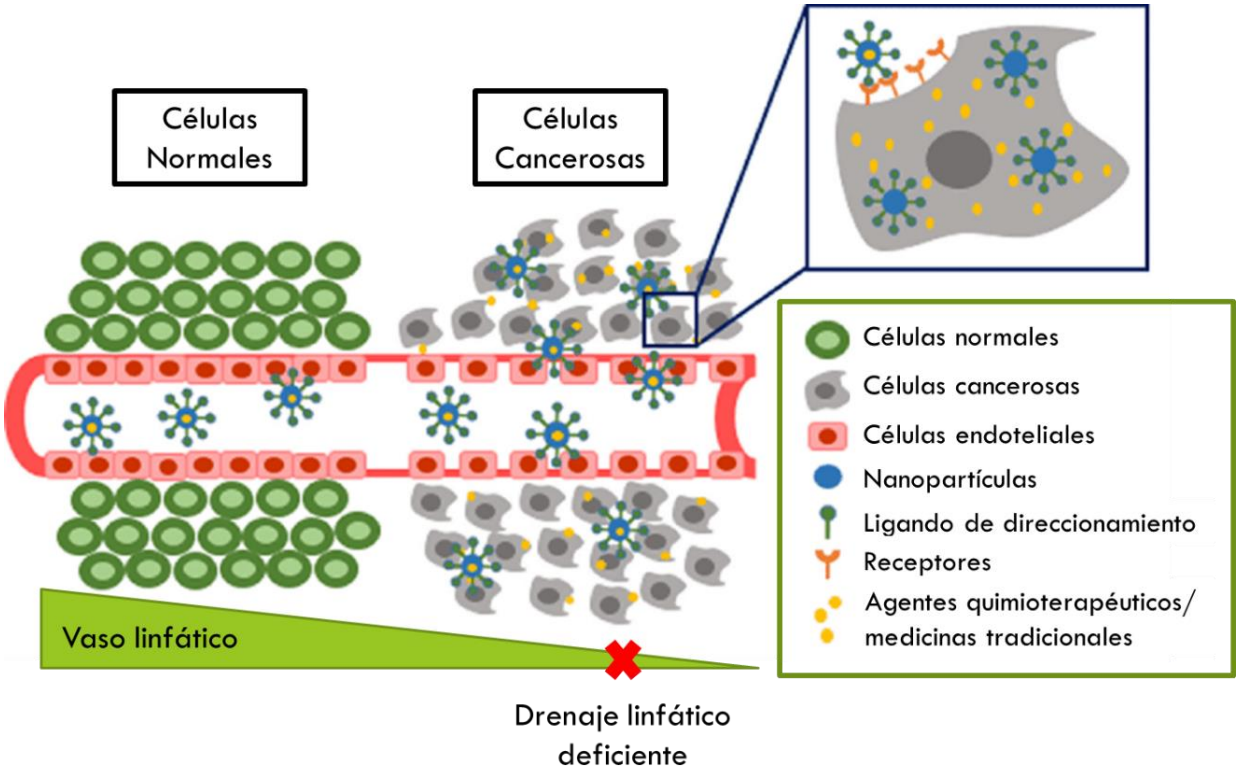

Figura 4. Direccionamiento pasivo y activo de sistemas nanométricos.

La **figura 4** esquematiza la extravasación de sistemas con dimensiones inferiores al tamaño de las fenestraciones en tejido vascular, originadas por el proceso angiogénico, sumado al reconocimiento ligando-receptor que favorece entregas específicas de los sistemas nanométricos. Aunado a ello, la retención de los mismos se ve aumentado debido al deficiente drenaje linfático que acompaña al microambiente tumoral.

Receptor del péptido liberador de gastrina y su función biológica en cáncer

El receptor del péptido liberador de gastrina (GRPr), es una proteína transmembranal, acoplada a la proteína G y con alta afinidad al péptido liberador de gastrina (GRP). El GRP es un péptido de 27 aminoácidos (Ala-Pro-Val-Ser-Val-Gly-Gly-Gly-Thr-Val-Leu-Ala-Lys-Met-Tyr-Pro-Arg-Gly-Asn-His-Trp-Ala-Val-Gly-His-Leu-Met-NH_2) que estimula la secreción de hormonas/neurotransmisores, la contracción muscular y tiene efectos sobre las células del sistema inmunológico entre muchas otras funciones (Pu et al., 2015).

En el GRPr pueden distinguirse tres regiones: 1) el dominio extracelular de unión al ligando, que es la región a la cual se une GRP, 2) 7 dominios hidrofóbicos que corresponden a los siete dominios transmembrana característicos de los receptores acoplados a proteína G, y 3) el dominio intracelular, encargado de activar el sistema de segundos mensajeros. Es importante destacar en la estructura de los siete dominios transmembrana los tres sitios de fosforilación para proteína-quinasa-C (PKC), uno en el tercer dominio transmembrana y dos en el cuarto, además de la secuencia cisteína-cisteína (Cys-Cys) en este último dominio, responsable del anclaje del receptor a la membrana celular.

Tanto del GRP como el GRPr se encuentran sobreexpresados en procesos tumorales, principalmente cáncer de mama, próstata, pulmón y páncreas. Por ello, la unión GRP/GRPr desencadena diferentes mecanismos de señalización, entre ellos, estimula a las fosfolipasas ($A_{2,16}$, $\beta_{1,3,17}$, D_{18}), AMPc y proteínas quinasas Raf-1, MEK y ERK; los cuales están involucrados con la estimulación del crecimiento, supervivencia, migración e invasión de las células cancerosas proliferación celular (Cornelio, Roesler, & Schwartsmann, 2007) (Morgat et al., 2017).

Se ha sugerido que el GRP modifica el comportamiento dinámico del citoesqueleto de actina a través de la activación de quinasas de adhesión focal, que conducen a cambios en el movimiento celular e interaccione célula-célula y célula-matriz, favoreciendo la migración y agresividad de las células de cáncer que sobre-expresan GRP/GRPr, por lo que se consideran como factor pronóstico y de monitoreo en la terapia contra cáncer (Chanda et al., 2010; Jafari et al., 2015).

Bombesina

La bombesina (BN) (**Figura 5**) es un péptido de 14 aminoácidos (pGlu-Gln-Arg-Leu-Gly-Asn-Gln-Trp-Ala-Val-Gly-His-Leu-Met-NH_2) análogo al GRP. BN y GRP comparten la secuencia C-terminal, concretamente los 7 últimos aminoácidos. Esta secuencia es la responsable de la unión al receptor y de su actividad biológica. Además, la metionina (Met) C-terminal debe ser amidada para que el péptido pueda tanto ser reconocido por anticuerpos como unirse a su receptor. La BN al igual que el GRP se introducen en el interior de la célula por endocitosis una vez que se unen a los receptores GRPr, estos receptores se reciclan o se degradan mientras que GRP o BN permanece en el citoplasma. Esata unión induce la proliferación, sobrevivencia y diferenciación celular, y participa en la migración y metástasis de las células de cáncer (Santos-Cuevas et al., 2011).

La unión entre BN y GRPr es una clara herramienta para la entrega específica de sistemas que se encuentren direccionados con el péptido, disminuyendo la interacción con tejido sano y permitiendo una mejorada terapia (Kulhari, Pooja, Singh, Kuncha, & Sistla, 2015; Kulhari, Pooja, Singh, & Sistla, 2014).

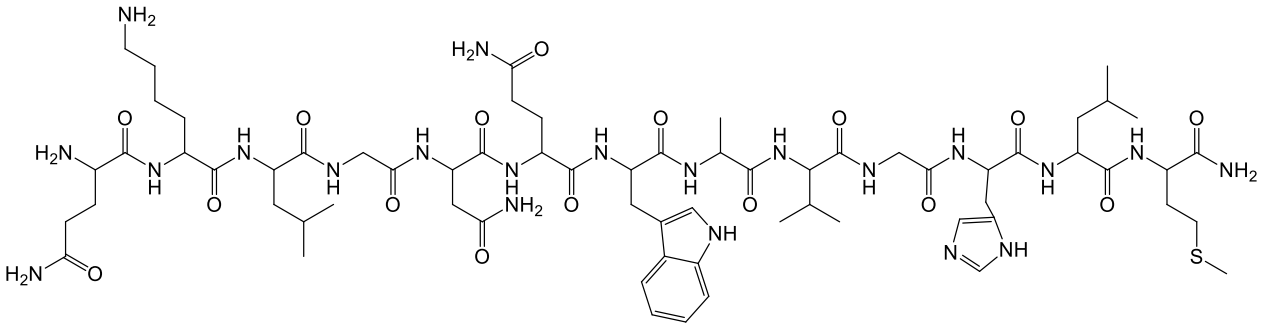

Figura 5. Estructura del péptido Bombesina

Análogos de Bombesina

Identificando la interacción BN/GRPr y la sobre-expresión del receptor en las células de cáncer, el GRPr ha sido considerado como blanco molecular para el diseño y desarrollo de nuevos agentes de diagnóstico y terapia de cáncer. Diferentes análogos de BN, incluidos Lys3-Bombesina, BN(7-14), BN (1-14) y Lys^{1}Lys3(DOTA)BN han sido exitosamente empleados con este fin.

Lys1Lys3(DOTA)-Bombesina, secuencia peptídica análoga a bombesina y al GRP, es una molécula modificada en la posición 1 y 3, con respecto a bombesina, la cual tiene incorporada en su estructura al agente quelante bifuncional (BFCA) DOTA.

El BFCA es parte importante en procesos de radiofármaco, ya que coordina al radionúclido y se encuentra unido covalentemente a la molécula marcadora directamente o a través de un conector (Ramos et al., 2013). La selección de un BFCA esta generalmente determinada por la naturaleza y estado de oxidación del ión metálico, el conector es frecuentemente usado para modificar las propiedades farmacocinéticas del radiofármaco y su biodistribución.

El DOTA (ácido 1,4,7,10-tetraazaciclododecano-*N*,*N'*,*N''*,*N'''*-tetraacético) y la familia de agentes bifuncionales cíclicos similares a DOTA, forman complejos muy estables con una variedad de elementos, en especial átomos trivalentes, tales como ^{68}Ga, ^{90}Y, ^{111}In, ^{149}Pm, ^{177}Lu, y divalentes como ^{27}Mg, ^{47}Ca, ^{64}Cu.

En este trabajo se propone el uso del quelante DOTA que, enlazado con Lys^{1}Lys^{3}(DOTA)-Bombesina (**Figura 6**) favorecería la entrega del radionúclido (^{177}Lu) hacia sitios de sobreexpresión de GRPr.

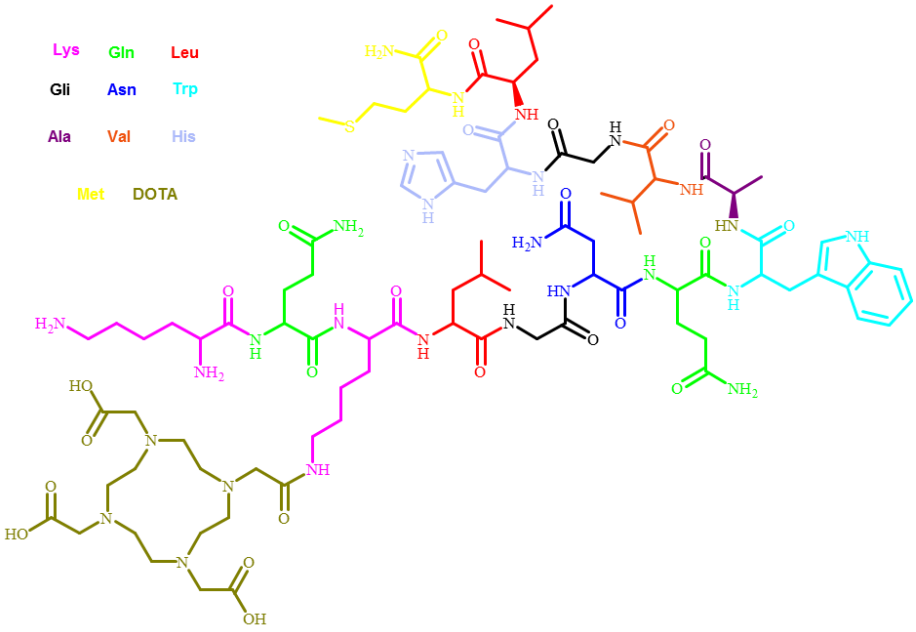

Figura 6. Lys^{1}Lys^{3}(DOTA)-Bombesina

1.3. Marcado

La radiación ionizante es un tipo de energía liberada por los átomos en forma de ondas electromagnéticas (rayos gamma o rayos X) o partículas (partículas alfa y beta o neutrones) por elementos inestables o radionúclidos (OMS). Cada radionúclido se caracteriza por el tipo de radiación que emite, la energía de la radiación, su abundancia y su semivida.

Los **radiofármacos**, sensores moleculares dirigidos hacia blancos específicos como tejidos o procesos *in vivo*, se usan en aplicaciones diagnósticas o terapéuticas. Identifican anormalidades en etapas tempranas en la progresión de una enfermedad (Ferro-Flores, Arteaga de Murphy, & Melendez-Alafort, 2006). Un radiofármaco generalmente contiene una biomolécula (BM), un conector, un radionúclido y un agente quelante bifuncional (BFCA) (Ramos, Ramos, Jesús, & García, 2013).

En particular, los radiofármacos de Lutecio (^{177}Lu), con reconocimiento molecular específico, se han propuesto como una nueva clase de radiofármacos teranósticos debido a las propiedades terapéuticas y diagnósticas del radionúclido (Mendoza-Nava et al., 2016).

Lutecio-177

Lutecio es el último miembro de la serie de lantanos, con 71 electrones dispuestos en la configuración [Xe] 4f145d16s2. Durante las reacciones químicas, los átomos de lutecio pierden los dos electrones más externos así como el único electrón 5d, generando así una especie catiónica +3. Los cationes trivalentes en solución se caracterizan por la fuerte tendencia de formar complejos con átomos donadores de electrones como O, F y N. El número de coordinación termodinámicamente muy estables suele ser 8 o 9, con ligandos de tipo poliaminopolicarboxilato acíclico o cíclico que tienen 8 o 9 átomos donantes (**Figura 7**).

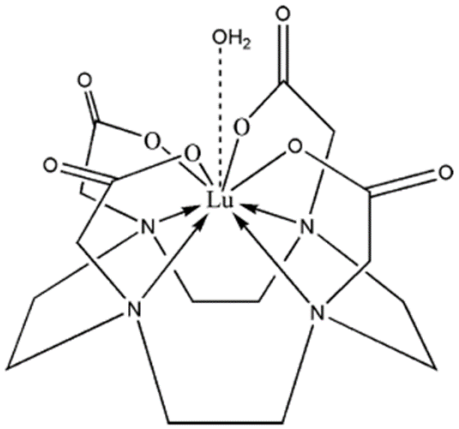

Figura 7. Complejo de Lutecio-DOTA

El ^{177}Lu, tiene vida media de 6.647 días, decae principalmente a través de emisión β^- (emisión β^- máxima de 497 keV) y presenta emisiones γ (113 y 208 keV), produciendo isótopos estables de hafnio (**Figura 8**). Estas emisiones son de interés en la práctica clínica debido a sus aplicaciones terapéuticas y de diagnóstico.

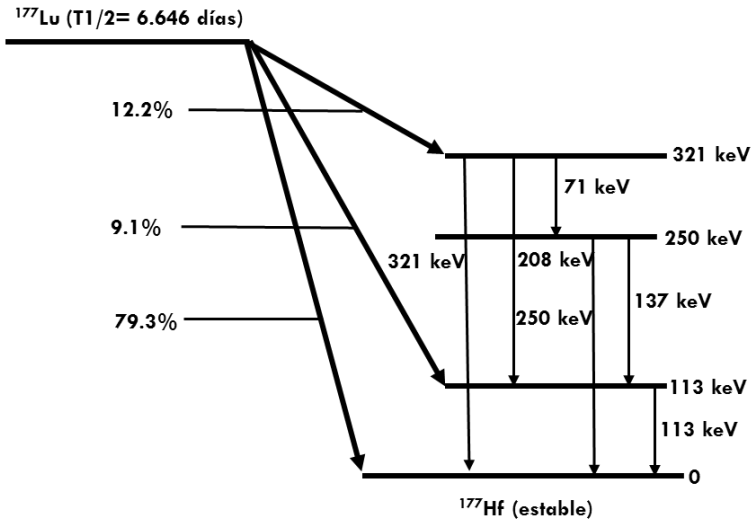

Figura 8. Esquema de decaimiento de Lutecio 177

Péptidos radiomarcados

Se han sintetizado diversos análogos de BN radiomarcados con ^{99m}Tc para detectar tumores malignos y para estadificar el cáncer de mama y de próstata, así como para identificar ganglios linfáticos afectados, por ejemplo: ^{99m}Tc-EDDA/HYNIC-[Lys3]BN) (Ferro-Flores, 2006), ^{99m}Tc(I)-2-picolilamina-N,N-ácido diacético-5-ácido amino valérico-BN (^{99m}Tc(I)-PADA-AVABN), ^{99m}Tc-Cys-6-amino-n-ácido hexanoico-BN (Varvarigou, 2002; Scopinaro, 2002; Scopinaro, 2005). Específicamente, el análogo Lys^3-Bombesina marcada con ^{99m}Tc utilizando como agente quelante a HYNIC o N_2S_2 se ha reportado como radiopéptido con alta estabilidad en suero, unión específica al receptor y rápida internalización (Jiménez-Mancilla et al., 2013).

Asimismo, los análogos de la BN o BN junto con ^{177}Lu se han utilizado en el desarrollo de radiofármacos para terapia, empleando como agentes quelantes, ciclos como DOTA, NOTA, NETA, etc. (Morales-Avila, Ortiz-Reynoso, Mirshojaei, & Ahmadi, 2015). Por ejemplo, ^{177}Lu-AMBA ha mostrado ser un agente terapéutico eficaz durante tratamientos *in vivo* ya que disminuye la tasa de crecimiento del tumor y permite la supervivencia libre de progresión en un modelo murino (Lantry et al., 2006).

Sin embargo, en la clínica se requiere de nuevos radiofármacos que permitan a) detectar y/o confirmar la presencia del tumor primario y metástasis, b) que permita explorar características bioquímicas de tejidos neoplásicos implicados en la estadificación del tumor y planeación del tratamiento y c) permita realizar la evaluación de la respuesta del tumor al tratamiento.

1.4. Paclitaxel

Paclitaxel (PTX, **Figura 9**), prototipo de la clase de los taxanos, es un fármaco antineoplásico aprobado para el tratamiento del cáncer de mama y ovario y, recientemente contra glioblastomas y metástasis cerebrales. Interactúa con los dímeros de tubulina en la fase mitótica de la división celular que promueve la polimerización de microtúbulos haciéndolos altamente estables, por lo tanto, evita la división celular. Sin embargo, a pesar de una medicación adecuada, la quimioterapia actual empleando una preparación comercial de PTX (Taxol ®) está asociada con efectos adversos

severos, tales como hipersensibilidad, neurotoxicidad y nefrotoxicidad, debido a que el vehículo de esta formulación es tóxico (Koudelka & Turánek, 2012; Ma & Mumper, 2013; Teow et al., 2013; Wang et al., 2012).

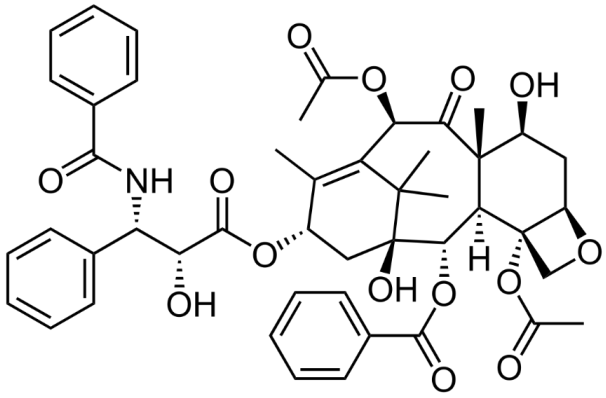

Figura 9. Paclitaxel

1.5. Sistemas Poliméricos para el transporte de Paclitaxel o radionúclidos

Los sistemas a base de PLGA y PAMAM han sido ampliamente descritos para la entrega selectiva y controlada de Paclitaxel o de Lutecio-177.

Sin embargo, no ha sido evaluada la capacidad de la entrega concomitante de ambos agentes en una misma plataforma.

2. JUSTIFICACIÓN

Debido a la urgente necesidad de alternativas que mejoren el diagnóstico y tratamiento del Cáncer, se buscan plataformas que combinen estas dos cualidades.

Las nanoestructuras poliméricas, han surgido como medios adecuados para el transporte dirigido y liberación controlada de fármacos en procesos tumorales mediante la incorporación en su estructura de ligandos de direccionamiento y, a su vez, se permite proponerlos como medios para el anclaje de radionúclidos para propósitos de imagen y que, a la vez, vuelvan más eficiente una formulación terapéutica propuesta.

Entre la amplia gama de fármacos disponibles para terapia contra el cáncer, Paclitaxel ha sido muy utilizado, sin embargo, debido a sus características de falta de selectividad y baja solubilidad, se han propuesto diversos medios a base de polímeros para poder transportarlo.

En este trabajo, se pretende preparar, caracterizar y evaluar radiofármacos basados en nanoestructuras poliméricas como sistemas de liberación de oncofármacos potencialmente útiles en la aplicación simultánea de terapia combinada (radioterapia dirigida y terapia farmacológica) y permitir, de manera concurrente el registro espacio temporal del tratamiento oportuno de cáncer de mama y de próstata. Específicamente se propone que al funcionalizar NPs de PLGA o dendrímeros de PAMAM con biomoléculas de reconocimiento molecular (Bombesina) por los receptores del péptido liberador de gastrina, los sistemas permitan la internalización selectiva en células que sobreexpresan dichos receptores, de manera que los agentes terapéuticos puedan ejercer su efecto farmacológico en el blanco seleccionado. Al mismo tiempo, que los sistemas marcados con el radiofármaco teranóstico 177Lu permitan realizar radioterapia dirigida e imagen molecular empleando el sistema multifuncional.

3. HIPÓTESIS

La funcionalización de estructuras poliméricas transportadoras de fármacos (PLGA(Paclitaxel) y/o PAMAM(Paclitaxel)) con ^{177}Lu-Bombesina, permitirá el reconocimiento específico, así como el incremento de la respuesta terapéutica, en células que sobreexpresan receptores del péptido liberador de gastrina.

4. OBJETIVOS

Objetivo general

Preparar, caracterizar y evaluar radiofármacos preparados a partir de nanoestructuras poliméricas (^{177}Lu-Bombesina-PLGA(PTX) y ^{177}Lu-Bombesina-PAMAM(PTX) como sistemas de liberación de oncofármacos potencialmente útiles en la aplicación simultánea de terapia combinada (radioterapia dirigida y terapia farmacológica) y permitir, de manera concurrente la detección y tratamiento oportuno de cáncer positivo a receptores del péptido liberador de gastrina.

Objetivos específicos

1. Obtener nanoestructuras poliméricas de PLGA y PAMAM cargadas con Paclitaxel
2. Realizar anclaje de bombesina a las estructuras poliméricas
3. Realizar el radiomarcado de los sistemas: Bombesina-PLGA-(PTX) y Bombesina-PAMAM-(PTX) con ^{177}Lu.
4. Caracterizar fisicoquímicamente los sistemas.
5. Evaluar la pureza radioquímica de los sistemas: ^{177}Lu-Bombesina-PLGA-(PTX) y ^{177}Lu-Bombesina-PAMAM-(PTX) por HPLC o por cromatografía en capa fina.
6. Evaluar *in vitro*: captación específica y viabilidad celular en células positivas al receptor del péptido liberador de gastrina.

5. DISEÑO DE LA INVESTIGACIÓN

5.1. ***Nanopartículas de PLGA***

5.1.1. Preparación de núcleos de PLGA y PLGA(PTX). Obtención por modificación del método de emulsión/evaporación del solvente, descrito por Stevanović y col. (Stevanovic, Jordovic, & Uskokovic, 2007).

5.1.2. Generación de grupos éster activos a partir de grupos carboxilo de PLGA, en medio básico, mediante el agente activador de carboxilos HATU (1-[Bis(dimetilamino)metilen]-1H-1,2,3-triazol[4,5-b]piridino 3-oxido hexafluorofosfato), y la posterior conjugación con el péptido Lys^1-Lys^3(DOTA)-BN.

5.1.3. Caracterización del sistema **BN-PLGA(PTX)** e intermediarios.

5.2. ***Dendrímeros de PAMAM***

5.2.1. Conjugación del agente quelante p-SCN-Bn-DOTA al dendrímero PAMAM generación 4 mediante la reacción del grupo isitiocianato presente en la estructura quelante y los grupos amino del dendrímero (Mendoza-Nava et al., 2016).

5.2.2. Activación de grupos carboxilo de Lys^1-Lys^3(DOTA)-BN utilizando HATU como agente activador y conjugación con grupos amino en el dendrímero.

5.2.3. Encapsulación de Paclitaxel mediante atrapamiento.

5.2.4. Caracterización del sistema **DOTA-DN(PTX)-BN** e intermediarios.

5.3. **Caracterización**

5.3.1. Fisicoquímica

Tamaño de partícula, Potencial Zeta, Microscopía Electrónica de Barrido o de Transmisión, Espectroscopia IR y UV-Vis.

5.3.2. Eficiencia de atrapamiento y eficiencia de carga.

5.3.3. Perfil de liberación

5.4. **Radiomarcado con ^{177}Lu**

5.4.1. Marcado de los sistemas BN-PLGA(PTX) y DOTA-DN(PTX)-BN mediante la técnica descrita por Vilchis-Juárez y col. (Vilchis-Juárez et al., 2014).

5.4.2. Purificación de los sistemas, por medio de ultra-centrifugación

5.4.3. Determinación de la pureza radioquímica de los complejos utilizando cromatografía de capa

fina

5.5. **Evaluación *in vitro***

5.5.1 Evaluación de la captación celular en células de cáncer positivas a GRPr.

5.5.2 Ensayo de Viabilidad Celular por medio del ensayo XTT.

5.6. **Estudios *in vivo***

Pruebas *in vivo* de acuerdo con las reglas y regulaciones de la Norma Oficial Mexicana NOM-062-ZOO-1999.

5.6.1 Inducción de tumores (líneas celulares positivas a GRPr) en ratones atímicos

5.6.2. Administración del sistema ^{177}Lu-BN-PLGA(PTX) o ^{177}Lu-DOTA-DN(PTX)-BN

5.6.3. Rastreo de los sistemas por SPECT.

5.6.4. Evaluación de la Biodistribución.

6. REFERENCIAS

1. Ahmed, N., Fessi, H., & Elaissari, A. (2012). Theranostic applications of nanoparticles in cancer. *Drug Discovery Today*, *17–18*, 928–934. https://doi.org/10.1016/j.drudis.2012.03.010
2. Barua, S., & Mitragotri, S. (2014). Challenges associated with penetration of nanoparticles across cell and tissue barriers: A review of current status and future prospects. *Nano Today*, *9*(2), 223–243. https://doi.org/10.1016/j.nantod.2014.04.008
3. Bertrand, N., Wu, J., Xu, X., Kamaly, N., & Farokhzad, O. C. (2014). Cancer nanotechnology: The impact of passive and active targeting in the era of modern cancer biology. *Advanced Drug Delivery Reviews*, *66*, 2–25. https://doi.org/10.1016/j.addr.2013.11.009
4. Chanda, N., Kattumuri, V., Shukla, R., Zambre, A., Katti, K., Upendran, A., … Kannan, R. (2010). Bombesin functionalized gold nanoparticles show in vitro and in vivo cancer receptor specificity. *Proceedings of the National Academy of Sciences of the United States of America*, *107*(19), 8760–8765. https://doi.org/10.1073/pnas.1002143107
5. Cornelio, D. B., Roesler, R., & Schwartsmann, G. (2007). Gastrin-releasing peptide receptor as a molecular target in experimental anticancer therapy. *Annals of Oncology*, *18*(9), 1457–1466. https://doi.org/10.1093/annonc/mdm058
6. Danhier, F., Ansorena, E., Silva, J. M., Coco, R., Breton, A. Le, & Préat, V. (2012). PLGA-based nanoparticles : An overview of biomedical applications. *Journal of Controlled Release*, *161*(2), 505–522. https://doi.org/10.1016/j.jconrel.2012.01.043
7. Di Mauro, P. P., & Borrós, S. (2014). Development of High Drug Loaded and Customizing Novel Nanoparticles for Modulated and Controlled Release of Paclitaxel. *Pharmaceutical Research*, (10), 3461–3477. https://doi.org/10.1007/s11095-014-1434-z
8. Ferro-Flores, G., Arteaga de Murphy, C., & Melendez-Alafort, L. (2006). Third Generation Radiopharmaceuticals for Imaging and Targeted Therapy. *Current Pharmaceutical Analysis*, *2*(4), 339–352. https://doi.org/10.2174/157341206778699555
9. Heidel, J. D., & Davis, M. E. (2011). Clinical developments in nanotechnology for cancer therapy. *Pharmaceutical Research*, *28*(2), 187–199. https://doi.org/10.1007/s11095-010-0178-7
10. Jafari, A., Salouti, M., Shayesteh, S. F., Heidari, Z., Rajabi, A. B., Boustani, K., & Nahardani, A. (2015). Synthesis and characterization of Bombesin- superparamagnetic iron oxide nanoparticles as a targeted contrast agent for imaging of breast cancer using MRI. *Nanotechnology*, *26*, 75101. https://doi.org/10.1088/0957-4484/26/7/075101
11. Jaimes-Aguirre, L., Gibbens-Bandala, B. V., Morales-Avila, E., Ocampo-García, B. E., Seyedeh-Fatemeh, M., & Amirhosein, A. (2016). Polymer-Based Drug Delivery Systems, Development and Pre-Clinical Status. *Current Pharmaceutical Design*, *22*(19), 2886–2903. https://doi.org/10.2174/1381612822666160217125028

12. Jiménez-Mancilla, N., Ferro-Flores, G., Santos-Cuevas, C., Ocampo-García, B., Luna-Gutiérrez, M., Azorín-Vega, E., … Torres-García, E. (2013). Multifunctional targeted therapy system based on 99m Tc/177 Lu-labeled gold internalized in nuclei of prostate cancer cells. *Journal of Labelled Compounds and Radiopharmaceuticals*, *56*(l), 663–671. https://doi.org/10.1002/jlcr.3087

13. Koudelka, Š., & Turánek, J. (2012). Liposomal paclitaxel formulations. *Journal of Controlled Release*, *163*(3), 322–334. https://doi.org/10.1016/j.jconrel.2012.09.006

14. Krasia-Christoforou, T., & Georgiou, T. K. (2013). Polymeric theranostics: using polymer-based systems for simultaneous imaging and therapy. *Journal of Materials Chemistry B*, *1*(24), 3002–3025. https://doi.org/10.1039/c3tb20191k

15. Kulhari, H., Pooja, D., Singh, M. K., Kuncha, M., & Sistla, R. (2015). Bombesin-conjugated nanoparticles improve the cytotoxic efficacy of docetaxel against gastrin-releasing but androgen-independent prostate cancer. *Nanomedicine (Lond.)*, *10*(18), 2847–2859. https://doi.org/10.2217/nnm.15.107

16. Kulhari, H., Pooja, D., Singh, M. K., & Sistla, R. (2014). Colloidal stability and physicochemical characterization of bombesin conjugated biodegradable nanoparticles. *Colloids and Surfaces A: Physicochemical and Engineering Aspects*, *443*, 459–466. https://doi.org/10.1016/j.colsurfa.2013.12.011

17. Kumari, A., Yadav, S. K., & Yadav, S. C. (2010). Biodegradable polymeric nanoparticles based drug delivery systems. *Colloids and Surfaces B: Biointerfaces*, *75*(1), 1–18. https://doi.org/10.1016/j.colsurfb.2009.09.001

18. Lammers, T., Kiessling, F., Hennink, W. E., & Storm, G. (2012). Drug targeting to tumors: Principles, pitfalls and (pre-) clinical progress. *Journal of Controlled Release*, *161*(2), 175–187. https://doi.org/10.1016/j.jconrel.2011.09.063

19. Lantry, L. E., Cappelletti, E., Maddalena, M. E., Fox, J. S., Feng, W., Chen, J., … Nunn, A. D. (2006). 177Lu-AMBA: Synthesis and Characterization of a Selective 177Lu-Labeled GRP-R Agonist for Systemic Radiotherapy of Prostate Cancer. *Journal of Nuclear Medicine*, *47*(7), 1144–1152.

20. Li, S.-D., & Huang, L. (2008). Pharmacokinetics and biodistribution of nanoparticles. *Molecular Pharmaceutics*, *5*(4), 496–504. https://doi.org/10.1021/mp800049w

21. Li, Y., Dong, H., Wang, K., Shi, D., Zhang, X., & Zhuo, R. (2010). Stimulus-responsive polymeric nanoparticles for biomedical applications. *Science China Chemistry*, *53*(3), 447–457. https://doi.org/10.1007/s11426-010-0101-4

22. Liechty, W. B., Kryscio, D. R., Slaughter, B. V., & Peppas, N. A. (2010). Polymers for Drug Delivery Systems. *Annual Review of Chemical and Biomolecular Engineering*, *1*, 149–173. https://doi.org/10.1146/annurev-chembioeng-073009-100847

23. Ma, P., & Mumper, R. J. (2013). Paclitaxel Nano-Delivery Systems: A Comprehensive Review. *Journal of Nanomedicine & Nanotechnology*, *4*(2), 164. https://doi.org/10.4172/2157-7439.1000164

24. Mei, L., Zhang, Z., Zhao, L., Huang, L., Yang, X.-L., Tang, J., & Feng, S.-S. (2013). Pharmaceutical nanotechnology for oral delivery of anticancer drugs. *Advanced Drug Delivery Reviews*, *65*(6), 880–890. https://doi.org/10.1016/j.addr.2012.11.005

25. Mendoza-Nava, H., Ferro-Flores, G., Ramírez, F. de M., Ocampo-García, B., Santos-Cuevas, C., Aranda-Lara, L., … Isaac-Olivé, K. (2016). 177 Lu-Dendrimer Conjugated to Folate and Bombesin with Gold Nanoparticles in the Dendritic Cavity: A Potential Theranostic Radiopharmaceutical. *Journal of Nanomaterials*, *2016*, 1–11. https://doi.org/10.1155/2016/1039258

26. Morales-Avila, E., Ortiz-Reynoso, M., Mirshojaei, S. F., & Ahmadi, A. (2015). Multifunctional radiolabeled nanoparticles: strategies and novel classification of radiopharmaceuticals for cancer treatment. *Journal of Drug Targeting*, *23*(3), 191–201. https://doi.org/10.3109/1061186X.2014.988216

27. Morgat, C., MacGrogan, G., Brouste, V., Vélasco, V., Sévenet, N., Bonnefoi, H., … Hindié, E. (2017). Expression of Gastrin-Releasing Peptide Receptor in Breast Cancer and Its Association with Pathologic, Biologic, and Clinical Parameters: A Study of 1,432 Primary Tumors. *Journal of Nuclear Medicine*, *58*(9), 1401–1407. https://doi.org/10.2967/jnumed.116.188011

28. Mukerjee, A., Ranjan, A. P., & Vishwanatha, J. K. (2012). Combinatorial Nanoparticles for Cancer Diagnosis and Therapy. *Current Medicinal Chemistry*, *19*(22), 3714–3721.

29. Peng, H., Liu, X., Wang, G., Li, M., Bratlie, K. M., Cochran, E., & Wang, Q. (2015). Polymeric multifunctional nanomaterials for theranostics. *Journal of Materials Chemistry B*, *3*, 6856–6870. https://doi.org/10.1039/C5TB00617A

30. Pu, F., Qiao, J., Xue, S., Yang, H., Patel, A., Wei, L., … Yang, J. J. (2015). GRPR-targeted Protein Contrast Agents for Molecular Imaging of Receptor Expression in Cancers by MRI. *Scientific Reports*, *5*, 1–14. https://doi.org/10.1038/srep16214

31. Ramos, E. L., Ramos, S. L., Jesús, C., & García, C. (2013). Agentes quelantes bifuncionales utilizados en la síntesis de radiofármacos. *Revista Mexicana de Ciencias Farmacéuticas*, *44*(1), 7–23.

32. Rojas-Aguirre, Y., Aguado-Castrejón, K., & González-Méndez, I. (2016). La nanomedicina y los sistemas de liberación de fármacos: ¿la (r)evolución de la terapia contra el cáncer? *Educación Química*, *27*(4), 286–291. https://doi.org/10.1016/j.eq.2016.07.002

33. Sadat Tabatabaei Mirakabad, F., Nejati-Koshki, K., Akbarzadeh, A., Yamchi, M. R., Milani, M., Zarghami, N., … Alimohammadi, S. (2014). PLGA-Based Nanoparticles as Cancer Drug Delivery Systems. *Asian Pacific Journal of Cancer Prevention*, *15*(2), 517–535. https://doi.org/10.7314/APJCP.2014.15.2.517

34. Santos-Cuevas, C. L., Ferro-Flores, G., Rojas-Calderón, E. L., García-Becerra, R., Ordaz-Rosado, D., Arteaga de Murphy, C., & Pedraza-López, M. (2011). 99m-Tc-N2S2-Tat (49-57)-bombesin internalized in nuclei of prostate and breast cancer cells : kinetics , dosimetry and effect on cellular proliferation. *Nuclear Medicine Communications*, *32*, 303–313.

https://doi.org/10.1097/MNM.0b013e328341b27f

35. Shen, J.-M., Gao, F.-Y., Yin, T., Zhang, H.-X., Ma, M., Yang, Y.-J., & Yue, F. (2013). cRGD-functionalized polymeric magnetic nanoparticles as a dual-drug delivery system for safe targeted cancer therapy. *Pharmacological Research*, *70*(1), 102–115. https://doi.org/10.1016/j.phrs.2013.01.009
36. Srivastava, A., Yadav, T., Sharma, S., Nayak, A., Kumari, A., & Mishra, N. (2016). Polymers in Drug Delivery. *Journal of Biosciences and Medicines*, *4*(1), 69–84. https://doi.org/10.4236/jbm.2016.41009
37. Stevanovic, M. M., Jordovic, B., & Uskokovic, D. P. (2007). Preparation and Characterization of Poly (D,L-Lactide-co-Glycolide) Nanoparticles Containing Ascorbic Acid. *Journal of Biomedicine and Biotechnology*, *2007*, 8 pages. https://doi.org/10.1155/2007/84965
38. Stockhofe, K., Postema, J. M., Schieferstein, H., & Ross, T. L. (2014). Radiolabeling of Nanoparticles and Polymers for PET Imaging. *Pharmaceuticals*, *7*, 392–418. https://doi.org/10.3390/ph7040392
39. Teow, H. M., Zhou, Z., Najlah, M., Yusof, S. R., Abbott, N. J., & D'Emanuele, A. (2013). Delivery of paclitaxel across cellular barriers using a dendrimer-based nanocarrier. *International Journal of Pharmaceutics*, *441*(1–2), 701–711. https://doi.org/10.1016/j.ijpharm.2012.10.024
40. Vilchis-Juárez, A., Ferro-Flores, G., Santos-Cuevas, C., Morales-Avila, E., Ocampo-García, B., Díaz-Nieto, L., … Gómez-Oliván, L. (2014). Molecular Targeting Radiotherapy with Cyclo-RGDfK(C) Peptides Conjugated to 177 Lu-Labeled Gold Nanoparticles in Tumor-Bearing Mice. *Journal of Biomedical Nanotechnology*, *10*(3), 393–404. https://doi.org/10.1166/jbn.2014.1721
41. Wang, Y., Wang, C., Gong, C., Wang, Y., Guo, G., Luo, F., & Qian, Z. (2012). Polysorbate 80 coated poly (e-caprolactone)-poly (ethylene glycol)-poly (e-caprolactone) micelles for paclitaxel delivery. *International Journal of Pharmaceutics*, *434*(1–2), 1–8. https://doi.org/10.1016/j.ijpharm.2012.05.015
42. Ye, Z., & Squillante, E. (2013). The development and scale-up of biodegradable polymeric nanoparticles loaded with ibuprofen. *Colloids and Surfaces A: Physicochemical and Engineering Aspects*, *422*, 75–80. https://doi.org/10.1016/j.colsurfa.2013.01.016

7. RESULTADOS

7.1 Gibbens-Bandala Brenda, Morales-Avila Enrique, Ferro-Flores Guillermina, Santos-Cuevas Clara, Meléndez-Alafort Laura, Trujillo-Nolasco Maydelid, Ocampo-García Blanca. **2019**. ^{177}Lu-Bombesin-PLGA(paclitaxel): A targeted controlled release nanomedicine for bimodal therapy of breast cancer. *Materials Science & Engineering C*.
https://doi.org/10.1016/j.msec.2019.110043
[Factor de impacto: 4.959]

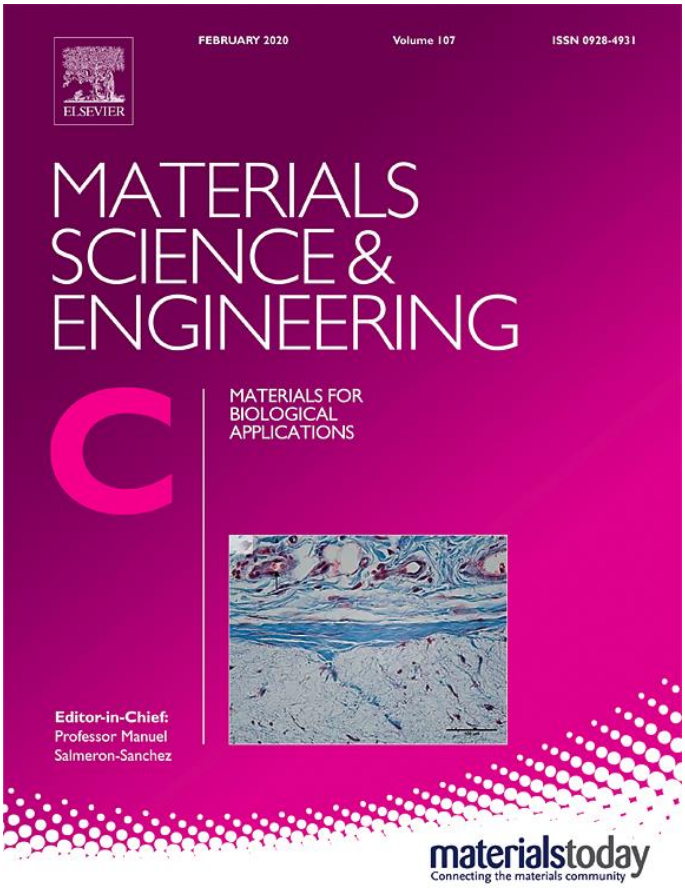

Materials Science & Engineering C 105 (2019) 110043

Contents lists available at ScienceDirect

Materials Science & Engineering C

journal homepage: www.elsevier.com/locate/msec

^{177}Lu-Bombesin-PLGA (paclitaxel): A targeted controlled-release nanomedicine for bimodal therapy of breast cancer

Brenda Gibbens-Bandala[a,b], Enrique Morales-Avila[b], Guillermina Ferro-Flores[a], Clara Santos-Cuevas[a], Laura Meléndez-Alafort[c], Maydelid Trujillo-Nolasco[a,b], Blanca Ocampo-García[a,*]

[a] Departamento de Materiales Radiactivos, Instituto Nacional de Investigaciones Nucleares, Carretera México-Toluca S/N, Ocoyoacac, Estado de México 52750, Mexico
[b] Facultad de Química, Universidad Autónoma del Estado de México, Paseo Tollocan S/N, Toluca, Estado de México 50180, Mexico
[c] Veneto Institute of Oncology IOV-IRCCS, Via Gattamelata 64, Padova 35128, Italy

ARTICLE INFO

Keywords:
Radiotherapy
Targeted therapy
Smart nanoparticles
Drug delivery
Cancer
Concomitant cancer treatment

ABSTRACT

The gastrin-releasing peptide receptor (GRPr) is overexpressed in > 75% of breast cancers. ^{177}Lu-Bombesin (^{177}Lu-BN) has demonstrated the ability to target GRPr and facilitate efficient delivery of therapeutic radiation doses to malignant cells. Poly(D,L-lactide-co-glycolide) acid (PLGA) nanoparticles can work as smart drug controlled-release systems activated through pH changes. Considering that paclitaxel (PTX) is a first-line drug for cancer treatment, this work aimed to synthesize and chemically characterize a novel polymeric PTX-loaded nanosystem with grafted ^{177}Lu-BN and to evaluate its performance as a targeted controlled-release nanomedicine for concomitant radiotherapy and chemotherapy of breast cancer.

PLGA(PTX) nanoparticles were synthesized using the single emulsification-solvent evaporation method with PVA as a stabilizer in the presence of PTX. Thereafter, the activation of PLGA carboxylic groups for BN attachment through the Lys^1-amine group was performed. Results of the chemical characterization by FT-IR, DLS, HPLC and SEM/TEM demonstrated the successful synthesis of BN-PLGA(PTX) with a hydrodynamic diameter of 163.54 ± 33.25 nm. The entrapment efficiency of paclitaxel was 92.8 ± 3.6%. The nanosystem showed an adequate controlled release of the anticancer drug, which increased significantly due to the pH change from neutral (pH = 7.4) to acidic conditions (pH = 5.3). After labeling with ^{177}Lu and purification by ultrafiltration, ^{177}Lu-BN-PLGA(PTX) was obtained with a radiochemical purity of 99 ± 1%.

In vitro and *in vivo* studies using MDA-MB-231 breast cancer cells (GRPr-positive) demonstrated a ^{177}Lu-BN-PLGA(PTX) specific uptake and a significantly higher cytotoxic effect for the radiolabeled nanosystem than the unlabeled BN-PLGA(PTX) nanoparticles. Using a pulmonary micrometastasis MDA-MB-231 model, the added value of ^{177}Lu-BN-PLGA(PTX) for tumor imaging was confirmed. The ^{177}Lu-BN-PLGA(PTX) nanomedicine is suitable as a targeted paclitaxel delivery system with concomitant radiotherapeutic effect for the treatment of GRPr-positive breast cancer.

1. Introduction

Recently, nanoradiopharmaceuticals have received more attention as suitable approaches for imaging and/or therapy for several cancer types. Nanoparticles (NPs) offer useful platforms for the design of more effective drug delivery systems. Moreover, NPs can be functionalized to allow target-specific recognition towards receptors overexpressed in malignant tissues. Particularly, polymeric nanoparticles have generated special interest in the field of cancer treatment due to their ability to encapsulate drugs and release them in a controlled manner [1]. Poly lactic-co-glycolic acid (PLGA) is approved for human use as a smart nanosystem for drug delivery due to its response to pH changes, biocompatibility and biodegradability [2,3]. Usually, a therapeutic agent is dispersed throughout the polymeric matrix or can be encapsulated in the hydrophobic nanoparticle core.

Paclitaxel (PTX) has become a first-line drug for the treatment of solid cancers. However, its use is hampered by its toxicity, poor bioavailability and severe side effects. Hence, the drug has been used as a

* Corresponding author at: Departamento de Materiales Radiactivos, Instituto Nacional de Investigaciones Nucleares, Carretera México-Toluca S/N, La Marquesa, Ocoyoacac, Estado de México C.P. 52750, Mexico.
E-mail address: blanca.ocampo@inin.gob.mx (B. Ocampo-García).

https://doi.org/10.1016/j.msec.2019.110043
Received 22 March 2019; Received in revised form 26 June 2019; Accepted 31 July 2019
Available online 01 August 2019
0928-4931/

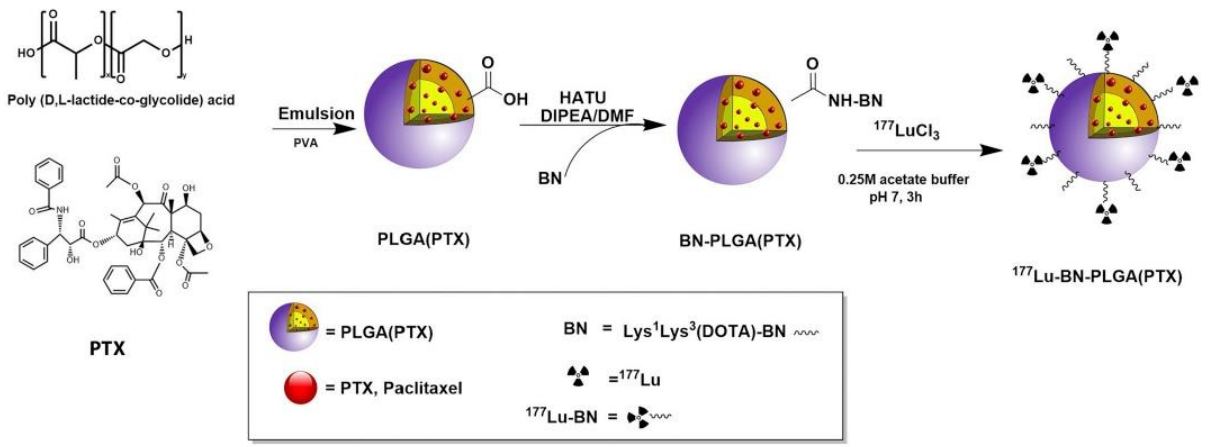

Fig. 1. Schematic representation of PLGA(PTX), BN-PLGA(PTX) and ^{177}Lu-BN-PLGA(PTX) nanosystems.

(μBondapak®, 10 μm 125A°, 3.9 × 150 mm) as the stationary phase and acetonitrile:water (60:40 v/v) as the mobile phase. Separation was carried out at a flow rate of 1 mL/min, with a run time of 5 min for each sample. PTX was measured at 227 nm on a Waters Empower system using a PTX calibration curve (r^2 of 0.997, 6.0–300.0 μg/mL). The experiments were conducted in triplicate.

The encapsulation efficiency (%EE) and drug loading (%DL) were evaluated through HPLC analysis. The concentration of non-encapsulated PTX in the filtered solution was obtained from the ultracentrifugation process (MWCO 30 kDa, 2500*g*, 20 min). These parameters, expressed as a percentage, were determined as follows:

$$\%EE = \left(\frac{Mass\ of\ PTX\ in\ nanoparticles}{Initial\ Mass\ of\ PTX}\right) \times 100 \quad (1)$$

$$\%DL = \left(\frac{Mass\ of\ PTX\ in\ nanoparticles}{Mass\ of\ nanoparticles}\right) \times 100 \quad (2)$$

2.8. In vitro PTX release

For the *in vitro* drug release studies, a solution of phosphate-buffered saline (PBS) containing 0.05% Tween-20, at pH 7.4 or pH 5.3, simulating physiological pH or tumor microenvironment, respectively, was used. Briefly, 10 mg of PLGA(PTX) were dispersed in 1 mL of release medium and placed in a dialysis membrane (MWCO 30 kDa). The dialysis bag was closed and immersed into a flask containing PBS (10 mL) at 37 °C and stirred at 110 rpm. At specified time points, an aliquot of 0.2 mL of the medium was collected and replaced with fresh PBS. Released PTX was measured through HPLC based on the previously described methodology [15].

2.9. Bombesin conjugation efficiency

Conjugation efficiency was determined by measuring free BN in the filtered solution after ultracentrifugation. The reverse-phase HPLC method was carried out using a C18 column (μBondapak® C18 10 μm 125A°, 3.9 × 300 mm) as a stationary phase and a gradient of water/acetonitrile containing 0.1% TFA from 95/5 (v/v) to 20/80 (v/v) as the mobile phase. Separation was carried out at a flow rate of 1 mL/min and a run time of 30 min. A BN standard curve (r^2 = 0.999, 0.07–2.2 mg/mL) was used in this analysis.

2.10. In vitro studies

2.10.1. Cell lines

MDA-MB-231 human breast cancer cells (GRPr-positive) [5,16,17] were originally obtained from the American Type Culture Collection (USA). The cells were routinely grown at 37 °C, with 5% CO_2 atmosphere and 85% humidity in RPMI medium supplemented with 10% newborn calf serum and antibiotics (100 μg/mL streptomycin, 100 U/mL penicillin).

2.10.2. In vitro binding assay and non-specific binding

MDA-MB-231cells were harvested through trypsinization and seeded in 24-well culture plates (1×10^5 cells/well, 0.5 mL). After 24 h, the medium was removed and the cells were incubated with adequate treatment dilution (^{177}Lu-BN-PLGA(PTX) or ^{177}Lu-BN, equivalent to 50 kBq per well) for 45 min at 37 °C. Each well was then rinsed twice with PBS. To displace the membrane-bound radiopharmaceutical fraction, cells were incubated twice (5 min, 37 °C) with 500 μL of 20 mM Gly/HCl, and the activity of the total withdrawn volume was transferred to counting tubes. The cells were then incubated twice with 500 μL of a 1 M NaOH solution (5 min, 37 °C); this fraction (cytoplasm and nucleus) represented nanosystem internalization. The total volume was transferred to counting tubes. Radioactivity in each tube was measured in a gamma NaI(Tl) detector (NML Inc., USA). An aliquot with the initial activity was measured as the radioactivity standard in each treatment. The uptake percentage was calculated. Non-specific binding (cells with blocked receptors) was determined in parallel, in the presence of 5.7 μM Lys^{1}Lys^3(DOTA)-BN with 10 min of pre-incubation.

2.10.3. Cytotoxicity studies

To compare the cytotoxic effect produced by ^{177}Lu-BN-PLGA(PTX), different treatments (PLGA, PLGA(PTX), BN-PLGA, ^{177}Lu-BN-PLGA(PTX), PTX, ^{177}Lu-BN) were evaluated in MDA-MB-231 cells, mainly to compare the PTX contribution since the effect produced by the β-emission of ^{177}Lu is well-documented. A sublethal dose was used to determine differences among treatments without the cell-killing effect. The concentration of nanosystems for radiolabeling was calculated in terms of PTX content and adjusted to 1.5 μM to use one-tenth of the lethal dose based on previous reports (breast cancer cells IC_{50} = 15 μM [18]).

The cytotoxic activity was measured using a Cell Proliferation Assay (XTT) kit, according to the manufacturer's protocol (Roche Diagnostics GmbH, Mannheim, Germany). Cells were seeded in a 96-well microtiter plate (1×10^4 cells/well) and incubated overnight to allow cell

attachment. Then, the medium was removed and 50 μL of each treatment and 200 μL of RPMI medium were placed in each well. The viability was evaluated after removing the medium at 72 h (37 °C, 5% CO_2 and 85% humidity).

2.10.4. Study of the synergistic therapeutic effect

To evaluate the chemotherapeutic (PTX) and radiotherapeutic (^{177}Lu) synergistic effect of the radiolabeled nanosystem on cell viability, 1×10^4 cells/well were exposed to ^{177}Lu-BN-PLGA(PTX) or unlabeled (BN-PLGA(PTX) nanosystems (30 μM in terms of PTX content). The viability was evaluated through the XTT protocol at 24, 48 and 72 h.

2.10.5. Estimation of radiation-absorbed doses to the MDA-MB-231cell nucleus

To estimate the radiation-absorbed doses to the MDA-MB-231 cell nucleus, the following equation was used:

$$D_{N \leftarrow Source} = (N_M \times DF_{N \leftarrow M}) + (N_C \times DF_{N \leftarrow C}) \quad (3)$$

where $D_{N \leftarrow Source}$ represents the mean absorbed dose to the nucleus from source regions (membrane and cytoplasm) and N_M and N_C are the total number of nuclear disintegrations that occurred in the membrane and cytoplasm. $DF_{N \leftarrow M}$ and $DF_{N \leftarrow C}$ denote the dose factors specific for ^{177}Lu, from membrane and cytoplasm regions to the nucleus configuration. The dose factor geometries were obtained from the S values reported by Goddu and Budinger (cell radius = 10 μm, nucleus radius = 5 μm) [19].

2.10.6. Hemocompatibility

For medical devices projected for direct or indirect blood exposure, hemocompatibility studies are required [20]. In this work, the potential of the nanosystems to disrupt red blood cells (RBC) was assessed by the hemolytic assay.

The hemolytic assay was performed in agreement with the standard ISO 10 993-4. Briefly, 200 μL of each treatment ($n = 3$) was placed in contact with 5% human RBC. Trials were immediately incubated at 37 °C for 1 h with negative (isotonic saline) and positive controls (distilled water). Optical density (OD) produced in each treatment was measured at 415 nm (Lambda Bio, Perkin Elmer, USA). The percentage of hemolysis was calculated according to Eq. 4.

$$\%Hemolysis = \frac{OD_{test} - OD_{negative}}{OD_{positive} - OD_{negative}} \times 10 \quad (4)$$

2.11. In vivo studies

In vivo studies in mice were carried out according to the Official Mexican Norm 062-ZOO-1999. Athymic female mice (6–7 weeks of age) were identified and transferred inside plastic cases, kept at a constant temperature, humidity, 12:12 light:dark periods and fed *ad libitum*.

2.11.1. Tumor induction

a) Tumor model for single-photon emission computed tomography (SPECT/CT) imaging and biodistribution studies

Athimic female mice received an intravenous (caudal vein, for pulmonary tumor model) or subcutaneous (upper back, for subcutaneous tumor model) inoculation of 1×10^6 MDA-MB-231 cancer cells suspended in 0.1 mL of phosphate-buffered saline, and 2 weeks after inoculation the animals were used for the imaging or biodistribution studies, respectively.

b) Tumor model for FDG-PET/CT (^{18}F-deoxyglucose-positron emission tomography/computed tomography) and SUV (standard uptake value) calculation.

To assess the extent of tumoral progression under exposure to different treatments, breast tumors (MDA-MB-231 cells, 1×10^6 in PBS) were subcutaneously inoculated on the upper back of 16 female athymic mice (5–6 weeks of age) and the inoculation site was observed for the development of a tumor. Mice survival and size tumor were monitored for 12 days.

2.11.2. Micro SPECT-CT imaging

To verify the *in vivo* nano-radiosystem retention in induced pulmonary tumors, SPECT-CT images were acquired using a micro-SPECT/CT scanner (Albira, ONCOVISION; Gem Imaging S.A., Valencia, Spain) 72 h after intravenous ^{177}Lu-BN-PLGA(PTX) administration (5 MBq in 0.1 mL PBS). Mice under 2% isoflurane anesthesia were placed in the prone position and imaging was performed. The micro-SPECT field of view was 60 mm; a symmetric 20% window was set at 140 keV, and pinhole collimators were used to acquire a three-dimensional SPECT image with a total of 64 projections of 30 s each over 360°. The image dataset was then reconstructed using the ordered-subset expectation maximization algorithm with the standard mode parameter, as provided by the manufacturer. CT parameters were 35 kV sure voltage, 700 μA current and 600 micro-CT projections.

2.11.3. Biodistribution

The subcutaneous tumor model animals received 5 MBq in 0.1 mL of ^{177}Lu-BN-PLGA(PTX). Seventy-two hours after injection, the mice were euthanized and the blood and main organs were removed and placed into pre-weighed plastic test tubes. The radioactivity was measured in a well-type scintillation Na(Tl) detector along with two aliquots of standards (representing 100% of injected activity) and expressed as percentages of the injected dose per gram (%ID/g) or per organ (%ID/organ).

2.11.4. FDG-PET/CT imaging

To assess the tumoral progression (Section 2.11.1), the female mice with MDA-MB-231 tumors were randomly separated into 4 groups. The mean volume of the tumors was 0.119 ± 0.035 cm^3, calculated as $V = \pi/6 * L * a^2$. The length (L) and width (a) were measured with Vernier calipers [21]. Mice were anesthetized with isofluorane 2% and administered intratumorally with each treatment as follows: a) 3 MBq of ^{177}Lu-BN-PLGA(PTX), b) 3 MBq of ^{177}Lu-BN-PLGA and the equivalent mass of c) PLGA(PTX) or d) PLGA as the control.

After 8 days of treatment, images were acquired on a micro-PET/CT scanner (Albira, ONCOVISION, Spain) and the tumor metabolic activity was measured through the Standardized Uptake Value (SUV) of ^{18}F-Deoxyglucose (FDG). The mice were administered with 70–100 μL (3–4 MBq) of FDG on the tail vein under anesthesia. After 1 h, whole body images were acquired in a micro-PET/CT, and the Standard Uptake Value (SUV) was calculated using PMOD Data Analysis software.

Finally, the mice were euthanized since the control tumor size was higher than 1.83 mm^3.

2.11.5. Tumor radiation absorbed dose estimation

The radiation-absorbed dose (the energy deposited by ionizing radiation per unit of mass expressed in Gy) of ^{177}Lu-BN-PLGA(PTX) and ^{177}Lu-BN-PLGA to tumor was calculated according to the following expressions:

$$N_{tumor} = \int_{t1}^{t2} A_h dt = A_0 \int_{0\,d}^{8\,d} e^{-\lambda t} = \frac{A_0}{\lambda}(1 - e^{-\lambda t}) \quad (5)$$

$$\bar{D}_{tumor \leftarrow tumor} = N_{tumor} DF_{tumor \leftarrow tumor} \quad (6)$$

where N = total number of disintegration in the tumor, $t_1 = 0$ day and $t_2 = 8$ day post-treatment, $\lambda = \ln 2/t_{1/2}$ or (ln2/6.7d), A_0 = initial administered Lu-177 activity (Bq), $\bar{D}_{tumor \leftarrow tumor}$ = mean absorbed dose to tumor from tumor, and DF is the dose factor for Lu-177.

The N value was introduced to Organ Level Internal Dose Assessment (OLINDA) code, (which provides conversion factors (DF)) to estimate the radiation-absorbed dose ($\bar{D}_{tumor \leftarrow tumor}$) delivered by Lu-177 administered with each treatment.

2.12. Statistical analysis

Differences in cell uptake between unblocked and blocked receptors were evaluated with the Student *t*-test. The cytotoxicity results were estimated by a two-sided ANOVA using OriginLab and GraphPrisma software, setting the statistical significance at $p < 0.05$.

3. Results and discussion

The application of polymeric nanoparticles for PTX release, GRPr targeting and targeted radiotherapy with ^{177}Lu has been studied in this research to achieve a dual therapeutic effect on MDA-MB-231 breast cancer cells.

3.1. Preparation of PLGA and PLGA(PTX) nanoparticles

In this research, minor modifications in the emulsion-solvent method [14] allowed us to obtain both the free-drug PLGA and paclitaxel-loaded PLGA nanoparticles. The hydrophobic hydrocarbon chains from the lactide moieties in PLGA enabled the interaction with hydrophobic PTX, allowing thermodynamic folding and the consequent nanoparticle formation [3].

Scanning Electron Microscopy and Transmission Electron Microscopy micrographs (Fig.2) showed that the designed nanosystems presented a well-shaped spherical form. The morphology was not modified by PTX incorporation or the grafted BN. All nanoparticle systems showed a hydrodynamic diameter < 200 nm (by DLS) and a monomodal distribution. A narrow polydispersity was observed for PLGA and PLGA(PTX) systems (Table 1). However, the PDI increased as a result of functionalization with BN (0.2896 and 0.2987). In general, a PDI smaller than 0.2 is considered as a narrow-size distribution [22]. Specifically, the size range was 104 nm to 201 nm for PLGA and 109 nm to 213 nm for PLGA(PTX), without significant differences ($p < 0.05$).

Table 1
Physicochemical characterization of nanoparticles.

Nanoparticle	Size (nm)	Polydispersity index (PDI)	Z potential (mV)
PLGA	152.90 ± 48.56	0.1977	−18.9
PLGA(PTX)	161.23 ± 52.27	0.1914	−19.0
BN-PLGA	156.19 ± 54.18	0.2896	−11.0
BN-PLGA(PTX)	163.54 ± 33.25	0.2987	−12.3

Negative zeta potential of PLGA nanoparticles (−18.9 mV) is attributed to the carboxylate groups on the nanoparticle surface. In PLGA(PTX), the Z potential remained unchanged in charge, which could mean that the paclitaxel remained entrapped in the nanoparticles, in agreement with the results of chemical characterization.

3.2. Conjugation of bombesin to PLGA or PLGA(PTX)

Bombesin was conjugated to the PLGA or PLGA(PTX) by the coupling peptide reaction, using HATU as the activator molecule. The attachment of BN onto the nanoparticle surface did not affect the translational diffusion coefficient, which can be understood as the maintenance in equivalent hydrodynamic diameter, keeping apparent nanoparticle sizes. However, the zeta potential showed a significant decrease from −18.9 mV to -11 mV in BN-PLGA and from −19.0 mV to −12.3 mV in BN-PLGA(PTX). The reduction in Z potential values suggests that the peptide interaction and arrangement on the nanoparticle surface originate changes in the electrostatic environment surrounding the nanoparticle. The positive amine, amide bonds and neutral hydrocarbon chains of Lys^{1}Lys^3(DOTA)-BN could contribute to the reduction

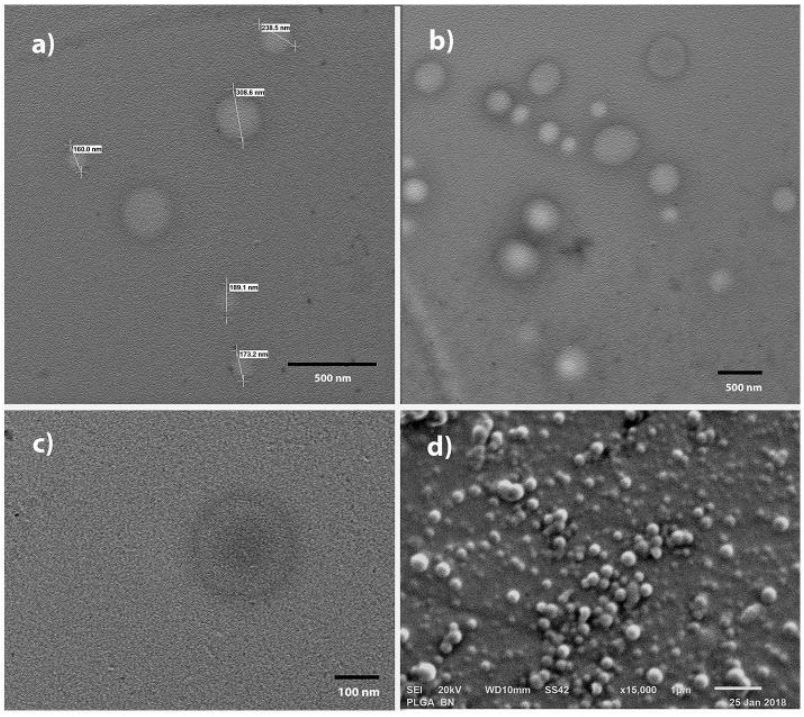

Fig. 2. Representative TEM micrograph of a) PLGA, b) PLGA(PTX), c) BN-PLGA(PTX) and d) SEM image of PLGA NPs.

of the zeta potential. BN conjugation efficiency, indirectly measured by HPLC, was calculated to be > 97%. The measured diameters of the nanoparticles could be affected by shrinking producing a structure modification. It is possible that NPs become highly porous, which could contribute to the changes observed in the nanoparticle average size evaluated by SEM with respect to DLS results, although without statistically significant differences.

In terms of physicochemical properties, a significant accumulation of bombesin-grafted nanoparticles on tumor tissue is expected by two different mechanisms, the enhanced permeability and retention (EPR) effect and active targeting thorough GRP cell receptors. Then, in the neovasculature of tumor, the characteristic fenestrations of 200–780 nm would allow the extravasation of ^{177}Lu-BN-PLGA(PTX) (200 nm) in the tumoral acid microenvironment, with the consequent PTX delivery and cancer cell internalization by simple PTX diffusion due to its small molecule size and lipophilic properties (< 1000 Da). ^{177}Lu-BN-PLGA(PTX) could also be actively incorporated into the cell by different endocytic pathways attributed to the specific recognition by the GRPr [12,23,24].

3.3. Radiolabeling efficiency and radiochemical purity

Radiolabeling efficiency of the nanosystems was determined by ultracentrifugation (45%), and after purification, radiochemical purity (evaluated by ITLC) was 99 ± 1%.

3.4. Infrared spectroscopy

The PLGA nanoparticle spectrum was consistent with that previously reported [11,14]. Characteristic vibrational modes were observed, such as $(C-H)_{\upsilon}$ from the co-polymer carbon skeletal between 2942 cm^{-1} and 2918 cm^{-1}, $(C=O)_{\upsilon}$ vibration of the ester group at 1752 cm^{-1}, $(C-H)_{\delta}$ from bonds between monomeric units of lactide-glycolide (L-G: 1376 cm^{-1}), glycolide-glycolide (G-G: 1425 cm^{-1}) and lactide-lactide (L-L: 1453 cm^{-1}) and $(C-O)_{\upsilon}$, $(O-H)_{\delta}$ and $(O-H)_{\upsilon}$ as evidence of stabilization with PVA (Fig. 3c).

IR analysis of the PTX was consistent with previous reports [25]. Briefly, the spectrum showed stretching (−N−H) vibrations characterized by a broad and asymmetric band centered at 3442 cm^{-1}. The band found at 2945 cm^{-1} was assigned to (−C−H) from asymmetric and symmetric stretching vibrations. The amide I region mainly associated with a (C═O) stretching vibration was identified at 1732 cm^{-1}, whereas (C−N) stretching was found at 1274 cm^{-1}. Aromatic hydrocarbons were identified by characteristic absorption bands in the region near to 1645 cm^{-1} and 1500–1400 cm^{-1}, produced by carbon-carbon stretching vibrations in the aromatic ring. The bands in the 1250–1000 cm^{-1} region were assigned to C−H in-plane bending, and finally, C−H stretching above 3000 cm^{-1} was also identified (Fig. 3a).

The IR spectrum corresponding to paclitaxel-loaded PLGA nanoparticles (Fig. 3d) showed no difference with regard to the empty nanoparticle spectrum. These spectra did not display the characteristic intense bands from free PTX; they may have been masked by the bands produced by the polymer. The possible absence of chemical interaction between the polymer and drug may indicate a complete encapsulation of paclitaxel into the nanoparticles [26,27].

The spectra of pure Lys^{1}Lys^3(DOTA)BN (Fig. 3b) showed characteristic peaks at 3283, 1646 and 1533 cm^{-1}, corresponding to −NH stretching, C═O stretching (Amide *I*) and −CN (amide II), as previously reported [28].

BN-conjugated nanoparticles (BN-PLGA(PTX) showed the contribution of characteristic vibrations from each component. The peaks at 1666 cm^{-1} and 1536 cm^{-1} on BN-PLGA(PTX) from amide stretching vibrations makes the presence of BN in PLGA nanoparticles evident (Fig. 3e).

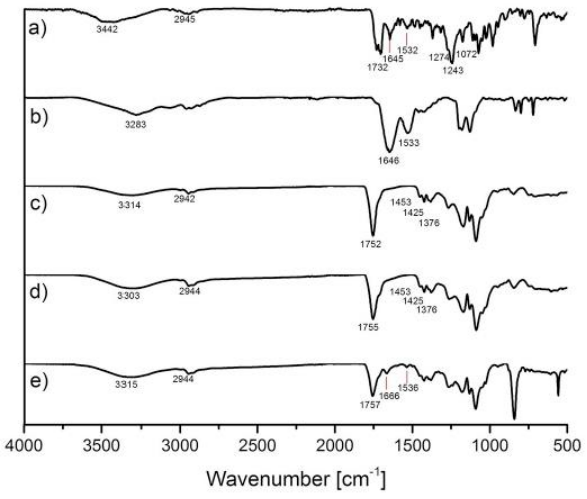

Fig. 3. Infrared spectra of a) paclitaxel, b) Lys^{1}Lys^3(DOTA)Bombesin, c) PLGA nanoparticles d) PLGA(PTX) nanoparticles and e) BN-PLGA(PTX) nanoparticles.

3.5. Encapsulation efficiency (EE) and drug loading (DL)

The efficiency of hydrophobic paclitaxel encapsulation in BN-PLGA(PTX) was calculated by subtracting the free drug measured in a filtered solution from the total amount used to prepare the nanoparticles. HPLC analysis was carried out at λ_{max} = 227 nm, using a standard curve related to the absorption and PTX concentration (6.0–300.0 μg/mL r^2 = 0.997). The efficiency of drug encapsulation was 92.8% ± 3.6, in agreement with similar reports [26,29,30]; and drug loading was 1.13 ± 0.13%. It was observed that loading capacity decreases in function of the size; thus high concentration of nanoparticles may be needed for therapeutic efficacy.

3.6. In vitro release

To evaluate the controlled release capacity of PTX from BN-PLGA(PTX), the nanosystem was evaluated in simulated physiological pH (7.4) and acidic microenvironment tumor conditions (pH 5.3). The cumulative release percentage of PTX is shown in Fig. 4.

The kinetic drug release profiles exhibited biphasic patterns with release during the first 25 h of 66.8% and 63.7% at pH 5.3 and 7.4,

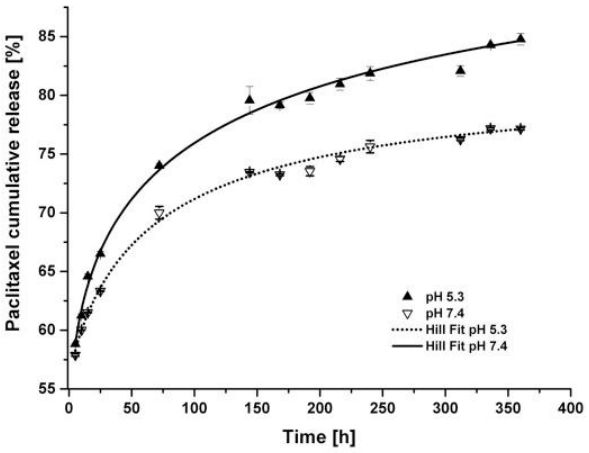

Fig. 4. *In vitro* release of PTX from paclitaxel-loaded PLGA nanoparticles in PBS (pH 5.3 and 7.4) fitted to the non-linear Hill model.

respectively, followed by a slow and continuous release during 15 days. Significant differences ($p < 0.05$) dependent on pH were observed, the maximum amount of drug release was reached at pH 5.3 (84.8%), whereas at pH 7.4 the maximum release was 77.1% of the total entrapped drug. As it is known, the higher release at pH 5.3 is attributed to the effect of hydrolysis and degradation of the polymer [31]. Therefore, paclitaxel release from BN-PLGA(PTX) in the acidic tumor microenvironment may have an improvement over anticancer drug delivery. The presented results support the proposal that loading hydrophobic molecules such as PTX on PLGA nanoparticles could enhance their accumulation on tumor tissues with the consequent decrease of the adverse effects produced by the drug.

3.7. In vitro uptake study

The therapeutic efficiency of paclitaxel-loaded PLGA depends on the nanosystem cell uptake, their intracellular distribution, and the release from internalized nanoparticles.

As previously reported, GRPr is overexpressed in several breast cancer cell lines such as MDA-MB-231 and T47D [16,17,32]. Cell uptake was evaluated comparing the behavior of ^{177}Lu-BN-PLGA(PTX) and ^{177}Lu-BN as a monomeric system. The results showed a specific uptake of ^{177}Lu-BN-PLGA(PTX) de 4.58 ± 0.42%, which was significantly reduced ($p < 0.05$) when GRP receptors of MDA-MB-231 cells were blocked by pre-incubation (10 min before treatment exposure) with free Lys^{1}Lys^{3}BN peptide (Fig. 5a). This evidence suggests that the active targeting was achieved due to the PLGA surface modification with BN.

The specific uptake of ^{177}Lu-BN was also confirmed. It was the highest uptake value observed (8.20 ± 0.49%), which was effectively diminished (1.6 ± 0.26%) when receptors were previously blocked in the presence of 5.7 μM Lys^{1}Lys^3(DOTA)-BN (10 min of pre-incubation) (Fig. 5a). While the free PTX does not require a ligand-receptor interaction to mediate endocytosis, ^{177}Lu-BN-PLGA(PTX) is introduced into the cell through several mechanisms. It has been demonstrated that nanoparticle systems conjugated to bombesin interact specifically with GRP receptors, increasing the ligand internalization by clathrin-mediated endocytosis, and thus allow a suitable delivery of paclitaxel into MDA-MB-231 cells; this enables the system to produce a higher level of toxicity [22,33].

Therefore, ^{177}Lu-BN-PLGA(PTX) nanosystems exhibited cellular uptake based on receptor-mediated endocytosis attributed to the interaction of BN with the GRP receptor. The active targeting was achieved by modifying the PLGA with BN. However, further information on the kinetics of internalization is needed to correlate the cargo delivery profile to understand the *in vitro* behavior.

3.8. Estimation of radiation-absorbed doses to the MDA-MB-231cell nucleus

Based on the uptake (radioactivity in the membrane) and internalization (radioactivity in cytoplasm) results as well as ^{177}Lu decay properties, the biokinetic models of ^{177}Lu-BN-PLGA(PTX) and ^{177}Lu-BN were obtained and the radiation absorbed doses calculated for MDA-MB-231 cells.

The total absorbed dose produced to the cell nuclei by ^{177}Lu-BN at 72 h was 0.659 Gy, 1.6 times higher than that produced by ^{177}Lu-BN-PLGA(PTX) (0.400 Gy, Table 2). All the estimated doses delivered by each treatment were lower than 1 Gy. In this regard, it is reported that a dose of 100 Gy is required to destroy cell function in non-proliferating systems, and the mean lethal dose for loss of proliferative capacity is about 2 Gy [34]. Moreover, a recent study demonstrated that the radiation-absorbed dose in the nucleus of 4.8 Gy on lymphoma cells induced DNA damage and produced an important increase in the apoptotic cell population (98%), mostly in late-stage (irreversible) apoptosis [35]. As previously mentioned, our intention during the cytotoxicity evaluation was to evaluate differences between ^{177}Lu treatments without inducing cell death, which is why doses below 2 Gy were used. However, for the study of the synergistic therapeutic effect, doses of 8 Gy were applied (Table 2).

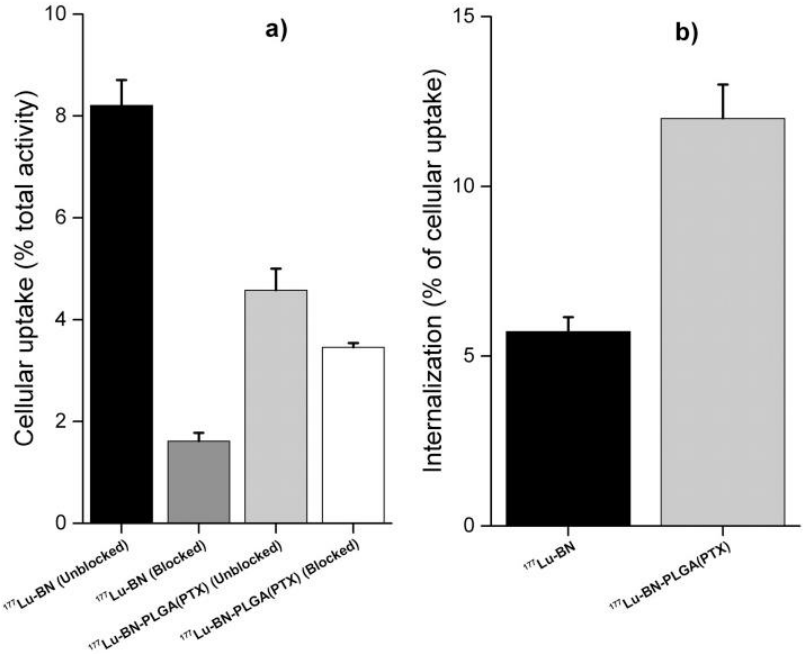

Fig. 5. a) ^{177}Lu-BN and ^{177}Lu-BN-PLGA(PTX) cellular uptake. Pre-incubated MDA-MB-231 cells with Lys^{1}Lys^3-DOTA-BN (blocked receptors) and without Lys^{1}Lys^3(DOTA)-BN pre-incubation (unblocked receptors) and b) internalization with regard to total uptake.

Table 2
Biokinetic model and radiation absorbed doses produced by 0.5 Bq/cell of ^{177}Lu-radiopharmaceuticals to the MDA-MB-231 cancer cell nuclei within 72 h.

Radiopharmaceutical cellular location	Biokinetic model $A(t)$	$N = \int_{t=0}^{t=72\,h} A(t)dt$	Dose (Gy)	Total dose to cell nuclei (Gy)
^{177}Lu-BN-PLGA(PTX)				0.400
Membrane	$A(t) = 0.089e^{-3.96t} + 3.730e^{-0.009t} + 0.780e^{-0.007t}$	8712	0.332	
Cytoplasm	$A(t) = 9.880e^{-10.004t} + 0.159e^{-0.008t} + 0.337e^{-0.008t}$	1004	0.075	
^{177}Lu-BN				0.659
Membrane	$A(t) = 0.422e^{-25.404t} + 6.25e^{-0.008t} + 1.98e^{-0.010t}$	15,912	0.594	
Cytoplasm	$A(t) = 0.439e^{-28.704t} + 0.132e^{-0.012t} + 0.337e^{-0.008t}$	904	0.065	

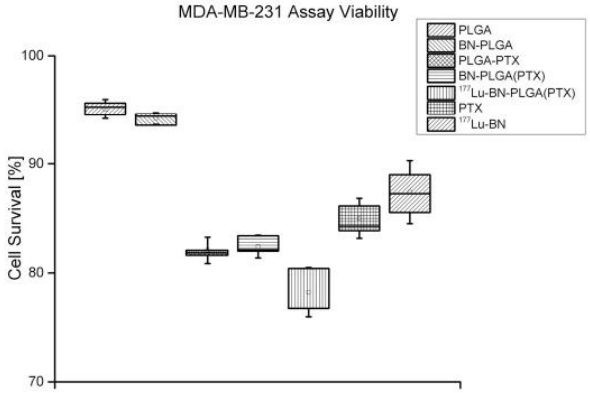

Fig. 6. Effect on cell viability after exposure of MDA-MB-231 cells to sublethal doses of paclitaxel (1.5 μM) and ^{177}Lu radiation doses (< 1 Gy) in different nanosystems.

3.9. In vitro cytotoxicity

Fig. 6 shows that ^{177}Lu-BN-PLGA(PTX) caused a significant decrease in cell viability when compared to BN-PLGA(PTX), ^{177}Lu-BN or PTX.

At 72 h of treatment, 0.40 Gy of radiation absorbed dose was deposited into the nucleus of an MDA-MB-231 cell treated with ^{177}Lu-BN-PLGA(PTX). At this time point, the viability decreased to 78.9 ± 2.61%, which was significantly different compared to BN-PLGA (94.1 ± 0.5%, $p < 0.001$), PLGA (92.2 ± 3.2%, $p < 0.001$), PTX (85.0 ± 1.8%, $p < 0.001$) and ^{177}Lu-BN (87.4 ± 3.3%, $p < 0.001$), even when in the latter, the radiation absorbed dose was 0.659 Gy (Table 2).

Since the *in vitro* binding assay demonstrated specific uptake at 45 min of treatment exposure, the uptake and consequent observed cell death without a significant difference ($p < 0.05$) for the PLGA(PTX) group (90.56 ± 7.30%), compared with BN-PLGA(PTX) (84.84 ± 2.52%), was attributed to the delivered PTX as a result of the unspecific invagination produced by the weak cooperative interactions between NPs and cells. Moreover, it was expected that the endocytic pathways having low efficiency were favored by the exposition time (72 h) for both treatments. [24,36].

After 72 h, the cell viability produced by 1.5 μM of free PTX (85.0 ± 1.8%) was significantly different ($p < 0.001$) when compared with the survival rate (78.9 ± 2.61%) produced by ^{177}Lu-BN-PLGA(PTX). At this time point, an important amount of PTX (74%) had been released, contributing to the cell toxicity (Fig. 3). These results are expected since a concentration of 15 μM of PTX is required to produce significant cell death [18]. Furthermore, the encapsulation of PTX on PLGA nanoparticles enhances the cytotoxic effect (Fig. 6).

In terms of radiosensitization, nanoparticles encapsulating chemical compounds have been proposed to enhance the response to radiation [37]. In Fig. 6, the synergistic effect between chemotherapy and radiotherapy is observed. The high decrease in viability produced by

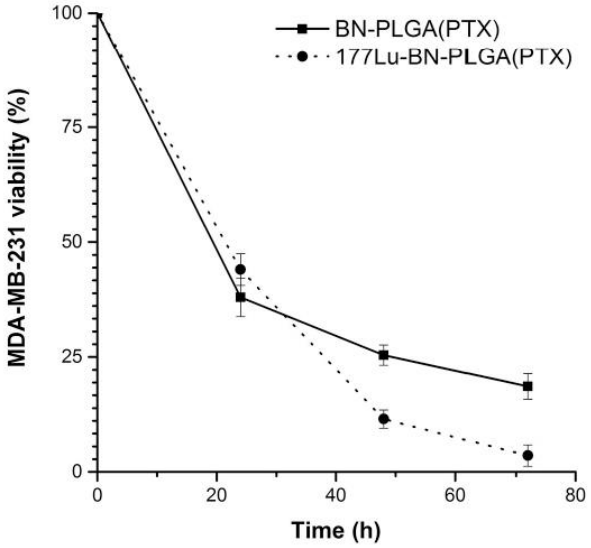

Fig. 7. Effect on MDA-MB-231cell viability after exposure to ^{177}Lu-BN-PLGA(PTX), compared to BN-PLGA(PTX). PTX = 30 μM, radiation dose = 8 Gy at 72 h.

^{177}Lu-BN-PLGA(PTX) between 24 and 48 h is mainly attributed to the radiosensitization effect produced by PTX.

The synergistic effect of chemotherapy and radiotherapy produced by the ^{177}Lu-BN-PLGA(PTX) nanosystem was evident when doses of PTX = 30 μM and radiation-absorbed doses of 8 Gy were used. As can be observed in Fig. 7, the greater cytotoxic effect for the radiolabeled nanosystem was observed between 24 and 72 h (highest slope) given that, at this time, a significant PTX and radiation dose delivery had occurred.

3.10. Hemocompatibility

The non-hemolytic behavior of the ^{177}Lu-BN-PLGA(PTX) supports its suitability for intravenous administration (0.97 ± 0.05%). The systems can be classified as non-hemolytic materials, based on the hemolysis value being lower than 2% [38].

3.11. In vivo studies

Fig. 8a shows a representative SPECT image of a mouse with an MDA-MB-231 pulmonary tumor model. The tumor-to-blood ratio reveals suitable contrast, with a significant accumulation of ^{177}Lu-BN-PLGA(PTX) nanomedicine in tumor tissue after 72 h of injection with a standard uptake value (SUV) of 3. The *ex vivo* biodistribution results of ^{177}Lu-BN-PLGA(PTX) also showed a high tumor uptake in MDA-MB-231 lesions (Fig. 8b). However, future studies are required to obtain a complete ^{177}Lu-BN-PLGA(PTX) biokinetic profile for the *in vivo*

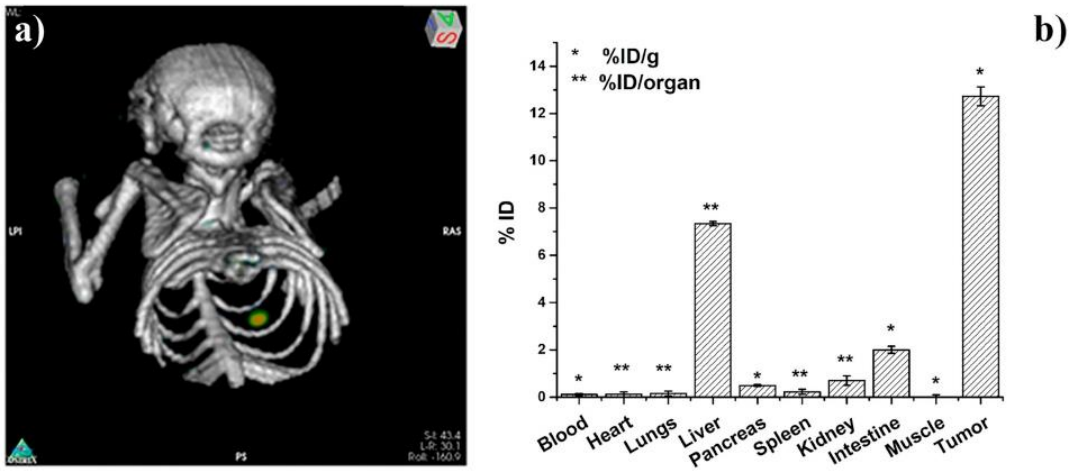

Fig. 8. a) Micro SPECT-CT image (72 h) in athymic mice with pulmonary tumor model (MDA-MB-231 cells) and b) biodistribution of ^{177}Lu-BN-PLGA(PTX) in athymic mice with subcutaneous tumor model (MDA-MB-231 cells), 72 h post-injection.

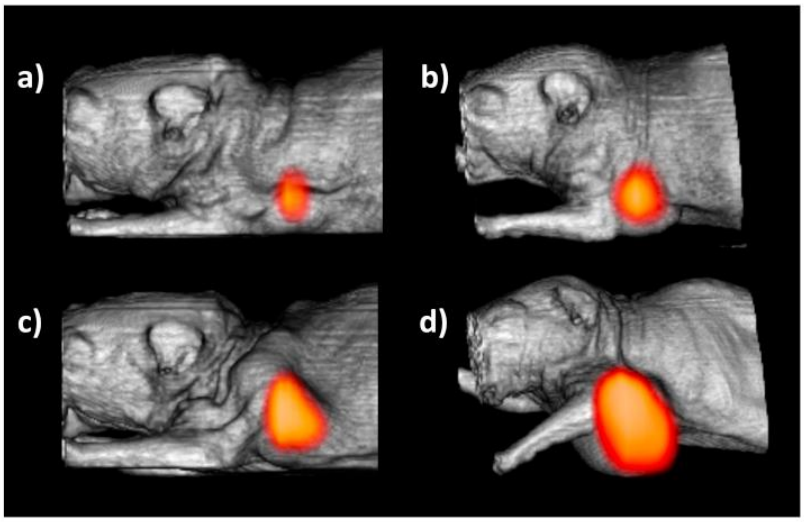

Fig. 9. Micro PET-CT images of a) ^{177}Lu-BN-PLGA(PTX), b) ^{177}Lu-BN-PLGA, c) PLGA(PTX) and d) PLGA as the control group, after 8 days post-administration of 3 MBq of ^{177}Lu-BN-PLGA(PTX), 3 MBq of ^{177}Lu-BN-PLGA and μg of PLGA(PTX) and PLGA. The heart FDG uptake was subtracted from the image to visualize the tumor uptake.

absorbed dose assessment and for the evaluation of its therapeutic efficacy in different breast cancer models.

Since the micro-PET/CT imaging at the end of the *in vivo* studies showed a tumor volume for the mice control group of 1.83 ± 0.54 cm^3, the combination of targeted radiotherapy (provided by ^{177}Lu-BN) and chemotherapy (provided by PTX) resulted in the highest inhibition of breast tumor growth for the mice administered with ^{177}Lu-BN-PLGA(PTX), which reached the lowest tumor proliferation (0.136 ± 0.04 cm^3). The group exposed to ^{177}Lu-BN-PLGA produced a final tumor of 0.654 ± 0.202 cm^3 and the PLGA(PTX) group produced a tumoral volume of 0.216 ± 0.072 cm^3. Therefore, the response to treatment was in this order: ^{177}Lu-BN-PLGA(PTX) > PLGA(PTX) > ^{177}Lu-BN-PLGA > PLGA (control).

The SUV data, related directly to the metabolic activity, were 42.43 ± 5.54, 24.31 ± 4.51, 14.74 ± 2.92 and 8.10 ± 1.06 for the control group, ^{177}Lu-BN-PLGA, PLGA(PTX), ^{177}Lu-BN-PLGA(PTX), respectively. Even though the average radiation-absorbed dose of ^{177}Lu-BN-PLGA(PTX) and ^{177}Lu-BN-PLGA delivered to the tumor was the same (36.9 ± 7.01 Gy), and this dose corresponds to that usually applied in radiotherapy treatments to breast cancer patients, the ^{177}Lu-BN-PLGA(PTX) conjugated showed the lowest tumoral metabolic activity (lowest SUV) and almost complete inhibition of the tumor progression (lowest tumoral volume). These results corroborate the synergistic effect between radiation therapy and chemotherapy in a single nanosystem (Fig. 9).

4. Conclusions

^{177}Lu-BN-PLGA(PTX) nanoparticles are suitable systems for the bimodal therapy of breast cancer due to the synergistic effect on cell viability of the ^{177}Lu radiation dose delivery and the controlled release of paclitaxel. The radiolabeling of BN-PLGA(PTX) with Lu-177 allows for the acquisition of GRPr overexpression images in breast cancer tumors, making the monitoring of disease progression possible. Further studies are needed to determine the therapeutic efficacy of ^{177}Lu-BN-PLGA(PTX) in different breast cancer preclinical models.

Funding statement

This study was supported by the International Atomic Energy

Agency (CRP—F22064, contract No. 18358) and was carried out as part of the activities of the "Laboratorio Nacional de Investigación y Desarrollo de Radiofármacos, CONACyT".

Declaration of competing interest

The authors declare that there are no conflicts of interest regarding the publication of this paper.

Acknowledgments

The authors thank Jorge E. Pérez del Prado for his support during SEM analyses. This study was partially supported by the National Council of Science and Technology (CONACyT-CB-A1S38087) and the International Atomic Energy Agency (CRP-F22064, Contract 18358). It was carried out as part of the activities of the "Laboratorio Nacional de Investigación y Desarrollo de Radiofármacos, CONACyT.

References

[1] S. Mann, A. Dufour, J. Glass, R. De Rose, S. Kent, G. Such, A. Johnston, Tuning the properties of pH responsive nanoparticles to control cellular interactions in vitro and ex vivo, Polym. Chem. 7 (38) (2016) 6015–6024.
[2] A. Srivastava, T. Yadav, S. Sharma, A. Nayak, A.A. Kumari, N. Mishra, Polymers in drug delivery, J Biosci Med 4 (01) (2015) 69.
[3] D. Kapoor, A. Bhatia, R. Kaur, R. Sharma, G. Kaur, S. Dhawan, PLGA: a unique polymer for drug delivery, Ther. Deliv. 6 (1) (2015) 41–58.
[4] S.-S. Feng, L. Mu, K.Y. Win, G. Huang, Nanoparticles of biodegradable polymers for clinical administration of paclitaxel, Curr. Med. Chem. 11 (4) (2004) 413–424.
[5] C. de Aguiar Ferreira, L.L. Fuscaldi, D.M. Townsend, D. Rubello, A.L.B. de Barros, Radiolabeled bombesin derivatives for preclinical oncological imaging, Biomed. Pharmacother. 87 (2017) 58–72.
[6] P. Fernandez, M. Debled, E. Hindié, Expression of gastrin-releasing peptide receptor in breast cancer and its association with pathologic, biologic, and clinical parameters: a study of 1,432 primary tumors, J. Nucl. Med. 58 (2017) 1401–1407.
[7] T. Maina, B.A. Nock, H. Kulkarni, A. Singh, R.P. Baum, Theranostic prospects of gastrin-releasing peptide receptor–radioantagonists in oncology, PET clinics 12 (3) (2017) 297–309.
[8] B.B.S. Cerqueira, A. Lasham, A.N. Shelling, R. Al-Kassas, Development of biodegradable PLGA nanoparticles surface engineered with hyaluronic acid for targeted delivery of paclitaxel to triple negative breast cancer cells, Mater. Sci. Eng. C. 76 (2017) 593–600.
[9] H. Mendoza-Nava, G. Ferro-Flores, F.d.M. Ramírez, B. Ocampo-García, C. Santos-Cuevas, E. Azorín-Vega, N. Jiménez-Mancilla, M. Luna-Gutiérrez, K. Isaac-Olivé, Fluorescent, plasmonic, and radiotherapeutic properties of the ^{177}Lu–dendrimer-AuNP–folate–bombesin nanoprobe located inside cancer cells, Mol. Imaging 16 (2017) (1536012117704768).
[10] N. Jiménez-Mancilla, G. Ferro-Flores, C. Santos-Cuevas, B. Ocampo-García, M. Luna-Gutiérrez, E. Azorín-Vega, K. Isaac-Olivé, M. Camacho-López, E. Torres-García, Multifunctional targeted therapy system based on 99mTc/^{177}Lu-labeled gold nanoparticles-Tat (49–57)-Lys3-bombesin internalized in nuclei of prostate cancer cells, J. Label. Compd. Radiopharm. 56 (13) (2013) 663–671.
[11] H. Kulhari, D. Pooja, S. Shrivastava, V. Naidu, R. Sistla, Peptide conjugated polymeric nanoparticles as a carrier for targeted delivery of docetaxel, Colloids Surf. B 117 (2014) 166–173.
[12] H. Kulhari, D. Pooja, M.K. Singh, M. Kuncha, D.J. Adams, R. Sistla, Bombesin-conjugated nanoparticles improve the cytotoxic efficacy of docetaxel against gastrin-releasing but androgen-independent prostate cancer, Nanomedicine 10 (18) (2015) 2847–2859.
[13] L. Bodei, M. Ferrari, A. Nunn, J. Llull, M. Cremonesi, L. Martano, G. Laurora, E. Scardino, S. Tiberini, G. Bufi, Lu-177-AMBA bombesin analogue in hormone refractory prostate cancer patients: a phase I escalation study with single-cycle administrations, European Journal of Nuclear Medicine and Molecular Imaging (2007) S221 SPRINGER 233 Spring Street, New York, NY 10013 USA.
[14] L. Jaimes-Aguirre, E. Morales-Avila, B.E. Ocampo-García, L.A. Medina, G. López-Téllez, B.V. Gibbens-Bandala, V. Izquierdo-Sánchez, Biodegradable poly(D,L-lactide-co-glycolide)/poly(L-γ-glutamic acid) nanoparticles conjugated to folic acid for targeted delivery of doxorubicin, Mater. Sci. Eng. C Mater. Biol. Appl. 76 (2017) 743–751.
[15] B. Gibbens-Bandala, B. Ocampo-García, G. Ferro-Flores, E. Morales-Avila, A. Ancira-Cortez, L. Jaimes-Aguirre, Multimeric system of RGD-grafted PMMA-nanoparticles as a targeted drug-delivery system for paclitaxel, Curr. Pharm. Des. 23 (23) (2017) 3415–3422.
[16] M. Miyazaki, N. Lamharzi, A.V. Schally, G. Halmos, K. Szepeshazi, K. Groot, R.Z. Cai, Inhibition of growth of MDA-MB-231 human breast cancer xenografts in nude mice by bombesin/gastrin-releasing peptide (GRP) antagonists RC-3940-II and RC-3095, Eur. J. Cancer 34 (5) (1998) 710–717.
[17] C. Chao, K. Ives, H.L. Hellmich, C.M. Townsend, M.R. Hellmich, Gastrin-releasing peptide receptor in breast cancer mediates cellular migration and interleukin-8 expression, J. Surg. Res. 156 (1) (2009) 26–31.
[18] N. Hasima, L.I.L. Aun, M.N. Azmi, A.N. Aziz, E. Thirthagiri, H. Ibrahim, K. Awang, 1′ S-1′-acetoxyeugenol acetate: a new chemotherapeutic natural compound against MCF-7 human breast cancer cells, Phytomedicine 17 (12) (2010) 935–939.
[19] S.M. Goddu, T.F. Budinger, MIRD cellular S. values: self-absorbed dose per unit cumulated activity for select radionuclides and monoenergetic electron and alpha particle emitters incorporated into different cell compartments, Society of Nuclear Medicine 1 (1997) 120.
[20] A. Escudero-Castellanos, B.E. Ocampo-García, M.V. Domínguez-García, J. Flores-Estrada, M.V. Flores-Merino, Hydrogels based on poly(ethylene glycol) as scaffolds for tissue engineering application: biocompatibility assessment and effect of the sterilization process, J Mater Sci Mater Med 27 (12) (2016) 176.
[21] A. Vilchis-Juárez, G. Ferro-Flores, C. Santos-Cuevas, E. Morales-Avila, B. Ocampo-García, L. Díaz-Nieto, M. Luna-Gutiérrez, N. Jiménez-Mancilla, M. Pedraza-López, L. Gómez-Oliván, Molecular targeting radiotherapy with cyclo-RGDFK (C) peptides conjugated to ^{177}Lu-labeled gold nanoparticles in tumor-bearing mice, J. Biomed. Nanotechnol. 10 (3) (2014) 393–404.
[22] C. Sengel-Turk, C. Hascicek, A. Dogan, G. Esendagli, D. Guc, N. Gonul, Surface modification and evaluation of PLGA nanoparticles: the effects on cellular uptake and cell proliferation on the HT-29 cell line, J Drug Deliv Sci Technol 24 (2) (2014) 166–172.
[23] M. Gaumet, A. Vargas, R. Gurny, F. Delie, Nanoparticles for drug delivery: the need for precision in reporting particle size parameters, Eur. J. Pharm. Biopharm. 69 (1) (2008) 1–9.
[24] J.s. Mosquera, I. García, L.M. Liz-Marzán, Cellular uptake of nanoparticles versus small molecules: a matter of size, Acc. Chem. Res. 51 (9) (2018) 2305–2313.
[25] J.G. Hiremath, N.S. Khamar, S.G. Palavalli, C.G. Rudani, R. Aitha, P. Mura, Paclitaxel loaded carrier based biodegradable polymeric implants: preparation and in vitro characterization, Saudi Pharm J 21 (1) (2013) 85–91.
[26] K.F. Martins, A.D. Messias, F.L. Leite, E.A. Duek, Preparation and characterization of paclitaxel-loaded PLDLA microspheres, Mater. Res. 17 (3) (2014) 650–656.
[27] F. Yerlikaya, A. Ozgen, I. Vural, O. Guven, E. Karaagaoglu, M.A. Khan, Y. Capan, Development and evaluation of paclitaxel nanoparticles using a quality-by-design approach, J. Pharm. Sci. 102 (10) (2013) 3748–3761.
[28] L. Aranda-Lara, G. Ferro-Flores, E. Azorín-Vega, F. de María Ramírez, N. Jiménez-Mancilla, B. Ocampo-García, C. Santos-Cuevas, K. Isaac-Olivé, Synthesis and evaluation of Lys 1 (α, γ-folate) Lys 3 (177 Lu-DOTA)-Bombesin (1-14) as a potential theranostic radiopharmaceutical for breast cancer, Appl. Radiat. Isot. 107 (2016) 214–219.
[29] R.K. Averineni, G.V. Shavi, A.K. Gurram, P.B. Deshpande, K. Arumugam, N. Maliyakkal, S.R. Meka, U. Nayanabhirama, PLGA 50: 50 nanoparticles of paclitaxel: development, in vitro anti-tumor activity in BT-549 cells and in vivo evaluation, Bull. Mater. Sci. 35 (3) (2012) 319–326.
[30] C. Fonseca, S. Simões, R. Gaspar, Paclitaxel-loaded PLGA nanoparticles: preparation, physicochemical characterization and in vitro anti-tumoral activity, J. Control. Release 83 (2) (2002) 273–286.
[31] H. Maleki, F. Dorkoosh, M. Adabi, M. Khosravani, H. Arzani, M. Kamali, Methotrexate-loaded plga nanoparticles: preparation, characterization and their cytotoxicity effect on human glioblastoma U87MG cells, Int J Med Nano Res 4 (1) (2017) 020.
[32] S. Giacchetti, C. Gauvillé, P.D. Crémoux, L. Bertin, P. Berthon, J.P. Abita, F. Cuttitta, F. Calvo, Characterization, in some human breast cancer cell lines, of gastrin-releasing peptide-like receptors which are absent in normal breast epithelial cells, Int. J. Cancer 46 (2) (1990) 293–298.
[33] D. Suresh, A. Zambre, N. Chanda, T. Hoffman, J. Smith, Bombesin peptide conjugated gold nanocages internalize via clathrin mediated endocytosis, Bioconjug. Chem. 25 (2014) 1565–1579.
[34] E.J. Hall, A.J. Giaccia, Radiobiology for the Radiologist, Lippincott Williams & Wilkins, Philadelphia, 2006.
[35] E. Azorín-Vega, E. Rojas-Calderón, B. Martínez-Ventura, J. Ramos-Bernal, L. Serrano-Espinoza, N. Jiménez-Mancilla, D. Ordaz-Rosado, G. Ferro-Flores, Assessment of cell death mechanisms triggered by ^{177}Lu-anti-CD20 in lymphoma cells, Appl. Radiat. Isot. 138 (2018) 73–77.
[36] P. Decuzzi, M. Ferrari, The role of specific and non-specific interactions in receptor-mediated endocytosis of nanoparticles, Biomaterials 28 (18) (2007) 2915–2922.
[37] J.W. Bergs, M.G. Wacker, S. Hehlgans, A. Piiper, G. Multhoff, C. Roedel, F. Roedel, The role of recent nanotechnology in enhancing the efficacy of radiation therapy, Biochim. Biophys. Acta 1856 (1) (2015) 130–143.
[38] A. Escudero-Castellanos, B.E. Ocampo-García, G. Ferro-Flores, K. Isaac-Olivé, C.L. Santos-Cuevas, A. Olmos-Ortiz, J. García-Quiroz, R. García-Becerra, L. Díaz, Preparation and in vitro evaluation of ^{177}Lu-iPSMA-RGD as a new heterobivalent radiopharmaceutical, J. Radioanal. Nucl. Chem. 314 (3) (2017) 2201–2207.

7.2 **Gibbens-Bandala Brenda,** Morales-Avila Enrique, Ferro-Flores Guillermina, Santos-Cuevas Clara, Luna-Gutiérrez Myrna, Ramírez-Nava Gerardo, Ocampo-García Blanca. 2019. 177Lu-DOTA-DN(PTX)-BN for Selective and Concomitant Radio and Drug – Therapeutic Effect on Breast Cancer Cells. *Polymers*.
https://doi.org/10.3390/polym11101572

polymers

MDPI

Article

Synthesis and Evaluation of ^{177}Lu-DOTA-DN(PTX)-BN for Selective and Concomitant Radio and Drug—Therapeutic Effect on Breast Cancer Cells

Brenda Gibbens-Bandala [1,2], Enrique Morales-Avila [2], Guillermina Ferro-Flores [1], Clara Santos-Cuevas [1], Myrna Luna-Gutiérrez [1], Gerardo Ramírez-Nava [1,3] and Blanca Ocampo-García [1,*]

1 Departamento de Materiales Radiactivos, Instituto Nacional de Investigaciones Nucleares, Carretera México-Toluca S/N, Ocoyoacac, Estado de México 52750, Mexico; bren_gbb@hotmail.com (B.G.-B.); ferro_flores@yahoo.com.mx (G.F.-F.); clara_letici@yahoo.com.mx (C.S.-C.); myrna.luna@inin.gob.mx (M.L.-G.); gerjul5420@hotmail.com (G.R.-N.)

2 Facultad de Química, Universidad Autónoma del Estado de México, Paseo Tollocan S/N, Toluca, Estado de México 50180, Mexico; enrimorafm@yahoo.com.mx

3 Departamento de Bioprocesos, UPIBI-Instituto Politécnico Nacional, Ciudad de México 07340, Mexico

* Correspondence: blanca.ocampo@inin.gob.mx; Tel.: +52-55-5329-7200 (ext. 13871); Fax: +52-55-5329-7306

Received: 31 July 2019; Accepted: 7 September 2019; Published: 27 September 2019

Abstract: The peptide-receptor radionuclide therapy (PRRT) is a successful approach for selectively delivering radiation within tumor sites through specific recognition of radiolabeled peptides by overexpressed receptors on cancer cell surfaces. The efficacy of PRRT could be improved by using polymeric radio- and drug- therapy nanoparticles for a concomitant therapeutic effect on malignant cells. This research aimed to prepare and evaluate, a novel drug and radiation delivery nanosystem based on the ^{177}Lu-labeled polyamidoamine (PAMAM) dendrimer (DN) loaded with paclitaxel (PTX) and functionalized on the surface with the Lys^{1}Lys^3(DOTA)-bombesin (BN) peptide for specific targeting to gastrin-releasing peptide receptors (GRPr) overexpressed on breast cancer cells. DN was first conjugated covalently to BN and DOTA (chemical moiety for lutetium-177 complexing) and subsequently loaded with PTX. The characterization by microscopic and spectroscopic techniques, in-vitro drug delivery tests as well as in in-vitro and in-vivo cellular uptake of ^{177}Lu-DOTA-DN(PTX)-BN by T47D breast cancer cells (GRPr-positive), indicated the formation of an improved delivery nanosystem with target-specific recognition by GRPr. Results of the ^{177}Lu-DOTA-DN(PTX)-BN effect on T47D cell viability (1.3%, compared with 10.9% of ^{177}Lu-DOTA-DN-BN and 14.0% of DOTA-DN-(PTX)-BN) demonstrated the concomitant radiotherapeutic and chemotherapeutic properties of the polymeric nanosystem as a potential agent for the treatment of GRPr-positive tumors.

Keywords: polymeric nanosystems; dendrimers; radiotherapy; GRPr; paclitaxel; lutetium-177

1. Introduction

In cases of metastatic or inoperable malignant diseases, the peptide-receptor radionuclide therapy (PRRT) is a viable option for selective delivering of radiation in tumors through specific recognition of radiolabeled peptides by receptors overexpressed on cancer cell surfaces [1].

Beta emitting radionuclides, such as lutetium-177 ($T_{1/2}$ = 6.7 d, βmax emission of 497 keV, γ-emission of 113 and 208 keV), are widely used in PRRT due to their relatively long-range in tissues (12 mm), which allows a cross-fire effect with the surrounding cells into the tumor.

Gastrin-releasing peptide receptors (GRPr) are overexpressed in breast, prostate, gastric, colon, and pancreatic tumors [2]. Various GRP analogs (e.g., bombesin or bombesin-modified peptides) labeled with Ga-68, Y-90, In-111, and Lu-177 have demonstrated a high in-vitro and in-vivo affinity for GRPr [3–5].

Among various approaches, the use of polymeric nanoparticles in cancer treatment has gained significant importance. Various drug delivery and drug targeting systems such as synthetic polymers, microcapsules, liposomes, and dendrimers, are now either already approved for clinical use or under development. The nanoparticles designed as drug delivery systems can improve the bioavailability and selective accumulation of drugs at the pathological site, overcoming the challenges faced by potent anticancer medicines related to the systemic side effects and multi-drug resistance [6].

Dendrimers are hyperbranched polymers with the distinctive 3D molecular arrangement, well-defined structure, and homogeneous composition. The high level of control over dendrimers structure and their multifunctional properties makes them attractive for drug delivery applications as well as nano-radiopharmaceutical devices. The functional groups in the outermost part of the dendrimer allow attaching moieties that can actively target specific cell receptors. A promising property of dendrimers in cancer diagnosis and treatment is the multimeric nature, which would potentially produce multivalent effects [7–9].

Polyamidoamine (PAMAM) dendrimers are described as carriers for anticancer drugs and can be easily modified at the terminal groups by to improve their specific targeting to tumor cells [10]. Paclitaxel (PTX) is one of the best anticancer drugs and is active against a wide spectrum of cancers. However, the major limitation in the clinical use of paclitaxel is its low solubility in water and most pharmaceutical grade solvents.

The efficacy of PRRT could be improved by using a polymeric radio—and drug—therapy nanosystem for a concomitant therapeutic effect on malignant cells. In this context, the aim of this research was to prepare and evaluate a novel drug and radiation delivery nanosystem based on the ^{177}Lu-labeled PAMAM dendrimer (DN) loaded with PTX and functionalized on the surface with the Lys^{1}Lys^{3}(DOTA)-bombesin (BN) peptide for specific targeting to gastrin-releasing peptide receptors (GRPr) overexpressed on breast cancer cells.

2. Materials

PAMAM dendrimer (DN) (ethylenediamine core, generation 4.0 solution 10 wt% in methanol) and Paclitaxel (PTX) were supplied by Sigma-Aldrich Chemical Co. (St. Louis, Missouri, USA). Bifunctional chelating agent S-2-(4-isothiocyanatobenzyl)-1,4,7,10-tetraazacyclododecane acid (p-SCN-Bn-DOTA) (DOTA) was obtained from Macrocyclics (Dallas, TX, USA). Lys^{1}Lys^{3}(DOTA)-Bombesin (bombesin, BN) was provided by International Atomic Energy Agency (through CRP-F2264). Lutetium-177 (^{177}Lu) as $^{177}LuCl_3$, was supplied from ITG (Germany). Dimethylformamide (DMF), diisopropylethylamine (DIPEA), 2-(1H-7-azabenzotriazol-1-yl)-1.1.3.3-tetramethyluroniumhexafluorophosphate (HATU), and all other reagents were analytical grades. 2,3-bis-(2-methoxy-4-nitro-5-sulfophenyl)-2H-tetrazolium-5-carboxanilide) (XTT) was obtained from Roche Diagnostics (Indianapolis, IN. USA). The T47-D cell line was obtained from ATCC (Atlanta, GA, USA).

3. Methods

3.1. Synthesis of DOTA-DN and DOTA-DN-BN

DOTA-DN was prepared according to the procedure described by Mendoza-Nava [11]. Briefly, PAMAM dendrimer methanol free (0.2859 μmol) and DOTA (4.3605 μmol) were dissolved in bicarbonate buffer (0.2 M, pH 9.5) and incubated at 37 °C during 1 h. Then, the DOTA-DN was purified by repetitive aqueous-washing until complete elimination of bicarbonate buffer (Ultra centrifugal filters, MWCO 3000 Da, Millipore, 2500 g, 30 min). Finally, the product was lyophilized (Figure 1).

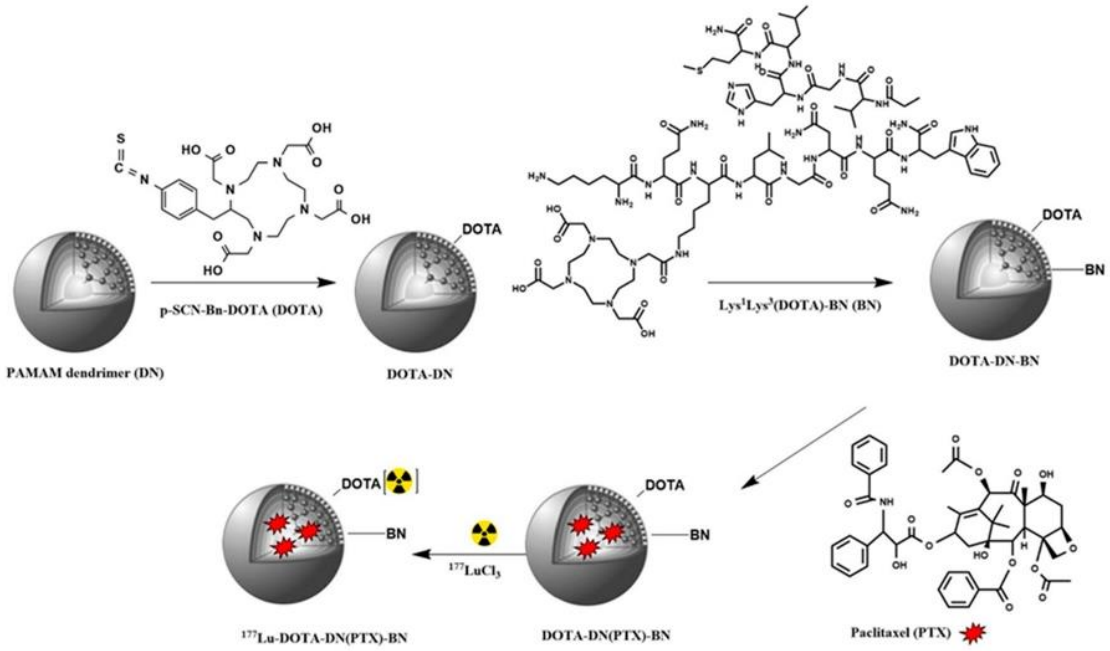

Figure 1. Schematic illustration of ^{177}Lu-DOTA-DN(PTX)-BN preparation.

In order to achieve carboxylate groups activation from Lys^{1}Lys^3(DOTA)-bombesin, the peptide (0.5 μmol) was incubated with HATU (HATU 1.3 μmol, DIPEA 19.1 μmol, and DMF as solvent) at room temperature for 15 min. The DOTA-DN (4.5 mg in bicarbonate buffer) was posteriorly added to the solution with active peptide. The mixture was then incubated during 1.5 h at room temperature. The obtained DOTA-DN-BN was purified and dried under vacuum. The Lys^{1}Lys^3(DOTA)-bombesin peptide was used as the biomolecule to reach the GRP receptor, where DOTA was used as the linker to form amide bounds with dendrimer. Since the carboxylate groups were activated and bound to primary amine, there are not enough chemical groups available to chelate Lu-177 in a stable coordination sphere at neutral pH.

For the preparation of Paclitaxel-loaded DN, a fraction of aqueous solution containing 5 mg of DOTA-DN-BN was mixed with Paclitaxel (1 mg, 1.17 μmol in methanol). The final mixture was stirred for 24 h at room temperature. The obtained PTX-loaded dendrimers were purified by ultracentrifugation and the pellet dried under vacuum to remove any non-incorporated PTX.

3.2. Radiolabeling of Dendrimeric Systems

Conjugated dendrimers were radiolabeled through bifunctional chelator DOTA with ^{177}Lu. Radiolabeling was carried out by adding a $^{177}LuCl_3$ solution (18.5 MBq in 10 μL) to DOTA-DN, DOTA-DN-BN and DOTA-DN(PTX)-BN (500 μL of 1 mg/mL in 1M acetate buffer, pH 5.0) and incubating each solution at 37 °C for 1 h.

Radiochemical purity analyses were performed by ultracentrifugation and instant thin-layer chromatography on silica gel (ITLC-SG, Gelman Sciences), using NaCl 0.9%/HCl 0.02% as mobile phase.

3.3. Physicochemical Characterization

3.3.1. Transmission Electron Microscopy (TEM)

Dendrimers were analyzed by TEM in JEOL JEM 2010 HT microscope operating at 200 kV to observe the two-dimensional, relative size, distribution, and morphology. A drop of the aqueous product was evaporated for analysis on a carbon-coated TEM copper grid. Approximately 1000 nanoparticles from 11 TEM micrographs were analyzed.

3.3.2. Fourier Transform Infrared Spectroscopy (FT-IR)

The FT-IR measurements were performed in transmission mode using a Perkin Elmer System 2000 spectrometer with the attenuated total reflection platform (Pike Technologies; Madison, WI, USA). The spectra were all acquired from 50 scans at a 0.4 cm^{-1} from 400 to 4000 cm^{-1}.

3.3.3. Entrapment Efficiency

Paclitaxel analysis was carried out by HPLC (μBondapak® C18 10 μm 125A°, 3.9 × 150 mm Column as stationary phase, and acetonitrile: water (60:40 *v/v*) as the mobile phase, flow rate of 1 mL/min, run time of 5 min). PTX was measured at 227 nm on a Waters Empower system using a PTX calibration curve (R^2 0.997, 6.0–300.0 μg/mL). The experiments were conducted in triplicate.

The amount of encapsulated paclitaxel was indirectly measured by subtracting the amount of non-encapsulated paclitaxel in the waste solution obtained from the amount of paclitaxel used to prepare the dendrimers. The encapsulation efficiency (*EE*%) was calculated as:

$$EE\ (\%) = \frac{Weight\ of\ PTX\ loaded}{Weight\ of\ PTX\ input} \times 100 \quad (1)$$

3.3.4. Conjugation Efficiency of DOTA and Bombesin

Conjugation efficiency was determined by measuring free DOTA or free Bombesin in the respective filtered solution via reverse-phase HPLC on a Waters Empower system using a C18 column (μBondapak® C18 10 μm 125A°, 3.9 × 300 mm Column) as a stationary phase and a gradient of water/acetonitrile containing 0.1% TFA from 95/5 (*v/v*) to 20/80 (*v/v*) as mobile phase (flow rate of 1 mL/min and time run 30 min). Bombesin standard curve (R^2 0.999, 0.07–2.2 mg/mL) was used in this analysis.

3.3.5. In Vitro PTX Release

For the in vitro drug release studies, a solution of phosphate-buffered saline (PBS, pH 7.4 or 5.3) containing 0.05% Tween-20 was used. Briefly, 10mg of DOTA-DN(PTX)-BN was dispersed in 1mL of release medium and placed in a dialysis membrane (MWCO 30,000 Da). The dialysis bag was closed and immersed into a flask containing PBS (10 mL) at 37 °C and continuously stirring at 110 rpm. At specific time intervals, an aliquot of release medium was collected, and replaced with fresh PBS. Released paclitaxel amount was measured by HPLC based on the previously described methodology.

3.3.6. Radiolabeling Stability

For the stability evaluation of the system in serum, ^{177}Lu-DOTA-DN(PTX)-BN and fresh human serum (dilution 1:10) were incubated at 37 °C. At given time points, an aliquot was taken and analyzed by radio-HPLC using a size-exclusion HPLC column (ProteinPak 300SW Waters; Milford, MA, USA) as stationary phase and 0.01M PBS as mobile phase (1 mL/min flow rate, and time run 30 min).

3.4. In Vitro Studies

3.4.1. Cell Line

T47D Breast Epithelial Ductal Carcinoma cells positive to GRPr were grown at 37 °C in an atmosphere of 5% CO_2 and 85% humidity in RPMI-1640 medium supplemented with 10% newborn calf serum and antibiotics (100 μg/mL streptomycin, 100 U/mL penicillin).

3.4.2. Cellular Uptake

For the measurement of the nanoradiopharmaceutical fraction on the cell membrane and the internalized fraction to the cytoplasm, T47D cells were harvested to be seeded in 24-well tissue culture

plates (1×10^5 cell/well, 0.5 mL) to allow adherence. After 24 h, the RPMI medium was removed, and the cells were incubated with 118 kBq (per well) of the following treatment: (^{177}Lu-DOTA-DN, ^{177}Lu-DOTA-DN-BN and ^{177}Lu-DOTA-DN(PTX)-BN) for 1 h at 37 °C. Then, each well was rinsed with PBS (2×) to eliminate the treatment. The plate was then incubated twice with 500 µL of glycine buffer (50 mM, pH 2.8) by 5 min at room temperature to obtain the fraction of cell uptake (radioactivity in the membrane). The cells were washed and incubated 5 min at room temperature with 500 µL of 1 M NaOH to evaluate the nanosystem internalization. Radioactivity was measured in a crystal scintillation well-type detector (Auto In-v-Tron 4010, NML Inc., Milwaukee, WI, USA). The uptake percentage was then calculated, considering the initial activity of each treatment as 100%. Non-specific binding was determined in parallel, in the presence of 175 nmol of Bombesin (500 times higher than the added concentration of treatments) to partially block the GRPr present in T47D cells. Additionaly, the saturation assay was performed as previously reported [12].

3.4.3. Cytotoxic Effect on T47D Cells

T47D cells were seeded in 96-well microtiter plate (1×10^4 cells/well) and incubated 24 h to allow adherence. The viability after exposure to 0.45 MBq of ^{177}Lu-DOTA-DN-BN, ^{177}Lu-DOTA-DN(PTX)-BN and $^{177}LuCl_3$ or 4µg of free PTX, DOTA-DN(PTX)-BN (in terms of paclitaxel amount) or equimolar concentration of DOTA-DN-BN, was evaluated at different time points (7 days, 37 °C, 5%°O_2 and 85% humidity). The cytotoxic activity was measured using a Cell Proliferation Assay (XTT) kit, according to the manufacturer's protocol (Roche Diagnostics GmbH, Mannheim, Germany).

3.4.4. Radiation-Absorbed Doses to the T47D Cell Nucleus

For estimation of the radiation-absorbed doses to the T47D cell nucleus, the following equation was used:

$$D_{N \leftarrow Source} = (N_M \times DF_{N \leftarrow M}) + (N_C \times DF_{N \leftarrow C}) \quad (2)$$

where $D_{N \leftarrow Source}$ represents the mean absorbed dose to the nucleus from source regions (membrane-M- and cytoplasm-C-) and N_M and N_C are the total number of nuclear disintegrations that occurred in the membrane and cytoplasm, respectively. $DF_{N \leftarrow M}$ and $DF_{N \leftarrow C}$ denote the dose factors specific for ^{177}Lu, from membrane and cytoplasm regions to the nucleus configuration. The dose factor geometries were obtained from the S values reported by Goddu and Budinger (cell radius = 10 µm, nucleus radius = 5 µm) [13].

3.4.5. In-Vitro Cell Treatment

The required radioactivity of ^{177}Lu-DOTA-DN(PTX)-BN to produce approximately the standard breast post-surgical radiotherapy (50 Gy) [14], was calculated by using the experimental biokinetic model fitted in Section 3.4.4. Half of this concentration was also prepared to evaluate the response related to PTX alone or ^{177}Lu/PTX. Therefore, 32.2 Bq and 16.1 Bq per cell was deposited on a 96-well plate containing 10,000 T47D cells per well. The identical unlabelled concentration of DOTA-DN(PTX)-BN was also evaluated at each level ($n = 6$).

3.5. In Vivo Studies

In vivo studies in mice were carried out according to the Official Mexican Norm 062-ZOO-1999. Athymic mice, 6–7 weeks old and 18–20 g weight, were kept in sterile cages with sterile wood-shaving beds, constant temperature, humidity, and 12:12 light: dark periods.

Tumor Induction. Animals ($n = 4$) received a subcutaneous inoculation (upper backsubcutaneous tumor model-) of 1×10^6 T47D cancer cells suspended in 0.1 mL of phosphate-buffered saline. 2.5 weeks after inoculation the animals were used for in vivo studies. One mouse was randomly selected for micro-SPECT/CT imaging, and a group of three mice was used to perform biodistribution studies.

3.5.1. SPECT-CT Imaging

To verify the in vivo ^{177}Lu-DOTA-DN(PTX)-BN retention in T47D induced tumors, micro-SPECT/CT images were acquired (Albira, ONCOVISION; Gem Imaging S.A., Valencia, Spain) 1.5 h, 9 h, 10 h, 24 h, 120 h after intratumoral administration of 9.25 MBq of the nanoradiopharmaceutical. The mouse, under 2% isoflurane anesthesia, was placed in the prone position and imaging was performed. The micro-SPECT field of view was 60 mm; a symmetric 20% window was set at 208 keV, and pinhole collimators were used to acquire a three-dimensional SPECT image with a total of 64 projections of 30 s each over 360°. The image was reconstructed using the ordered-subset expectation-maximization algorithm with the standard mode parameter, as provided by the manufacturer. CT parameters were 35 kV positive voltage, 700 μA current, and 600 micro-CT projections.

3.5.2. Biodistribution

The subcutaneous tumor model animals (n = 3) received 9.25 MBq of the radiolabeled system (^{177}Lu-DOTA-DN(PTX)-BN). After 120 h post-injection, the mice were euthanized, and the blood and main organs were removed. The radioactivity accumulated in organs was measured in a calibrated Na(Tl) detector and expressed as %ID/g (percentage of the injected dose per gram of tissue) or %ID/organ (percentage of the injected dose per organ).

4. Results and Discussion

PAMAM dendrimers have extensively been reported as drug delivery systems for carrying therapeutic and diagnostic agents, but their capacity for concomitant applications of chemotherapy (Paclitaxel) and radiotherapy (^{177}Lu) in a target-specific multifunctional platform has not been reported.

PAMAM dendrimer generation 4.0 contains 64 terminal amine groups available for firstly grafting with p-SCN-Bn-DOTA, via the irreversible formation of thiourea derivative. Bombesin conjugation was attained via one carboxyl lateral arm from the DOTA macrocycle, which was linked to the PAMAM amine group. The calculated DN:DOTA and DN:Bombesin molar ratio was 1:15 and 1:3, respectively.

A variety of delivery systems of PTX have been reported, including entrapment of the molecule [15–17], or conjugation to the surface [18–20]. In this research, the dendrimeric system allowed 97.72 ± 0.26% of PTX encapsulation.

As shown in Figure 2, microscopic transmission electron analysis (TEM) revealed well-defined dendritic structures (Figure 2b). The mean particle size of DOTA-DN was 13.05 nm, 16.01 nm for DOTA-DN-BN, and 16.37 nm in the case of DOTA-DN(PTX)-BN. The BN grafting, influenced on increasing the particle size ($p < 0.05$). Also, the population width distribution increased with bombesin and paclitaxel incorporation.

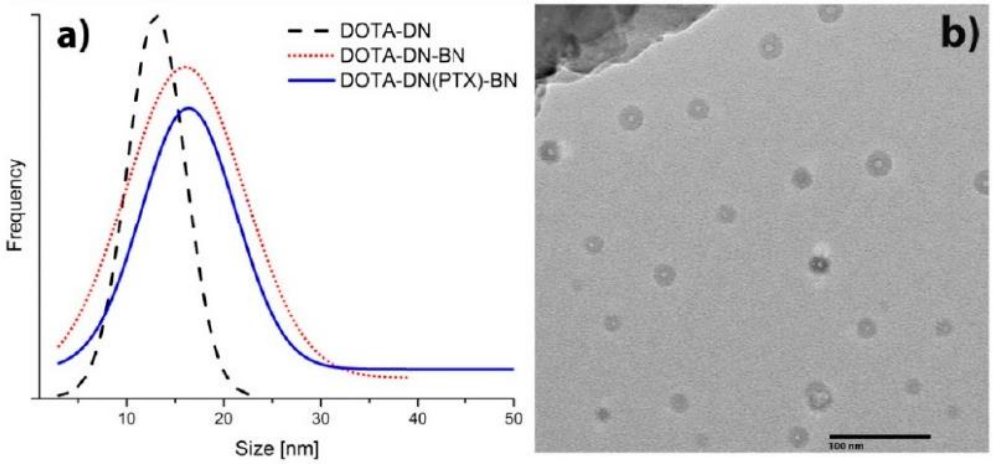

Figure 2. (**a**) Size distribution of the different nanosystems (**b**) TEM of DOTA-DN(PTX)-BN.

4.1. Infra-Red Spectroscopy

FT-IR analysis of the DOTA-DN(PTX)-BN dendrimeric system showed some characteristic bands of its components (Dendrimer, DOTA, bombesin, and paclitaxel) which changed in intensity and position because of the conjugation reactions.

The IR-spectrum of pure PAMAM G4.0 (Figure 3a) showed bands at 3261 cm^{-1} and 3074 cm^{-1} attributed to N-H stretch vibrations of amine groups. The bands at 2935 cm^{-1} and 2831 cm^{-1} correspond to aliphatic C-H stretches. The amide carbonyl absorption (HNC = O) from the PAMAM dendrimer was observed at 1630 cm^{-1}, while at 1543 cm^{-1}, the amide N-C stretching was identified [21–24].

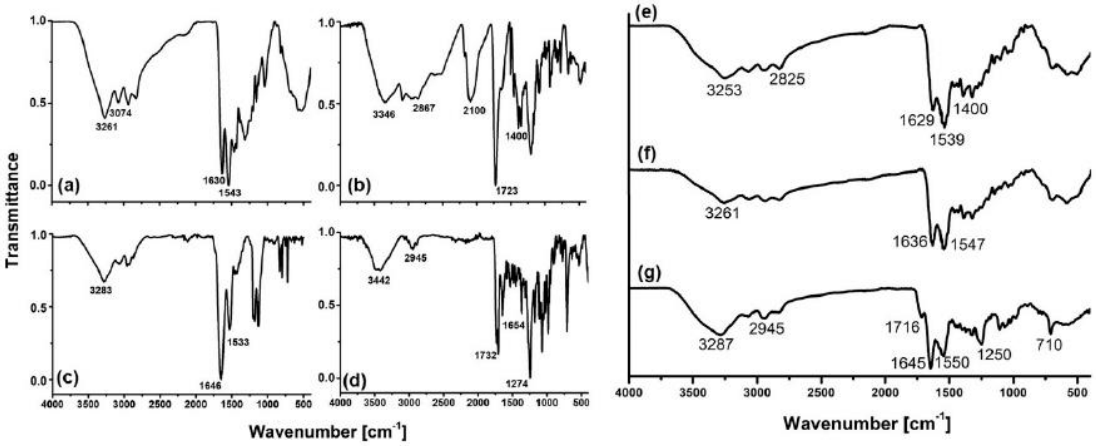

Figure 3. The FT-IR spectrum of (**a**) PAMAM Dendrimer (DN), (**b**) pSCN-Bn-DOTA (DOTA), (**c**) Lys^1Lys^3(DOTA)-BN (BN), (**d**) Paclitaxel (PTX), (**e**) DOTA-DN, (**f**) DOTA-DN-BN, (**g**) DOTA-DN(PTX)-BN.

The p-SCN-Bn-DOTA IR-spectrum (Figure 3b) showed a well-defined band at 2100 cm^{-1}, which was assigned to the isothiocyanate motif vibration. At 2960–2867 cm^{-1} and 1400 cm^{-1} appear vibrations attributed to the C-H stretch, and at 3346 cm^{-1} the presence of amine groups were identified. At 1723 cm^{-1} the C=O stretch and at 1500 cm^{-1} the aromatic C-C stretch were also observed.

After p-SCN-DOTA conjugation to dendrimer, the DOTA-DN (Figure 3e) showed a shift compared to the main dendrimer bands in the region at 3000–2900cm^{-1}. New bands in the amide I and amide II region were observed. The isothiocyanate region from the bifunctional agent was absent, which suggested a conformational and dipole change when conjugation was carried out. Amide formation involves the use of carboxylic groups, which was not observed after conjugation. The new band at 1400 cm^{-1} region indicated the presence of DOTA in the dendrimer structure.

The IR-spectrum of pure BN (Lys^1Lys^3(DOTA)BN) (Figure 3c) showed bands at 3283 cm^{-1}, 1646 cm^{-1} and 1533 cm^{-1} assigned to $(–NH)_\upsilon$, $(C=O)_\upsilon$ (Amide I) and (–CN) (amide II) respectively, as previously reported [25].

After grafting DOTA-DN with Bombesin peptide, the infrared spectrum showed essential changes. The new product DOTA-DN-BN (Figure 3f) show significant shifts in the amine and amide region, but no new bands were observed.

The IR analysis of PTX (Figure 3d) was consistent with the previously reported [26]. Briefly, spectrum showed $(–NH)_\upsilon$ vibrations characterized by a broad and asymmetric band centered at 3442 cm^{-1}, the band found at 2945 cm^{-1} was assigned to (–C-H) from asymmetric and symmetric stretching vibrations. Amide I region mainly associated with $(C=O)_\upsilon$ vibration was identified at 1732 cm^{-1} whereas $(C-N)_\upsilon$ was found at 1274 cm^{-1}. Aromatic hydrocarbons were identified by characteristic absorption bands in the region near to 1645 and 1500–1400 cm^{-1} produced by carbon-carbon stretching vibrations in the aromatic ring. The bands at 1250–1000 cm^{-1} region were assigned to (C–H) in-plane bending, and finally, $(C–H)_\upsilon$ above 3000 cm^{-1} were also identified.

After PTX interaction (Figure 3g), the infrared spectrum showed bands of PTX at 1716 cm^{-1} and 710 cm^{-1} from amide I, additionally, an increase of intensity was observed in the well-defined bands at 1645 cm^{-1} and 1400 cm^{-1} from Ar(C-C) and 1250 cm^{-1} due to the contribution of amine groups. A significant increase on band intensity and change on band shape near to 3650–3150 cm^{-1} region respect to DOTA-DN-BN were identified, suggesting an increase on H-bond formation associated to the interaction of O-H and N-H groups as proton donor groups from PTX, BN, and DN.

4.2. In Vitro Paclitaxel Release

For evaluation of the controlled release capacity of paclitaxel from DOTA-DN(PTX)-BN, accumulative (%) drug release was determined in different analysis conditions.

The release profile of PTX was prolonged. The PTX desorption was dependent on pH and resulted to be higher under acidic conditions than under neutral conditions (Figure 4, Hill Model) through disturbance and disruption of hydrogen bonding. Hence, the observed release rate of DOTA-DN(PTX)-BN at pH 5.3 is favorable for cancer therapy. Additionally, it would be expected that acidic intra-cellular conditions (intracellular lysosomal environment) improve the PTX release with the consequent increase of local drug concentration.

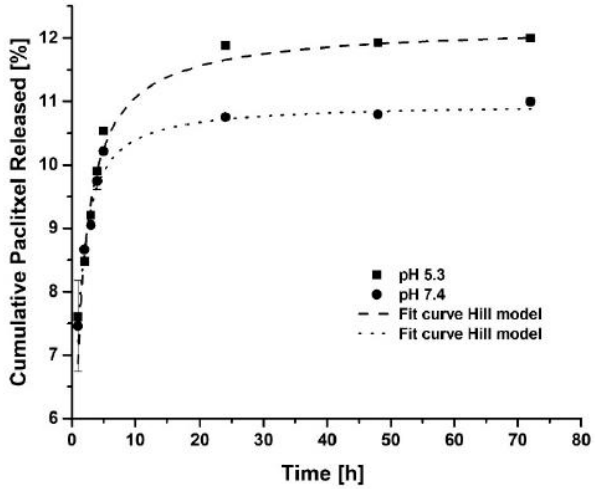

Figure 4. In vitro release profile of Paclitaxel from DOTA-DN(PTX)-BN system at pH 5.3 and 7.4 (mean ± SD, $n = 3$).

The relatively slow PTX-releasing rate observed in vitro could be enhanced by the in vivo high oncotic pressure in tumors, since previous reports have demonstrated that the PTX release from dendrimeric systems gradually speeds up with the osmotic pressure [27].

4.3. Serum Stability

^{177}Lu-DOTA-DN(PTX)-BN demonstrates high stability in human serum. After 0.5, 1 and 24 h of incubation <10% of the radiopharmaceutical was bound to plasma proteins. These results suggest that ^{177}Lu-DOTA-DN(PTX)-BN was not significantly catabolized in serum, and therefore has suitable metabolic stability.

4.4. In Vitro Studies

4.4.1. Cell Uptake

In order to demonstrate the specific uptake of nanoradiopharmaceuticals via Bombesin-GRPr recognition, uptake and internalization assays in T47D cells (GRPr-positive) were carried out (Figure 5). The ANOVA (1 way) for multiple comparisons showed a statistical significant difference between

^{177}Lu-DOTA-DN(PTX)-BN and ^{177}Lu-DOTA-DN ($p < 0.05$) (cell uptake of 6.67% vs 5.31%, respectively), which confirmed the active uptake mechanism through the interaction Bombesin-GRPr. There was no significant difference between nanosystems containing the molecular recognition molecule (^{177}Lu-DOTA-DN-BN, 6.67% and ^{177}Lu-DOTA-DN(PTX)-BN, 6.70%).

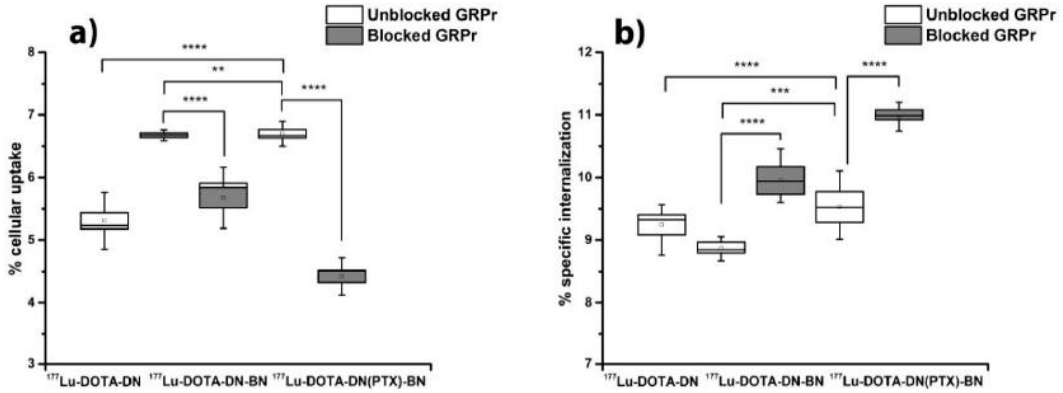

Figure 5. Uptake (**a**) and internalization (**b**) of ^{177}Lu-DOTA-DN, ^{177}Lu-DOTA-DN-BN, and ^{177}Lu-DOTA-DN(PTX)-BN in T47D cells (vacuum boxes). Cells with blocked receptors were pre-incubated with excess (500 times) of Bombesin peptide (full boxes) to determine specific uptake. Whisker represents SD ($n = 6$).

Figure 5b shows the internalization of each radiolabelled treatment to the cytoplasm. This process was favored with the pre-incubation with BN and attributed to cationic surface charge conferred by BN, which promotes interaction of the nanoparticles with the membrane and therefore, increases the rate and extent of internalization [28].

When GRPr were previously blocked with a BN concentration 500 higher than the BN present at nanosystems, the uptake decreased one-fold and two-fold for ^{177}Lu-DOTA-DN-BN and ^{177}Lu-DOTA-DN(PTX)-BN, respectively. This result suggests that the process of specific binding between Bombesin and GRPr is taking place through an endocytic pathway in high rate for ^{177}Lu-DOTA-DN(PTX)-BN rather than the non-targeted nanosystem, which could be favored by the high molecular weight conferred by PTX inside the cavities. This specific coupling provided a significant uptake and internalization (internalization of 8.86% in ^{177}Lu-DOTA-DN-BN and 9.53% in ^{177}Lu-DOTA-DN(PTX)-BN). However, it was evident that passive uptake was carried out by a surface phenomenon between nanoparticles and the cell surface. The ^{177}Lu-DOTA-DN(PTX)-BN concentration needed to achieve the half-maximum binding at equilibrium (Kd) resulted in 32.49 ± 9.01 nM.

4.4.2. Cell Viability

The surface coating has been reported to determine the cytotoxicity/biocompatibility for many nanoparticles. Particularly for PAMAM dendrimers, toxicity is mainly attributed to surface amine groups, but also dependent upon molecular weight, the number of surface amine groups, and generation of PAMAM dendrimers. Several studies have reported that after surface modification, the toxicity of PAMAM dendrimers can be reduced [29].

As shown in Figure 6, the dendrimer surface modification with DOTA and Bombesin, allowed the preparation of a non-toxic system DOTA-DN-BN (97.14 ± 10.12% of viability), mainly attributed to the surface end groups [7].

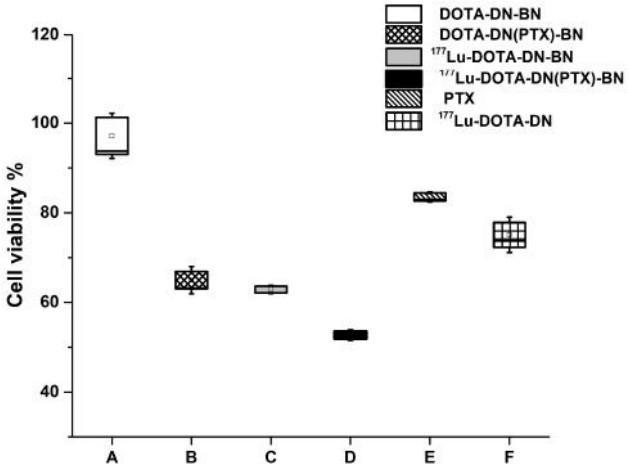

Figure 6. Cell viability after seven days of treatment with DOTA-DN-BN (**A**), DOTA-DN(PTX)-BN (**B**), ^{177}Lu-DOTA-DN-BN (**C**), ^{177}Lu-DOTA-DN(PTX)-BN (**D**), Paclitaxel (**E**), ^{177}Lu-DOTA-DN (**F**).

Reduction on cell viability was inherent to the presence of PTX or ^{177}Lu. The effect of combining ^{177}Lu with PTX was the highest on reducing viability on T47D cells treated with ^{177}Lu-DOTA-DN(PTX)-BN (Figure 6). At seven days post-treatment, viability percentage was only 54.15 ± 3.05% for ^{177}Lu-DOTA-DN(PTX)-BN, which was significantly different ($p < 0.05$) when compared with the unlabeled system DOTA-DN(PTX)-BN (64.58 ± 6.32%), or free-PTX system ^{177}Lu-DOTA-DN-BN (59.03 ± 5.48%).

As expected, there was no statistical significance between the cell uptake of DOTA-DN(PTX)-BN when compared with ^{177}Lu-DOTA-DN-BN ($p > 0.05$). This therefore implies that the produced cytotoxic effect caused by ^{177}Lu and PTX was at the same level.

The in vitro therapeutic efficacy studies confirmed that ^{177}Lu-DOTA-DN-(PTX)-BN nanosystem nanoparticles are more effective than a non-radiolabeled nanoparticle. The synergistic effect of chemotherapy and radiotherapy produced by the ^{177}Lu-DOTA-DN-(PTX)-BN nanosystem was observed when doses of PTX = 26.79 μM and radiation-absorbed doses of 122 Gy (delivered by 32.19 Bq/cell) were used (Table 1). As can be observed in Figure 7, the cytotoxic effect for the radiolabeled nanosystem was observed between 24 h and 48 h (highest slope). The effect was statistically significant after 48, 96, and 120 h. At 120 h of treatment, the total delivered radiation dose was 122 Gy, and the concentration of PTX was 26.79 μM.

Table 1. Biokinetic model and radiation absorbed doses produced by Bq/cell of ^{177}Lu-DOTA-DN-(PTX)-BN to the T47D cancer cell nuclei within 168 h.

^{177}Lu-DOTA-DN-(PTX)-BN Cellular Location	Biokinetic Model A(t)	$N = \int_{t=0}^{t=168h} A(t)dt$	Dose (Gy/Bq)	Total Dose to Cell Nuclei (Gy/Bq)
Membrane	$A(t) = 6.190e^{-0.014t} + 0.243e^{-0.008t} + 0.049e^{-0.008t}$	15012	1.12	4.23
Cytoplasm	$A(t) = 8.580e^{-0.014t} + 0.345e^{-0.008t}$	20700	3.11	

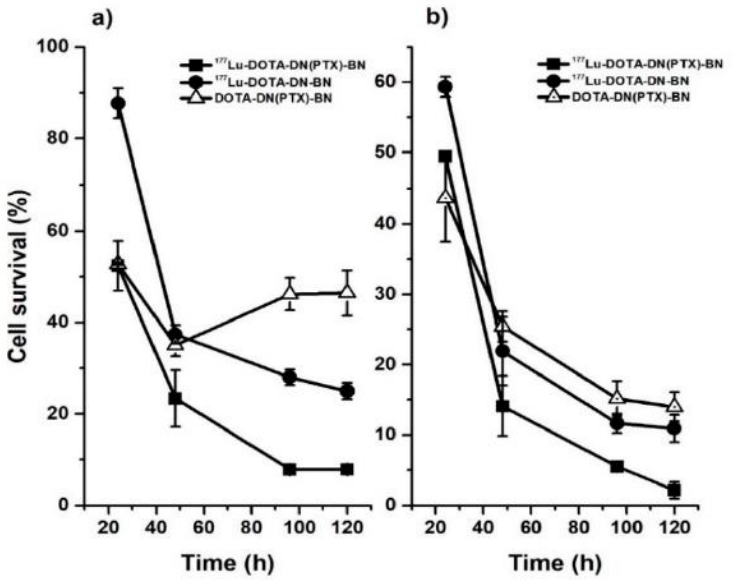

Figure 7. In vitro therapeutic efficacy of ^{177}Lu-DOTA-DN-(PTX)-BN on T47D cell line, (**a**) cell survival fraction resulted from 16.1 MBq per cell and the equimolar concentration of the unlabeled nanosystem, (**b**) cell survival fraction resulted from 32.2 MBq per cell and the equimolar level of the unlabeled nanosystem.

Nanosystems containing and delivering both, chemo—and radiotherapy are more effective than nanoparticles containing only PTX. When T47D breast cells were treated with the targeted nanosystem providing only PTX (DOTA-DN-(PTX)-BN) at 13.40 μM, the cell viability increased after 48 h (Figure 7a). This behavior was attributed to the DNA repair rate. The concentration of delivered PTX was unsuccessful in producing disrupting of microtubules. After 120 h of treatment with DOTA-DN-(PTX)-BN, the cell viability was 14.00 ± 2.06%. The viability of cells treated with ^{177}Lu-DOTA-DN-BN was 10.93 ± 1.17%, and the treatment of cells with ^{177}Lu-DOTA-DN-(PTX)-BN resulted in the lowest viability of 1.32 ± 0.71%. These results demonstrated that the combination of PTX and Lu-177 in the same nanoprobe was more effective than PTX or Lu-177 alone.

4.4.3. In Vivo Studies

The ^{177}Lu-DOTA-DN-(PTX)-BN nanosystem showed high retention in the tumor volume. No significant leakage was observed after 120 h associated with the specific receptor binding [11], which suggest that this nano-approach has a strong potential to be used for the treatment of solid tumor over-expressing GRPr. (Ethical Approval number: NOM-062-ZOO-1999 and approval date: 7 March 2018 for animal experiments).

Figure 8 shows micro-SPECT images of a mouse with a T47D subcutaneous tumor model. The tumor-to-blood ratio reveals suitable contrast, with a significant accumulation of ^{177}Lu-DOTA-DN(PTX)-BN in tumor tissue after (a) 1.5 h, (b) 9 h, (c) 10 h, (d) 24 h, and (e) 120 h. The ^{177}Lu-DOTA-DN(PTX)-BN nanosystem remains into the tumor delivering both, targeted radiotherapy and PTX-chemotherapy.

The measured volume of the tumor at the beginning of the imaging studies (1.5 h) was 0.32 cm^3. The biokinetic model based on the standard uptake value obtained at each time point, was adjusted to a function in OLINDA/EXM. The estimated absorbed radiation dose was 3.01 Gy/MBq at infinite time (Table 2). Therefore, to produce a tumoral radiation absorbed dose of 50 Gy in the murine model (which is usually applied in radiotherapy treatments to breast cancer patients), 16.61 MBq should be administered.

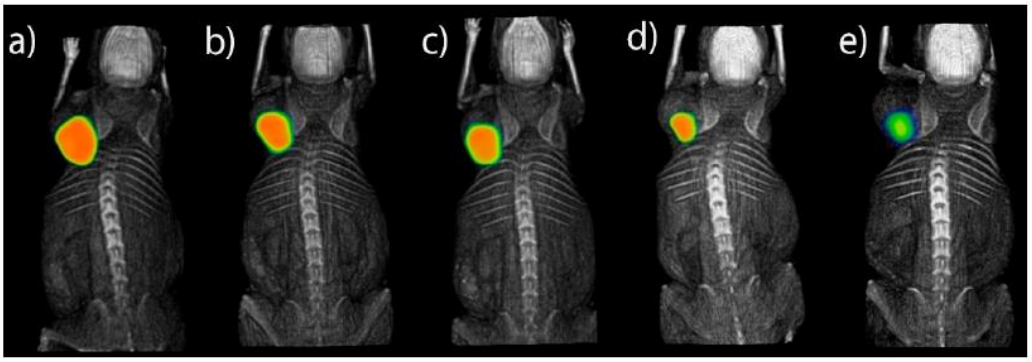

Figure 8. Subcutaneous tumoral model. Intratumoral administration of ^{177}Lu-DOTA-DN(PTX)-BN after (**a**) 1.5 h, (**b**) 9 h, (**c**) 10 h, (**d**) 24 h, (**e**) 120 h.

Table 2. Biokinetic model and radiation absorbed dose produced by MBq of ^{177}Lu-BN-PLGA(PTX) to the T47D tumor (intratumoral administration).

Biokinetic Model A(t)	$N = \int_{t=0}^{t=\infty} A(t)dt$	Dose (Gy/MBq)
$A(t) = 7.70e^{-0.418t} + 8.65e^{-0.008t} + 0.57e^{-0.004t}$	11.73	3.01

The radiopharmaceutical was cleared from the tumor with three components: 7.7% of the total dose (total activity of the administered radiopharmaceutical) was removed quickly with an effective half-life (*Te*) of 1.65 h, 8.6% with a *Te* of 86 h and 0.57% with prolonged *Te* of 173 h (Table 2).

The ^{177}Lu-DOTA-DN(PTX)-BN remained into the tumor delivering both, targeted radiotherapy and PTX-chemotherapy. The final tumor size was reduced 15.6% and the volume at 120 h was 0.27 cm^3.

Nano-radiopharmaceuticals have to be injected intratumorally or peritumorally due to the nanoparticles nature since they accumulate significantly in the reticuloendothelial system when the intravenous administration is used. The biodistribution of ^{177}Lu-DOTA-DN(PTX)-BN after 120 h (Figure 9) demonstrated that 36.25% of the radioactivity remained into the tumor, with only a 3.93% in the pancreas and 1.53% in kidney, which are organs widely reported to express GRPr [30].

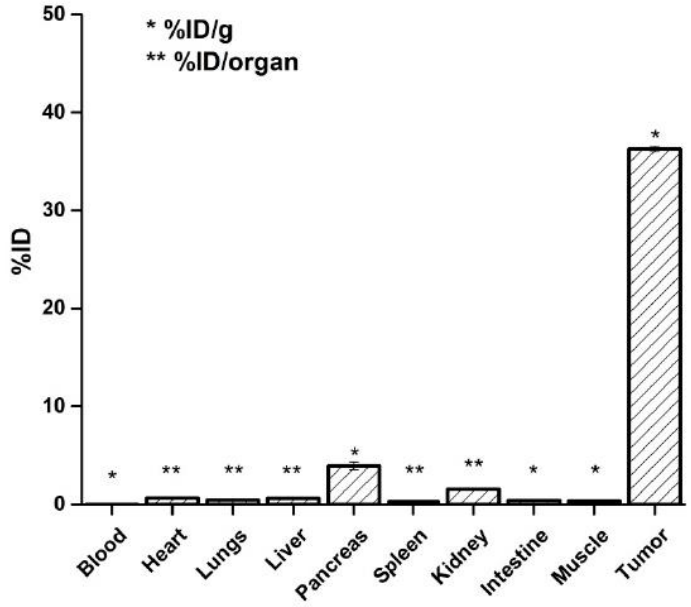

Figure 9. Biodistribution of ^{177}Lu-DOTA-DN(PTX)-BN 72h post intratumoral administration.

5. Conclusions

In this research, targeted polymeric nanoparticles designed to produce a simultaneous effect of radiotherapy and chemotherapy were successfully prepared. The ^{177}Lu-DOTA-DN(PTX)-BN nanoparticles exhibited high affinity towards GRP receptors, which enabled them to selectively and concomitantly deliver ^{177}Lu as the radiotherapeutic agent and PTX as the chemotherapeutic component. ^{177}Lu-DOTA-DN(PTX)-BN showed suitable characteristics for combined targeted therapy applications in GRPr-positive tumors.

Author Contributions: B.G.B., B.O.G. and G.F.F. conceived and designed the experiments; B.G.B., B.O.G., E.M.A., and M.L.G. performed the experiments and analyzed results; C.S.C. and G.R.N. acquired the micro-SPECT images, biokinetic models and dosimetry; and B.G.B., B.O.G., and G.F.F wrote the paper.

Funding: This study was supported by the grant CONACyT-CB-A1S38087 and the International Atomic Energy Agency (CRP-F2264). It was performed as part of the activities of the "Laboratorio Nacional de Investigación y Desarrollo de Radiofármacos, CONACyT".

Conflicts of Interest: The authors declare no conflict of interest.

References

1. Ferro-Flores, G.; Arteaga de Murphy, C.; Melendez-Alafort, L. Third Generation Radiopharmaceuticals for Imaging and Targeted Therapy. *Curr. Pharm. Anal.* **2006**, *2*, 339–352. [CrossRef]
2. de Ferreira, C.A.; Fuscaldi, L.L.; Townsend, D.M.; Rubello, D.; de Barros, A.L.B. Radiolabeled bombesin derivatives for preclinical oncological imaging. *Biomed. Pharmacother.* **2017**, *87*, 58–72. [CrossRef] [PubMed]
3. Brabander, T.; Teunisse, J.; Van Eijck, C.; Franssen, G.J.; Feelders, R.A.; de Herder, W.W.; Kwekkeboom, D.J. Peptide Receptor Radionuclide Therapy for Neuroendocrine Tumors. *Best Pract. Res. Clin. Endocrinol. Metab.* **2016**, *30*, 103–114. [CrossRef] [PubMed]
4. Baratto, L.; Jadvar, H.; Iagaru, A. Prostate Cancer Theranostics Targeting Gastrin-Releasing Peptide Receptors. *Mol. Imaging Biol.* **2018**, *20*, 501–509. [CrossRef] [PubMed]
5. Cornelio, D.B.; Roesler, R.; Schwartsmann, G. Gastrin-releasing peptide receptor as a molecular target in experimental anticancer therapy. *Ann. Oncol.* **2007**, *18*, 1457–1466. [CrossRef] [PubMed]
6. Jaimes-Aguirre, L.; Gibbens-Bandala, B.V.; Morales-Avila, E.; Ocampo-García, B.E.; Seyedeh-Fatemeh, M.; Amirhosein, A. Polymer-Based Drug Delivery Systems, Development and Pre-Clinical Status. *Curr. Pharm. Des.* **2016**, *22*, 2886–2903. [CrossRef] [PubMed]
7. Palmerston Mendes, L.; Pan, J.; Torchilin, V.P. Dendrimers as nanocarriers for nucleic acid and drug delivery in cancer therapy. *Molecules* **2017**, *22*, 1401. [CrossRef] [PubMed]
8. Cai, X.; Hu, J.; Xiao, J.; Cheng, Y. Dendrimer and cancer: A patent review (2006–present). *Expert Opin. Ther. Pat.* **2013**, *23*, 515–529. [CrossRef]
9. Madaan, K.; Kumar, S.; Poonia, N.; Lather, V.; Pandita, D. Dendrimers in drug delivery and targeting: Drug-dendrimer interactions and toxicity issues. *J. Pharm. Bioallied Sci.* **2014**, *6*, 139–150. [CrossRef]
10. Zhang, W.W.; Wang, Y.C.; Kan, X.M.; Wang, X.M.; Geng, D.M. Preparation and evaluation of peptide-dendrimer-paclitaxel conjugates for treatment of heterogeneous stage 1 non-small cell lung cancer in 293T and L132 cell lines. *Trop. J. Pharm. Res.* **2017**, *16*, 737–742. [CrossRef]
11. Mendoza-Nava, H.; Ferro-Flores, G.; Ramírez, F.D.; Ocampo-García, B.; Santos-Cuevas, C.; Aranda-Lara, L.; Azorín-Vega, E.; Morales-Avila, E.; Isaac-Olivé, K. 177 Lu-Dendrimer Conjugated to Folate and Bombesin with Gold Nanoparticles in the Dendritic Cavity: A Potential Theranostic Radiopharmaceutical. *J. Nanomater.* **2016**, *2016*, 1–11. [CrossRef]
12. Escudero-Castellanos, A.; Ocampo-García, B.; Ferro-Flores, G.; Santos-Cuevas, C.; Morales-Ávila, E.; Luna-Gutiérrez, M.; Isaac-Olivé, K. Synthesis and preclinical evaluation of the 177 Lu-DOTA-PSMA(inhibitor)-Lys 3 -bombesin heterodimer designed as a radiotheranostic probe for prostate cancer. *Nuclear Med. Commun.* **2019**, *40*, 278–286. [CrossRef] [PubMed]
13. Goddu, S.M.; Budinger, T.F. *MIRD Cellular, S. Values: Self-Absorbed Dose Per Unit Cumulated Activity for Select Radionuclides and Monoenergetic Electron and Alpha Particle Emitters Incorporated into Different Cell Compartments*; Society of Nuclear Medicine: Reston, VA, USA, 1997.

14. Haviland, J.S.; Mannino, M.; Griffin, C.; Porta, N.; Sydenham, M.; Bliss, J.M.; Yarnold, J.R. Late normal tissue effects in the arm and shoulder following lymphatic radiotherapy: Results from the UK START (Standardisation of Breast Radiotherapy) trials. *Radiother Oncol.* **2018**, *126*, 155–162. [CrossRef] [PubMed]
15. Tekade, R.K.; Tekade, M.; Kumar, M.; Chauhan, A.S. Dendrimer-stabilized smart-nanoparticle (DSSN) platform for targeted delivery of hydrophobic antitumor therapeutics. *Pharm. Res.* **2015**, *32*, 910–928. [CrossRef] [PubMed]
16. Ma, J.; Yao, H. Dendrimer-paclitaxel complexes for efficient treatment in ovarian cancer: Study on OVCAR-3 and HEK293T cells. *Acta Biochim. Pol.* **2018**, *65*, 219–225. [CrossRef] [PubMed]
17. Devarakonda, B.; Judefeind, A.; Chigurupati, S.; Thomas, S.; Shah, G.V.; Otto, D.P.; de Villiers, M.M. The effect of polyamidoamine dendrimers on the in vitro cytotoxicity of paclitaxel in cultured prostate cancer (PC-3M) cells. *J. Biomed. Nanotechnol.* **2007**, *3*, 384–393. [CrossRef]
18. Rompicharla, S.V.K.; Kumari, P.; Ghosh, B.; Biswas, S. Octa-arginine modified poly(amidoamine) dendrimers for improved delivery and cytotoxic effect of paclitaxel in cancer. *Artif. Cells Nanomed. Biotechnol.* **2018**, *46* (Suppl. 2), 847–859. [CrossRef] [PubMed]
19. Cline, E.N.; Li, M.H.; Choi, S.K.; Herbstman, J.F.; Kaul, N.; Meyhöfer, E.; Skiniotis, G.; Baker, J.R.; Larson, R.G.; Walter, N.G. Paclitaxel-Conjugated PAMAM Dendrimers Adversely Affect Microtubule Structure through Two Independent Modes of Action. *Biomacromolecules* **2013**, *14*, 654–664. [CrossRef] [PubMed]
20. Teow, H.M.; Zhou, Z.; Najlah, M.; Yusof, S.R.; Abbott, N.J.; D'Emanuele, A. Delivery of paclitaxel across cellular barriers using a dendrimer-based nanocarrier. *Int. J. Pharm.* **2013**, *441*, 701–711. [CrossRef] [PubMed]
21. Gautam, S.P.; Keservani, R.K.; Gautam, T.; Gupta, A.K.; Sharma, A.K. An Alternative Approach for Acetylation of Amine Terminated Poly- amidoamine (PAMAM) Dendrimer. *Ars Pharm.* **2015**, *56*, 155–159. [CrossRef]
22. Zhang, Y.; Liu, X.; Li, L.; Guo, Z.; Xue, Z.; Lu, X. An electrochemical paracetamol sensor based on layer-by-layer covalent attachment of MWCNTs. *Anal. Methods* **2016**, *8*, 2218–2225. [CrossRef]
23. Shadrack, D.M.; Mubofu, E.B.; Nyandoro, S.S. Synthesis of Polyamidoamine Dendrimer for Encapsulating Tetramethylscutellarein for Potential Bioactivity Enhancement. *Int. J. Mol. Sci.* **2015**, *16*, 26363–26377. [CrossRef] [PubMed]
24. Narmani, A.; Yavari, K.; Mohammadnejad, J. Imaging, biodistribution and in vitro study of smart 99mTc-PAMAM G4 dendrimer as novel nano-complex. *Colloids Surf. B Biointerfaces* **2017**, *159*, 232–240. [CrossRef] [PubMed]
25. Aranda-Lara, L.; Ferro-Flores, G.; Azorín-Vega, E.; de María Ramírez, F.; Jiménez-Mancilla, N.; Ocampo-García, B.; Santos-Cuevas, C.; Isaac-Olivé, K. Synthesis and evaluation of Lys 1 (α,γ-Folate)Lys 3 (177 Lu-DOTA)-Bombesin(1-14) as a potential theranostic radiopharmaceutical for breast cancer. *Appl. Radiat. Isot.* **2016**, *107*, 214–219. [CrossRef] [PubMed]
26. Hiremath, J.G.; Khamar, N.S.; Palavalli, S.G.; Rudani, C.G.; Aitha, R.; Mura, P. Paclitaxel loaded carrier based biodegradable polymeric implants: Preparation and in vitro characterization. *Saudi Pharm. J.* **2013**, *21*, 85–91. [CrossRef] [PubMed]
27. Yang, R.; Mao, Y.; Ye, T.; Xia, S.; Wang, S.; Wang, S. Study on enhanced lymphatic exposure of polyamidoamin-alkali blue dendrimer for paclitaxel delivery and influence of the osmotic pressure on the lymphatic targeting. *Drug Deliv.* **2016**, *23*, 2617–2629. [CrossRef]
28. Kumari, A.; Yadav, S.K.; Yadav, S.C. Biodegradable polymeric nanoparticles based drug delivery systems. *Colloids Surf. B Biointerfaces* **2010**, *75*, 1–18. [CrossRef] [PubMed]
29. Naha, P.C.; Mukherjee, S.P.; Byrne, H.J. Toxicology of Engineered Nanoparticles: Focus on Poly (amidoamine) Dendrimers. *Int. J. Environ. Res. Public Health* **2018**, *15*, 338. [CrossRef]
30. Ischia, J.; Patel, O.; Bolton, D.; Shulkes, A.; Baldwin, G.S. Expression and function of Gastrin-releasing peptide (GRP) in normal and cancerous urological tissues. *BJU Int.* **2014**, *113* (Suppl. 2), 40–47. [CrossRef]

8. CONCLUSIONES GENERALES

Se sintetizaron los sistemas BN-PLGA(PTX) y DOTA-DN(PTX)-BN como medios para la entrega selectiva y controlada de paclitaxel en sitios tumorales que sobreexpresan el receptor del péptido liberador de gastrina.

Las técnicas caracterización como espectroscopía vibracional, microscopía electrónica y cromatografía líquida de alta resolución evidenciaron la formación de sistemas nanométricos, funcionalizados con el péptido bombesina y cargados con el antineoplásico Paclitaxel, que permiten la liberación controlada del mismo.

El radiomarcado de los sistemas con Lutecio-177 se logró con purezas radioquímicas del 99%.

Se comprobó que los sistemas ^{177}Lu-BN-PLGA(PTX) y ^{177}Lu-DOTA-DN(PTX)-BN presentan una adecuada estabilidad en suero, necesaria para su posterior evaluación *in vivo*.

Las pruebas *in vitro* demostraron que los sistemas cuentan con capacidad de reconocimiento en sitios de expresión de receptores del péptido liberador de gastrina.

La presencia concomitante del radionúclido y del agente antitumoral resultó en una mayor disminución de la viabilidad celular, en comparación con la actividad citotóxica ejercida por cada componente de forma aislada.

Mediante la SPECT/CT se obtuvieron imágenes evidenciando la captación de los radio-sistemas que, aunado a los estudios de biodistribución, confirmaron la captación y retención tumoral ^{177}Lu-BN-PLGA(PTX) y de ^{177}Lu-DOTA-DN(PTX)-BN tras su administración en modelos murinos.

Se ha evidenciado, por lo tanto, que los nanosistemas poliméricos ^{177}Lu-BN-PLGA(PTX) y ^{177}Lu-DOTA-DN(PTX)-BN cuentan con propiedades teranósticas, que pueden ser aplicados en investigaciones posteriores.

9. PERSPECTIVAS

En el presente trabajo se desarrollaron sistemas basados en nanopartículas poliméricas que permitan la entrega selectiva y controlada del agente antineoplásico Paclitaxel y el radionúclido Lutecio-177, con la finalidad de ser herramientas con aplicaciones teranósticas.

La demanda de mejores medios terapéuticos y diagnóstico en tratamientos contra el cáncer, motiva a la búsqueda de herramientas que permiten el registro espacio-temporal de eventos moleculares, de la evolución de la enfermedad y mejores resultados terapéuticos.

Es por ello que, los sistemas propuestos en el presente trabajo, sirven de base para estudios que permitan proponer estrategias de eficiencias de carga mayores y mayores capacidades de marcado para poder incrementar terapéuticos.

10. ANEXOS

Ocampo-García B. et al. (2019) Dual-Targeted Therapy and Molecular Imaging with Radiolabeled Nanoparticles. In: Khoobchandani M., Saxena A. (eds) Biotechnology Products in Everyday Life. EcoProduction (Environmental Issues in Logistics and Manufacturing). Springer, Cham

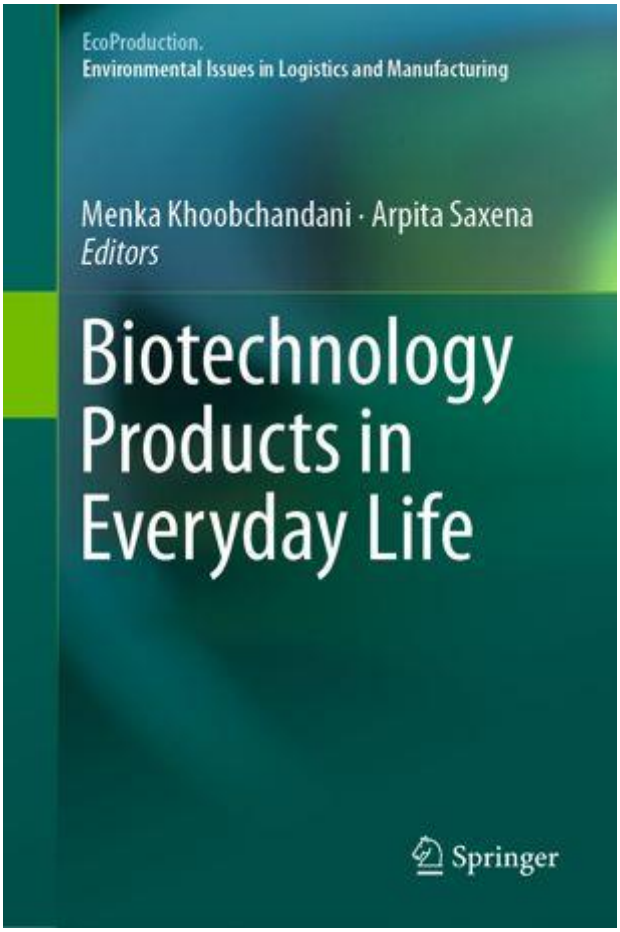

Dual-Targeted Therapy and Molecular Imaging with Radiolabeled Nanoparticles

Blanca Ocampo-García, Brenda Gibbens-Bandala, Enrique Morales-Avila, Laura Melendez-Alafort, Menka Khoobchandani, Maydelyd Trujillo-Nolasco and Kattesh V. Katti

Abstract Radiolabeled targeted nanoparticles have been extensively studied for medical applications. Their multifunctionality and multivalency (among other properties) make them suitable candidates to target different diseases by means of pharmacophore groups for molecular, cellular, and/or tissue targeting. They have been used for molecular imaging and as drug delivery systems to improve drug efficacy and decrease side effects by passive accumulation of drugs in healthy tissues. Metallic nanoparticles can be radiolabeled or be radioactive themselves in order to deposit a large amount of energy into malignant cells, which produces irreversible damage. Because of their high surface area, these can be functionalized with small molecules and biomacromolecules for targeted radiotherapy. Moreover, their quantum size effect and resulting properties recently proved to produce hyperthermia. Polymeric nanoparticles are also acquiring importance in molecular imaging as diagnostic and therapeutic agents, due to their biocompatibility, biodegradability, and pharmacokinetic advantages, including the ability for controlled drug release or targeted radiotherapy. Both metallic and polymeric nanoparticles have been proposed as new, smart, pharmaceutical devices to produce dual-targeted therapy and molecular imaging. In this chapter, we will discuss the development and potential medical applications of radiolabeled metallic and polymeric nanoparticles as intelligent targeted systems.

B. Ocampo-García (✉) · B. Gibbens-Bandala · M. Trujillo-Nolasco
Departamento de Materiales Radiactivos, Instituto Nacional de Investigaciones Nucleares, Carretera México-Toluca S/N, Ocoyoacac 52750, Estado de México, Mexico
e-mail: ocampo_be@yahoo.com.mx; blanca.ocampo@inin.gob

B. Gibbens-Bandala · E. Morales-Avila · M. Trujillo-Nolasco
Facultad de Química, Universidad Autónoma Del Estado de México, Paseo Tollocan S/N, Toluca 50180, Estado de México, Mexico

L. Melendez-Alafort
Instituto Oncologico Veneto IOV-IRCCS, via Gattamelata 64, 35138 Padua, Italy

M. Khoobchandani · K. V. Katti
Department of Radiology, Institute of Green Nanotechnology, University of Missouri Cancer Nanotechnology Platform, University of Missouri, One Hospital Drive, Columbia, MO 65212, USA

M. Khoobchandani and A. Saxena (eds.), *Biotechnology Products in Everyday Life*, EcoProduction, https://doi.org/10.1007/978-3-319-92399-4_14

Keywords Radiolabeled nanoparticle · SPECT imaging · PET imaging
Cerenkov imaging · Polymeric nanoparticle · Inorganic nanoparticle
Nuclear imaging · Targeting · Drug release

1 Introduction

Nanoparticles (NPs) play an important role in life science research. Particularly, nanosystems that enable molecular imaging of biological processes and therapeutic applications have been successfully developed based on their capacity to produce multifunctional and multivalent effects.

In the medical field, these nanosensors can be designed to target pharmacophore groups in select cells in order to produce a desired in vitro or in vivo effect. NPs have been purposed as in vitro approaches for diagnosis, in vivo molecular imaging or targeted delivery, and in vivo tissue engineering [1].

For human applications, only a few nanosystems or nanoplatforms have been approved for use in patients. Several shortcomings, mainly safety issues, have challenged their translation to clinical applications. Among them, their inherent toxicity produced by the accumulation in the reticuloendothelial system (RES) originated by their relatively slow hepatic uptake and biliary excretion continues to hamper their widespread use in vivo [2].

Molecular imaging for clinical use refers to the implementation of imaging techniques with highly sensitive and specific recognition with an additional high degree of spatial resolution. Modalities based on nuclear techniques combined with nuclear resonance imaging (NMR) promise a high degree of efficiency, increasing the diagnostic accuracy. Additionally, radiolabeled techniques extend the possibility for their therapeutic application using proper surface architecture to guarantee selectivity by molecular targeting.

Nuclear imaging modalities include single-photon emission computed tomography (SPECT), positron emission tomography (PET), and more recently, Cerenkov luminescence (CL) has also gained prominence. By using these imaging modalities, several approaches based on nanoparticles are being currently studied.

In this chapter, we discuss the development and potential medical applications of radiolabeled metallic and polymeric nanoparticles as intelligent targeted systems for applications in molecular imaging and therapy.

2 Multitargeting Receptors

In several diseases, including cancer, the heterogeneity of overexpressed receptors is well known. This fact opens the possibilities to target concurrently multiple receptors in vivo, in order to improve the detection sensitivity. In general, there are three different strategies for multireceptor targeting [3]:

(a) Heteromultivalent ligands, which allow simultaneous binding to different receptors.
(b) The co-injection of multiple radiotracers.
(c) The sequential injection of different imaging agents.

NPs have emerged as heteromultivalent and multifunctional systems that enable targeting of more than one receptor site to enable both therapy and imaging [4]. In the medical field, multifunctional nanoparticles that combine therapeutic molecules, molecular targeting, and diagnostic imaging abilities and exhibit appropriate features for in vivo use can improve the efficacy of cancer therapy and disease diagnosis. Although most of the nanosystems studied have demonstrated a wide variety of properties, multifunctional and multivalent nanoapproaches that simultaneously exhibit all needed functionalities for human applications are currently limited. Essential functionalities for multifunctional nanocarriers comprise:

- In vivo stability before attainment the target sites.
- Long circulation time in the bloodstream.
- Sensitivity to local stimuli to produce controlled release (temperature and/or pH).
- High drug loading content.
- Ability to specifically accumulate in the target sites.
- Ability to effect the intracellular drug uptake behavior.
- Capability to monitor disease advancement.

Targeting molecules that are capable of attaching onto the surface of nanoparticles include peptides, aptamers, small molecules, and antibodies [5].

3 Nuclear Imaging Based on Nanoparticles

A wide number of nanoplatforms have the capability for chemical conjugation to a chelator or to be radiolabeled on a chelator-free way. The selection of radionuclide to be attached or adsorbed onto the nanoparticle surface depends on the usefulness of that nanoplatform. Some features to be considered include the emission mode, emitted energies, and physical half-life. Gamma-emitting radionuclides with a short half-life are preferred for imaging, and beta-particle emitters are chosen for therapeutic purposes. Radionuclides that enable both imaging and therapeutic capabilities are called "theranostic" (^{177}Lu, ^{90}Y or ^{198}Au). In nuclear imaging, gamma radiation emitted by different radionuclides in diverse decay modes allows the acquisition of images (Fig. 1).

Positron emission tomography (PET) allows measurement of physiologic processes. This imaging can be performed by the annihilation of a positron emitted from a radionuclide with an electron. In this phenomenon, two 511 keV photons are emitted at 180°, which pass through the body and are detected by a ring of detectors around the subject. Radiolabeled NPs can be imaged in a quantitative mode to define the tumor uptake provided by the radiolabeled NPs [5]. Among PET radionuclides,

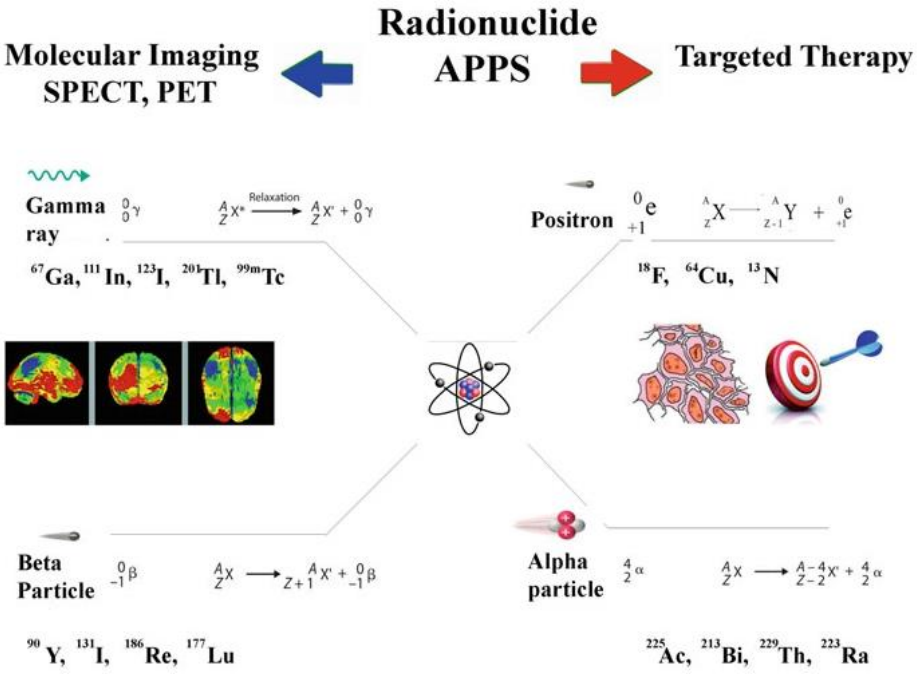

Fig. 1 Decay modes for nuclear imaging and therapy

^{68}Ga ($t_{1/2} = 68$ min) has a $t_{1/2}$ necessary to produce in vivo imaging of NPs and has been used for both PET and Cerenkov imaging. The ^{18}F ($t_{1/2} = 110$ m) radionuclide is also employed to label NP. For longer in vivo PET imaging, ^{64}Cu ($t_{1/2} = 12.7$ h), ^{89}Zr ($t_{1/2} = 78.4$ h), and ^{124}I ($t_{1/2} = 4.18$ d) are commonly used [6].

In single-photon emission computed tomography (SPECT), the emission of a gamma photon originated by the nucleus produces regional foci of the in vivo distribution. Collimators are used to detect a specific range of photon energies. Usually, two opposite detectors are used to obtain images through rotating from multiple angles around the field of view, which are then reconstructed to render three-dimensional images [7].

Cerenkov imaging is produced by the visible light wavelength produced by a charged particle traveling through a dielectric medium faster than the speed of light in that medium [8]. Radionuclides ^{177}Lu and ^{90}Y are used as imaging and therapeutic agents. Moreover, other radionuclides can be used in combination with NPs to obtain a theranostic agent [5].

4 Radiolabeling of Nanoparticles

In general, there are four main strategies to radiolabel nanoparticles:

- Bifunctional approach using chelators to coordinate radionuclides, chemically bound to the nanoparticle surface.
- A chelator-free radiolabeling method whereby radionuclides can be directly bound to the nanoparticle surface.
- Direct bombardment with neutrons or protons to produce some radioactive atoms in the nanoparticle.
- Radionuclides can be embedded into the nanoparticle.

In nuclear imaging, several chelators have been used to bind radionuclides onto the nanoparticle surface. NOTA (1,4,7-triazacyclononane-1,4,7-triyltriacetic acid), DOTA(1,4,7,10-tetra-azacyclododecane-1,4,7,10-tetrayltetra-acetic acid), *p*-SCN-Bn-DOTA (S-2-(4-isothiocyanatobenzyl)-1,4,7,10-tetraazacyclododecane tetraacetic acid), and diethylenenetriaminepentaacetic acid (DTPA) are bifunctional complexing agents which bind radioactive atoms to a target biomolecule.

The conditions of radiolabeling include reaction temperature, incubation time, and biomolecule degradation control, making some modifications on affinity, binding properties, and consequent pharmacokinetic behavior, possible.

5 Radiolabeled Metallic Nanoparticles

Stable inorganic NPs have been prepared using different approaches. Mainly, NPs for biomedical applications are based on nanocolloids formed by heavy metal suspensions stabilized with a coating process using polymers, proteins, or polysaccharides. The coating provides NPs colloidal biocompatibility, stability, and increases their circulation time reducing their uptake by the RES. Nanoparticle biodistribution generally depends on their coating but also on their size. Small NPs with a mean diameter less than 10 nm undergo fast renal filtration; unlike NPs with a diameter greater than 200 nm are quickly removed by the RES system from the bloodstream. Therefore, NPs with diameters between 10 and 100 nm have achieved a higher accumulation at the target site, as a result of their longer circulation times. Furthermore to minimize the opsonization and clearance processes, generally NPs can be coated with some polymers as poly(ethylene glycol) (PEG) [9].

The most investigated inorganic NPs are gold NPs (AuNPs) and iron oxide NPs (IONPs), but there are also some reports of other noble metals such as silver and copper. Nanoparticles offer two key advantages as targeted agents: Firstly, nanoparticle geometry consists of a core, typically with thousands of detectable atoms such as iron and gold; secondly, they can be coated with targeting peptides, antibodies, or any molecules with biological activity. In addition, they have a large surface area, which is ideal not only for efficient modification but also can incorporate various functional moieties on the surface to produce systems with multiple receptor targeting at the same time. This produces multivalent effects caused by multiple simultaneous interactions between the surface of the nanoparticle and that of the cell [10–12].

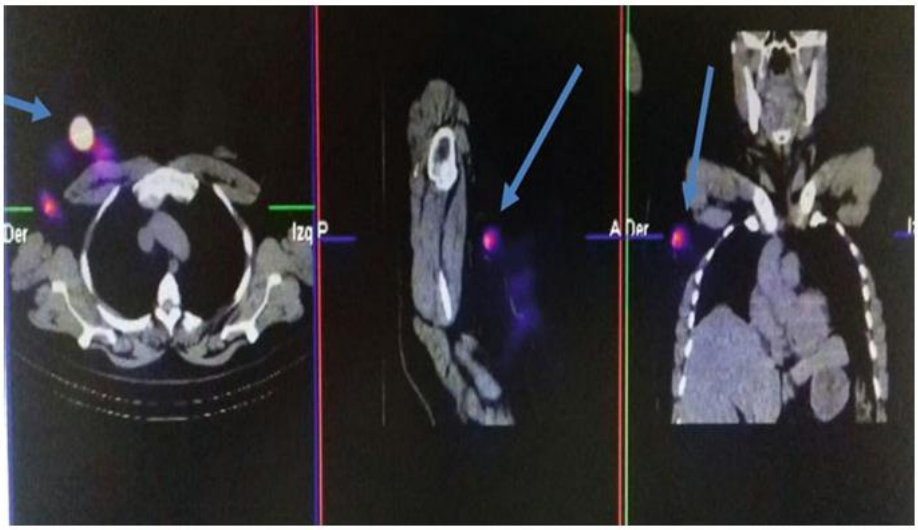

Fig. 2 Sentinel node localization by SPECT/CT in patient with breast cancer (24 h ^{99m}Tc-AuNP-mannose post-administration). Image courtesy of National Cancer Institute (Mexico)

5.1 Radiolabeled Gold Nanoparticles (AuNPs)

Gold nanoparticles continue to show great potential for clinical applications. In recent years, important breakthroughs have been made in the development of gold radiolabeled nanoparticles, which can be used as novel diagnostic tools in multimodality imaging systems. Some multimeric systems of AuNPs radiolabeled with ^{99m}Tc have been reported as suitable target-specific drugs for molecular imaging of tumors and sentinel lymph node detection [13, 14]. Moreover, ^{177}Lu-AuNPs conjugated to different targeting peptides have been proposed as theranostic radiopharmaceuticals [15–18]. Recently, Ferro-Flores et al. (2017) developed an antiangiogenic cancer-specific dual-targeting ^{177}Lu-Au-nanoradiopharmaceutical based on AuNPs. The nuclear localization sequence (NLS)-Arg-Gly-Asp peptide and an aptamer (HS-pentyl-pegaptanib) to target both the α(v)β(3) integrin and the vascular endothelial growth factor (VEGF) overexpressed in the tumor neovasculature has been demonstrated. The nanosystem showed properties of angiogenesis inhibition [19].

Only few examples of AuNPs have demonstrated successful clinical applications, but several approaches are still in clinical trials [20]. To localize sentinel lymph node in breast cancer patients (Fig. 2), ^{99m}Tc-AuNP-mannose radiopharmaceutical showed a suitable response by using 1-day or 2-day conventional protocols [21].

Plasmonic Gold Nanoparticles for Photothermal Therapy

NPs of noble metals have a broad absorption band in the visible spectrum, due to plasmon resonance. Metallic nanomaterials display strong absorption in the near-infrared (NIR) region (700–1100 nm); mostly, it converts optical energy into thermal energy. This effect is called photothermal ablation and can be used to destroy tumor cells by local heating. Photothermal ablation therapy has gained increasing attention because of its minimally invasive approach for cancer treatment. Several specific targeting approaches for photothermal heating with gold nanoparticles have been widely reported [22–26]. The plasmon resonance for common gold 20-nm nanosphere is 520 nm and redshift in NIR region from 800–1200 nm. Further, these materials can be conjugated with specific targeting molecules for better efficacy [27, 28].

In order to elucidate the temperature increase necessary to produce cell death by photothermal therapy when AuNPs in different tissues are irradiated with a Nd-YAG laser (532 nm), the optical properties (coefficient of extinction, absorption, and scattering) were calculated [29].

Recently, a new generation of nanosystems, which enables more than one pathway of producing therapy and imaging, has emerged. As expected, these systems have demonstrated clear advantages to those of individual therapy approaches. The photothermal and radiotherapeutic potential of the ^{177}Lu-dendrimer conjugated toward folate and bombesin conjugated with gold nanoparticles in the dendritic cavity (^{177}Lu-DenAuNP-folate-bombesin) was demonstrated. The intense NIR fluorescence emitted at 825 nm from the conjugate inside breast cancer cells corroborated the effectiveness of ^{177}Lu-DenAuNP-folate-bombesin for optical imaging [30]. Moreover, the synergistic interaction in a breast cancer model between heat produced by photoconversion and cytotoxicity with doxorubicin was demonstrated by small AuNPs (less than 20 nm) when irradiated by laser [31].

Intrinsically Radiolabeled Gold Nanoparticles

Au-198 can be used for tumor therapy because of its half-life of 2.7 days and higher energy β-emission ($\beta_{max} = 0.96$ meV) which enables it to penetrate up to 11 mm in tissue to produce therapeutic cross-fire effect on the tumor cells with a minimal radiation dose to the normal tissue surrounded. In vitro/in vivo biocompatible of Au-198 compounds was produced and evaluated the first time by Katti et al. [32, 33]. They prepared trigonal and tetrahedral gold compounds functionalized with biocompatible water-soluble hydroxymethyl phosphine that showed suitable in vivo clearance by renal and hepatobiliary pathways. The present article also demonstrates antitumor properties of these complexes against some types of human cancer established in mice and dogs as lung, breast, non-Hodgkin's lymphoma, prostate, and pancreatic tumors [34]. The promising radiochemical and biodistribution properties of these Au-198 nanoparticles encouraged their stabilization with other polymers as epigallocatechin gallate (EGCG) and gum arabic glycoprotein (GAP) [35]. The utility of amino acid-based phosphines for reducing gold salt into gold nanoparticles has

allowed to prepare biocompatible ^{198}AuNPs for theranostic applications [36, 37]. Recently, Axiak-Bechtel et al. used dogs to develop a human-mimicking prostate cancer model. They found that dogs with spontaneous prostatic tumors treated with a single dose of GAP-^{198}AnNP (105 Gy) did not show short-term toxicity.

In addition, the combination of imaging modalities (CT/SPECT) revealed that, following the injection of GAP-^{198}AuNP, the therapeutic agent was mainly localized in the prostate, with some loss in the bladder and urethra [38]. Advantageous Au-198 radiochemical properties also encouraged Chanda et al. to conjugate ^{198}AuNPs with BBN peptides in order to develop a tumor-targeted therapeutic agent. ^{198}AuNP-BBN in vitro and in vivo studies in mice evidenced a high binding affinity (IC_{50}) in microgram ranges and a selective uptake in GRP-receptor-rich organs such as the pancreatic acne in normal mice and the tumors in prostate tumor-bearing mice. The difference in prostate tumor sites between the mice treated with ^{198}AuNP-BBN and the pretreated group demonstrated the realistic clinical potential of these targeted nanoparticles [39]. Radioactive AuNP has been also functionalized with mangiferin, a promising xanthonoid for tumor targeting. The therapeutic efficacy studies of MGF-^{198}AuNPs provided conclusive evidence that the nanosystem has the ability to reduce tumors volume and did not cause any adverse radiotoxicity [40].

5.2 *Radiolabeled Iron Oxide Nanoparticles*

Iron oxide nanoparticles (IONPs) are one of the most widely studied NPs for imaging applications over the past two decades, because they can enable contrast in MRI through the production of localized magnetic field inhomogeneities. IONP size can range from several nanometers to microns and can be classified according to their hydrodynamic diameter into: ultra-small paramagnetic iron oxide (USPIO) NPs below 50 nm; superparamagnetic iron oxide (SPIO) from 60 to 250 nm; and micron-sized iron oxide particles (MPIO) from 1 to 8 μm [41].

Iron oxide NPs are produced by physical, chemical, and biological methods. However, chemical synthesis methods based on the co-precipitation of Fe^{2+} and Fe^{3+} aqueous salt solutions by addition of a base are the most commonly used due to their low production cost and the high yield. In addition, using these methods is easy to control the size, composition, and the shape of the NPs produced, changing some factors as the Fe^{2+} and Fe^{3+} ratio, the type of salts used (e.g., chlorides, sulfates, nitrates, or perchlorates), pH, and the ionic strength. Other chemical methods such as precipitation (solgel and gas/aerosol gel preparation) have been developed [42].

Functionalized IONPs provide the opportunity to develop tumor-specific thermal therapy for metastatic cancer when inductively heated by an externally applied, alternating magnetic field. To be used as targeted agents, however, IONP cores have to be first stabilized with an adsorbed layer of a biocompatible polymer (such as dextran, chitosan, or polymethacrylate) and then conjugate the target-specific molecules such as antibodies, proteins, peptides [9].

IONPs have been radiolabeled with SPECT and PET imaging isotopes using direct, indirect labeling, and doping approaches, in order to develop multimodality imaging agents for dual PET/MR or SPECT/MRI, as well as trimodality imaging (MR/NIR/PET or SPECT) when conjugated to fluorescent near-infrared optical agents [41].

Several dual-mode imaging probes for PET/MRI using ^{64}Cu have been reported. Jarrett et al. designed iron oxide nanoparticles coupled with ^{64}Cu for the diagnosis of vascular inflammation. Glaus et al. reported ^{64}Cu-DOTA-PEG-IONPs showed strong MR and PET signals and stability in mouse serum. ^{64}Cu-bis (dithiocarbamate-bisphosphonate) conjugated to IONPs has also been reported for in vivo lymphatic imaging. To image $\alpha_v\beta_3$ expression, multifunctional ^{64}Cu-labeled IONPs conjugated to the RGD (Arg-Gly-Asp) peptide have been developed and demonstrated a specific glioblastoma tumor-targeting capability by PET/MRI dual imaging [43]. Xie et al. dual-labeled IONPs encapsulated into human serum albumin matrices with ^{64}Cu-DOTA and Cy5.5, and using in vivo PET/NIR fluorescence/MRI trimodality imaging in a subcutaneous U87MG xenograft mouse model, demonstrated a huge accumulation in lesions, a high extravasation rate, and low uptake by macrophages in tumor microenvironment [44].

Both Ga-67 and Ga-68 have been used for multimodal imaging. Jalilian et al. reported a ^{67}Ga-labeled IONP-folate system with adequate cell membrane permeability and paramagnetic properties for thermotherapy. This system showed excellent stability at room temperature, low liver uptake, and high blood circulation after 24 h. Stelter et al. covalently bonded the transfection agent HIV-1 Tat, the fluorescent dye fluorescein isothiocyanate, and ^{68}Ga to IONPs, and demonstrated that the radionanoconjugate can be applied to efficient cell labeling, subsequent multimodal molecular imaging, and possible thermoablative therapy [44].

Madru et al. prepared ^{99m}Tc-labeled IONPs for the SPECT/MRI imaging multimodality of sentinel lymph nodes. The labeling was carried out through polyethylene glycol coated over the solid iron oxide core. SPECT/MRI imaging confirmed its potential applications in the diagnosis of breast cancer and malignant melanoma, due to the accumulation of ^{99m}Tc-IONPs in animal lymph nodes. Shanehsazzadeh et al. evaluated the biodistribution in mice of dextran-coated IONPs labeled with ^{99m}Tc and found high uptake in the reticuloendothelial system.

In order to study the concomitant efficacy of heating injected magnetic nanoparticles, ^{111}In-labeled ChL6 was conjugated to carboxylated polyethylene glycol (PEG) in different-sized, dextran-coated IONPs, with one to two ChL6 antibodies per nanoparticle. Using athymic mice bearing the human breast cancer model, it was observed that heating the nanoparticles with an externally applied AMF caused tumor necrosis in all cases. SPECT imaging showed a tumor uptake of 14% of the injected dose per gram at 48 h. However, although the heating capacity of the large nanoparticles (30 and 100 nm) was several times greater, the tumor-targeting efficacy was significantly less than that of their 20-nm-sized counterparts [43].

Also, beta-particle emitters such as I-131 have been conjugated to NPs for radiotherapy purposes. For example, Liang et al. radiolabeled IONPs with Re-188 using a direct method with a labeling efficiency of 90% and good in vitro stability and

Table 1 Radiolabeled iron oxide nanoparticles for SPECT/PET MR imaging

Nanoparticle	Application	References
^{99m}Tc-IONPs/diethylene triamine pentaacetic acid (DTPA) and 1,4,7-triazacyclononane-triacetic acid (NOTA)	Multimodality contrast agents for sentinel lymph node mapping	[45]
^{99m}Tc-PEG-BP-USPIO/Poly etilenglycol-bisphosphonates (BP)	Visualization of blood vessels and vascular organs with high spatial definition	[46]
^{99m}Tc-USPIO-bevacizumab	Targeted imaging of hepatocellular carcinoma	[47]
^{99m}Tc-PEG-SPIONs	Molecular imaging for sentinel lymph node (SLN)	[48]
^{111}In-antimesothelin antibody (mAbMB)-SPION	Early diagnosis and treatment planning of mesothelin-expressing cancers using SPECT-MR imaging	[49]
^{64}Cu-DTPA-SPION-Fluorochrome	Trimodality reporter for macrophage and inflammatory plaque components	[50]
^{68}Ga/^{111}In-TAT-FITC-aminosilated-SPIONs	Cell labeling for trimodal imaging	[51]
^{64}Cu-PEG-fosfolipid-SPIONs	Dual PET-MRI imaging agent	[52]
^{64}Cu-bifosfonate-dextran-SPIONs	PET-MR dual modality for draining lymph nodes image	[6]
^{64}Cu-DOTA-polyaspartic acid (PASP)-IONPs-RGD	Dual PET and MRI of tumor integrin expression	[53]
Intrinsically radiolabeled [^{59}Fe]-SPIONs	Dual SPECT-MR detection	[54]
$^{67}Ga^{3+}$ and Cu^{2+}-labeled SPIONs	Multimodal PET/SPECT-MRI agent	[55]

demonstrated the ability of ^{188}Re-IONPs to kill liver cancer cells. Cao et al. prepared silica-coated magnetite nanoparticles immobilized with histidine and linked the Re-188 onto their surface, obtaining a labeling yield of 91%. Chen et al. reported the development of ^{131}I-anti-VEGF cross-linked to dextran-coated IONPs and investigated their therapeutic effects in nude mice with induced liver tumors. Tumor growth delay and tumor inhibition were observed. Therefore, their results suggested that the radioimmunotherapy of an intratumoral injection of ^{131}I-anti-VEGF-IONP is effective for the treatment of liver cancer [44] (Table 1).

5.3 Radiolabeled Silver Nanoparticles

Silver NPs (AgNPs) have been used as antimicrobial agents because they can be incorporated into plastics, textiles, and other materials. However, little is known about in vivo trafficking and deposition of AgNPs. Therefore, a few studies have been reported recently to study the accumulation of AgNPs in organs and their toxicological implications. Ichedef et al. [56] reported a synthesis method for radiolabeled silver nanoparticles from proton activation of silver metal powder, enriched in Ag-107, with a 30.7 meV proton beam to produce the γ-emitter Ag-105 g (half-life of 41.29 days). Following the activation, the powder was dissolved in concentrated nitric acid in order to form silver nitrate ($AgNO_3$), which was used to synthesize the ^{105}AgNP. Chrastina and Schnitzer [57] developed a rapid method for the radiolabeling of AgNPs with I-125 in order to track in vivo tissue uptake of silver nanoparticles after systemic administration by SPECT imaging. Biodistribution analysis revealed uptake of the nanoparticles in the liver (24.5% ID/g) and spleen (41.5% ID/g) at 24 h. Similar results were obtained by Ashraf et al. [58] using water-based suspension of bare silver nanoparticles and dextran-coated AgNPs (dextran AgNPs) radiolabeled with Tc-99m. Both ^{99m}Tc-AgNPs and Tc-99m-dextran-AgNPs were mainly accumulated in the liver/spleen region although dextran delayed liver uptake, enhancing the blood retention time. Farrag et al. reported a simple and rapid method for radiolabeling of three types of Ag NPs using I-125, with high labeling yields (>90%), without disturbing the optical properties. After intravenous injection of the radiocompound in normal and solid tumor-bearing mice, they found that ^{125}I-AgNPs was localized in the tumor site for a long period of time [59].

5.4 Radiolabeled Copper Nanoparticles

Synthesis of intrinsically radiolabeled nanoparticles is an emerging concept in cancer theranostics and is expected to play an imperative role in translating nanotechnology research. Therefore, recently Zhou et al. [60] synthesized radioactive ^{64}CuS NPs, in which ^{64}Cu is an integral building block of CuS rather than a chelate to the NPs. These simple to make ^{64}CuS NPs demonstrated to possess excellent stability and to be suitable both for PET imaging and as photothermal coupling agents for photothermal ablation. Furthermore, the ^{64}CuS NPs showed a passive targeting preference over the tumor site and a strong NIR absorption that mediated ablation of U87 tumor cells after either intratumoral or intravenous injection. Based on these results, a viable strategy for a large-scale production (GBq level) of Cu-64 using medium flux research reactors was explored. Biological studies of ^{64}CuS NPs produced with this method on mice-bearing melanoma tumors revealed a significant tumor uptake (4.64 ± 1.71% ID/g) within 4 h post-injection, with good tumor-to-background contrast [61].

A smart nanosystem was developed for tumor-targeting drug delivery and PET/MR imaging. The nanocarrier is based on superparamagnetic iron oxide

nanoparticles radiolabeled with ^{64}Cu and demonstrated favorable properties for combined targeted anticancer drug delivery and PET/MRI dual-modality imaging of tumors overexpressing integrin $\alpha_v\beta_3$. The size (hydrodynamic diameter) was 68 ± 2 nm and was pH-sensitive in order to deliver Doxorubicin. The in vivo ^{64}Cu-labeled cRGD-conjugated SPIO nanocarrier uptake was mainly in the tumor and liver, but not in most normal tissues. The system demonstrated good tumor-targeting capability and successful tumor contrast [4].

6 Radiolabeled Polymeric Nanoparticles

Polymeric nanoparticles have been extensively reported as effective carriers to therapeutic pharmaceuticals and are recently emerging as a new class of molecular imaging (MI) agents for detection and treatment of human diseases [62]. An optimal polymeric nanosystem for MI applications possesses the following components: (a) controlled- and sustained-release properties; (b) smaller size (5–250 nm) to facilitate internalization and probing of cells and they do not have rapid renal clearance; (c) their surface is easily modified with molecular signaling and receptor-targeting molecules; (d) payload-carrying capacity delivers high concentrations of imaging agents to desired region; (e) multimodal potential offers visualization in more than one imaging modality; and (f) theranostic capability enables detection and treatment of disease using a single platform [63].

A wide variety of natural or synthetic polymers (chitosan, PLA, PGA, PLGA, PEG, HPMA, and other acrylate derivatives) with outstanding biocompatibility and biodegradability and nanoparticle preparation techniques (nanoparticles obtained by polymerization of a monomer or obtained directly from a preformed polymer) have been described for polymeric nanoparticle production [64]. There is no exclusive polymer for the encapsulation of any therapeutic or imaging agent, and not all molecules can be incorporated in all polymers. Both the physicochemical properties of the polymer and candidate molecule to be incorporated must be considered.

There are two general methods for the generation of polymeric nanosystems for imaging applications. The first is **covalent conjugation** of contrast agents to a polymeric matrix, followed by the formation of nanoparticles by conventional techniques or the conjugation can be in the surface of preformed nanoparticles. The second is the **physical encapsulation** of the contrast agent within polymeric nanoparticles.

The major advantage of grafted polymers is that the contrast agent is covalently bound to the polymer; thus, the burst release does not occur. However, disadvantages include poor loading efficiency and nonhomogeneous distribution of contrast agents within the polymeric matrix. The physical encapsulated systems may have superior advantages over the covalently bound polymer because of high loading efficiency within the polymeric matrix. However, controlling the burst release contrast agents from nanoconjugates within a biological system remains a significant challenge [65].

For nuclear imaging, radionuclides such as ^{11}C, ^{18}F, ^{64}Cu, ^{76}Br, ^{99m}Tc, ^{111}In, and ^{90}Y have been used with a wide range of copolymers to formulate robust nanosized

Table 2 Examples of polymeric nanoparticles used in nuclear imaging

Polymeric system	Agent	Modality	References
^{99m}Tc-PLGA	^{99m}Tc	SPECT	[66]
HPMA-LMA	^{18}F	PET	[67, 68]
Poly(*t*-butyl acrylate), PEG, methyl acrylate, styrene	^{64}Cu	PET	[69]
Poly-glycidyl-methacrylate(poly-2,3-epoxy-propylmethacrylate)	^{68}Ga	PET	[70]
Polyethylene glycol-coated micelles dually labeled	Cy^7, ^{111}In	SPECT, NIR, FL	[71]
PVPh	^{124}I	PET	[72]
PAMAM dendrimer-entrapped gold NPs	^{99m}Tc	SPECT/CT	[73]
PEG-b-PPA/DNA micellar nanoparticles	^{111}In	SPECT/CT	[74]
PEGylated dendrimer poly(amidoamine) (PAMAM)-folic acid conjugates	^{99m}Tc	SPECT	[75]
Poly(*N*-vinylimidazole-co-*N*-vinylpyrrolidone)g-poly(D,L-lactide)	^{123}I	SPECT/CT	[76]
Dextran nanoparticles	^{89}Zr	PET/MR	[77]

CT, Computed tomography; *FL*, Fluorescence

delivery systems. Additionally, the fluorescence imaging technique is integrated with polymeric NPs to develop the image-guide drug delivery system to monitor drug pharmacokinetics, intratumoral drug distribution, and drug tumor accumulation in real time.

The versatility of these nanomaterials makes them an attractive platform for developing highly sensitive molecular imaging agents. Table 2 covers the recent use of polymeric nanoparticles as carriers of molecular MI agents.

7 Discussion

Many different types of nanoparticles have been designed and evaluated over the years. Initially, nanosystems were primarily used for therapeutic purposes, that is, for a more efficient delivery of therapeutic drugs to pathologic sites, while reducing their accumulation in potentially endangered healthy tissues. Currently, some therapeutic nanoparticles are used clinically, and more of these so-called nanomedicine formulations are being evaluated in preclinical and clinical trials. However, in recent years, interest for nanoparticles as diagnostic agents has increased.

Radiolabeled nanoparticles developed as a smart multifunctional platform, designed for in vivo imaging and/or therapy have demonstrated high potential to be used in medical applications. The use of noninvasive nuclear imaging modalities such as PET, SPECT, or CL allows for the study of NP biodistribution in animal models, which can provide essential information for clinical translation of radiolabeled nanosystems to human trials. Medical applications of multifunctional nanoparticles could be reached if therapeutic agents could be incorporated in the same platform as molecular targeting agents with diagnostic imaging capabilities.

The potential of using nanoparticles for molecular imaging is compromised because their pharmacokinetic properties are difficult to control. Among the challenges to translate, these nanoapproaches to human application for imaging and/or therapy are the lack of ability to administer them intravenously and their low specific activities are the main shortcomings to deal with. Nanoparticles would either have to be administered by an intratumoral injection or directly deposited on an artery that feeds a target organ to avoid RES in order to achieve therapeutic applications in humans. It is important to note that in order to facilitate the clinical translation of radiolabeled nanoparticles, appropriate dosimetry and toxicological studies should be included.

Acknowledgements This study was supported by the International Atomic Energy Agency (CRP-F22064, Contract No. 18358) and the Universidad Autónoma del Estado de México, through project No. 4288/2017/CI. This research was carried out as part of the activities of the "Laboratorio Nacional de Investigación y Desarrollo de Radiofármacos, CONACyT".

Conflicts of Interest The authors declare no conflict of interest.

References

1. Choi, H., Lee, Y.-S., Hwang, D.W., Lee, D.S.: Translational radionanomedicine: a clinical perspective. Eur. J. Nanomed. **8**(2), 71–84 (2016)
2. Ma, Y., Mou, Q., Zhu, X., Yan, D.: Small molecule nanodrugs for cancer therapy. Mater. Today Chem. **4**, 26–39 (2017)
3. Reubi, J.C., Maecke, H.R.: Approaches to multireceptor targeting: hybrid radioligands, radioligand cocktails, and sequential radioligand applications. J. Nucl. Med. **58**(Supplement 2), 10S–16S (2017)

4. Yang, X., Hong, H., Grailer, J.J., Rowland, I.J., Javadi, A., Hurley, S.A., et al.: cRGD-functionalized, DOX-conjugated, and 64 Cu-labeled superparamagnetic iron oxide nanoparticles for targeted anticancer drug delivery and PET/MR imaging. Biomaterials **32**(17), 4151–4160 (2011)
5. Pratt, E.C., Shaffer, T.M., Grimm, J.: Nanoparticles and radiotracers: advances toward radionanomedicine. Wiley Interdisc. Rev.: Nanomed. Nanobiotechnol. **8**(6), 872–890 (2016)
6. Torres Martin de Rosales, R., Tavaré, R., Glaria, A., Varma, G., Protti, A., Blower, P.J.: ^{99m}Tc-bisphosphonate-iron oxide nanoparticle conjugates for dual-modality biomedical imaging. Bioconjug. Chem. **22**(3), 455–465 (2011)
7. Goel, S., Chen, F., Ehlerding, E.B., Cai, W.: Intrinsically radiolabeled nanoparticles: an emerging paradigm. Small **10**(19), 3825–3830 (2014)
8. Thorek, D.L., Robertson, R., Bacchus, W.A., Hahn, J., Rothberg, J., Beattie, B.J., et al.: Cerenkov imaging-a new modality for molecular imaging. Am. J. Nucl. Med. Mol. Imaging **2**(2), 163 (2012)
9. Abou, D.S., Pickett, J.E., Thorek, D.L.J.: Nuclear molecular imaging with nanoparticles: radiochemistry, applications and translation. Br. J. Radiol. **88**, 2015 (1054). https://doi.org/10.1259/bjr.20150185. PubMed PMID: WOS:000363315800012
10. Montet, X., Funovics, M., Montet-Abou, K., Weissleder, R., Josephson, L.: Multivalent effects of RGD peptides obtained by nanoparticle display. J. Med. Chem. **49**(20), 6087–6093 (2006). https://doi.org/10.1021/jm060515m. PubMed PMID: ISI:000240826200023
11. Montet, X., Montet-Abou, K., Reynolds, F., Weissleder, R., Josephson, L.: Nanoparticle imaging of integrins on tumor cells. Neoplasia **8**(3), 214–222 (2006). https://doi.org/10.1593/neo.05769. PubMed PMID: ISI:000239282800007
12. Khoobchandani, M., Katti, K., Maxwell, A., Fay, W.P., Katti, K.V.: Laminin receptor-avid nanotherapeutic EGCg–AuNPs as a potential alternative therapeutic approach to prevent restenosis. Int. J. Mol. Sci. **17**(3), 316 (2016)
13. Ocampo-García, B., Ferro-Flores, G., Morales-Avila, E., de María, Ramírez F.: Kit for preparation of multimeric receptor-specific ^{99m}Tc-radiopharmaceuticals based on gold nanoparticles. Nucl. Med. Commun. **32**(11), 1095–1104 (2011)
14. Orocio-Rodríguez, E., Ferro-Flores, G., Santos-Cuevas, C.L., Ramírez, FdM, Ocampo-García, B.E., Azorín-Vega, E., et al.: Two novel nanosized radiolabeled analogues of somatostatin for neuroendocrine tumor imaging. J. Nanosci. Nanotechnol. **15**(6), 4159–4169 (2015)
15. Ferro-Flores, G., E Ocampo-García, B., L Santos-Cuevas, C., de Maria Ramirez, F., Azorin-Vega, E., Meléndez-Alafort, L.: Theranostic radiopharmaceuticals based on gold nanoparticles labeled with ^{177}Lu and conjugated to peptides. Curr. Radiopharm. **8**(2), 150–159 (2015)
16. Vilchis-Juárez, A., Ferro-Flores, G., Santos-Cuevas, C., Morales-Avila, E., Ocampo-García, B., Díaz-Nieto, L., et al.: Molecular targeting radiotherapy with cyclo-RGDFK (C) peptides conjugated to ^{177}Lu-labeled gold nanoparticles in tumor-bearing mice. J. Biomed. Nanotechnol. **10**(3), 393–404 (2014)
17. Luna-Gutiérrez, M., Ferro-Flores, G., Ocampo-García, B.E., Santos-Cuevas, C.L., Jiménez-Mancilla, N., León-Rodríguez, D., et al.: A therapeutic system of ^{177}Lu-labeled gold nanoparticles-RGD internalized in breast cancer cells. J. Mex. Chem. Soc. **57**(3), 212–219 (2013)
18. Jiménez-Mancilla, N., Ferro-Flores, G., Santos-Cuevas, C., Ocampo-García, B., Luna-Gutiérrez, M., Azorín-Vega, E., et al.: Multifunctional targeted therapy system based on ^{99m}Tc/^{177}Lu-labeled gold nanoparticles-Tat(49-57)-Lys3-bombesin internalized in nuclei of prostate cancer cells. J. Labelled Compd. Radiopharm. **56**(13), 663–671 (2013)
19. González-Ruíz, A., Ferro-Flores, G., Azorín-Vega, E., Ocampo-García, B., de Maria, Ramírez F., Santos-Cuevas, C., et al.: Synthesis and in vitro evaluation of an antiangiogenic cancer-specific dual-targeting ^{177}Lu-Au-nanoradiopharmaceutical. J. Radioanal. Nucl. Chem. **314**(2), 1337–1345 (2017)
20. Anselmo, A.C., Mitragotri, S.: A review of clinical translation of inorganic nanoparticles. AAPS J. **17**(5), 1041–1054 (2015)

21. Ocampo-García, B.E., Ramírez, FdM, Ferro-Flores, G., De León-Rodríguez, L.M., Santos-Cuevas, C.L., Morales-Avila, E., et al.: ^{99m}Tc-labelled gold nanoparticles capped with HYNIC-peptide/mannose for sentinel lymph node detection. Nucl. Med. Biol. **38**(1), 1–11 (2011)
22. Alberti, C.: From molecular imaging in preclinical/clinical oncology to theranostic applications in targeted tumor therapy. Eur. Rev. Med. Pharmacol. Sci. **16**(14), 1925–33 (2012). PubMed PMID: WOS:000313936400006
23. Pissuwan, D., Valenzuela, S.M., Cortie, M.B.: Therapeutic possibilities of plasmonically heated gold nanoparticles. Trends Biotechnol. **24**(2), 62–67 (2006). https://doi.org/10.1016/j.tibtech.2005.12.004. PubMed PMID: ISI:000235574900004
24. Abadeer, N.S., Murphy, C.J.: Recent progress in cancer thermal therapy using gold nanoparticles. J. Phys. Chem. C **120**(9), 4691–4716 (2016)
25. Fekrazad, R., Naghdi, N., Nokhbatolfoghahaei, H., Bagheri, H.: The combination of laser therapy and metal nanoparticles in cancer treatment originated from epithelial tissues: a literature review. J. Lasers Med. Sci. **7**(2), 62 (2016)
26. Mendoza-Nava, H., Ferro-Flores, G., Ocampo-García, B., Serment-Guerrero, J., Santos-Cuevas, C., Jiménez-Mancilla, N., et al.: Laser heating of gold nanospheres functionalized with octreotide: in vitro effect on HeLa cell viability. Photomed. Laser Surg. **31**(1), 17–22 (2013)
27. Ocampo-Garcia, B.E., Ramirez, F.D., Ferro-Flores, G., De Leon-Rodriguez, L.M., Santos-Cuevas, C.L., Morales-Avila, E., et al.: Tc-99m-labelled gold nanoparticles capped with HYNIC-peptide/mannose for sentinel lymph node detection. Nucl. Med. Biol. **38**(1), 1–11 (2011). https://doi.org/10.1016/j.nucmedbio.2010.07.007. PubMed PMID: ISI:000286574800001
28. Patra, C.R., Bhattacharya, R., Mukhopadhyay, D., Mukherjee, P.: Application of gold nanoparticles for targeted therapy in cancer. J. Biomed. Nanotechnol. **4**(2), 99–132 (2008). https://doi.org/10.1166/jbn.2008.016. PubMed PMID: ISI:000257794200001
29. Carrillo-Cazares, A., Jiménez-Mancilla, N., Luna-Gutiérrez, M., Isaac-Olivé, K., Camacho-López, M.: Study of the optical properties of functionalized gold nanoparticles in different tissues and their correlation with the temperature increase. J. Nanomater. (2017)
30. Mendoza-Nava, H., Ferro-Flores, G., Ramírez, FdM, Ocampo-García, B., Santos-Cuevas, C., Azorín-Vega, E., et al.: Fluorescent, plasmonic, and radiotherapeutic properties of the ^{177}Lu–Dendrimer–AuNP–Folate–Bombesin nanoprobe located inside cancer cells. Mol. Imaging **16**, 1536012117704768 (2017)
31. Mendes, R., Pedrosa, P., Lima, J.C., Fernandes, A.R., Baptista, P.V.: Photothermal enhancement of chemotherapy in breast cancer by visible irradiation of gold nanoparticles. Sci. Rep. **7**(1), 10872 (2017)
32. Berning, D.E., Katti, K.V., Barnes, C.L., Volkert, W.A., Ketring, A.R.: Chemistry in environmentally benign media. 7. Chelating hydroxymethyl-functionalized bisphosphines as building blocks to water-soluble and in-vitro-stable gold(I) complexes. Synthesis, characterization, and x-ray crystal structures of Au{(HOH2C)(2)PC6H4P(CH2OH)(2)}(2) Cl and AU(2){(HOH2C)(2)PCH2CH2P(CH2OH)(2)}(2) Cl-2. Inorg. Chem. **36**(13), 2765–2769 (1997). https://doi.org/10.1021/ic961396b. PubMed PMID: WOS:A1997XF30900013
33. Berning, D.E., Katti, K.V., Volkert, W.A., Higginbotham, C.J., Ketring, A.R.: Au-198-labeled hydroxymethyl phosphines as models for potential therapeutic pharmaceuticals. Nucl. Med. Biol. **25**(6), 577–583 (1998). https://doi.org/10.1016/s0969-8051(98)00023-7. PubMed PMID: WOS:000075024800010
34. Higginbotham, M.L., Henry, C.J., Katti, K.V., Casteel, S.W., Dowling, P.M., Pillarsetty, N.: Preclinical tolerance and pharmacokinetic assessment of MU-Gold, a novel chemotherapeutic agent, in laboratory dogs. Vet. Ther. **4**(1), 76–82 (2003). PubMed PMID: WOS:000220158900008
35. Katti, K.V., Kannan, R., Katti, K., Kattumori, V., Pandrapraganda, R., Rahing, V., et al.: Hybrid gold nanoparticles in molecular imaging and radiotherapy. Czechoslovak J. Phys. **56**, D23–D34 (2006). PubMed PMID: WOS:000206057500003

36. Berning, D.E., Katti, K.V., Barnes, C.L., Volkert, W.A.: Chemical and biomedical motifs of the reactions of hydroxymethylphosphines with amines, amino acids, and model peptides. J. Am. Chem. Soc. **121**(8), 1658–1664 (1999)
37. Kannan, R., Rahing, V., Cutler, C., Pandrapragada, R., Katti, K.K., Kattumuri, V., et al.: Nanocompatible chemistry toward fabrication of target-specific gold nanoparticles. J. Am. Chem. Soc. **128**(35), 11342–11343 (2006)
38. Axiak-Bechtel, A.M., Upendran, A., Lattimer, J.C., Kelsey, J., Cutler, C.S., Selting, K.A., et al.: Gum arabic-coated radioactive gold nanoparticles cause no short-term local or systemic toxicity in the clinically relevant canine model of prostate cancer. Int. J. Nanomed. **9**, 5001–5011 (2014). https://doi.org/10.2147/ijn.s67333. PubMed PMID: WOS:000343863800001
39. Chanda, N., Kattumuri, V., Shukla, R., Zambre, A., Katti, K., Upendran, A., et al.: Bombesin functionalized gold nanoparticles show in vitro and in vivo cancer receptor specificity. Proc. Natl. Acad. Sci. U. S. A **107**(19), 8760–8765 (2010). https://doi.org/10.1073/pnas.1002143107. PubMed PMID: WOS:000277591200049
40. Al-Yasiri, A., Khoobchandani, M., Cutler, C., Watkinson, L., Carmack, T., Smith, C., et al.: Mangiferin functionalized radioactive gold nanoparticles (MGF-198 AuNPs) in prostate tumor therapy: green nanotechnology for production, in vivo tumor retention and evaluation of therapeutic efficacy. Dalton Trans. **46**(42), 14561–14571 (2017)
41. de Barros, A.L.B., Tsourkas, A., Saboury, B., Cardoso, V.N., Alavi, A.: Emerging role of radiolabeled nanoparticles as an effective diagnostic technique. EJNMMI Res. **2** (2012). https://doi.org/10.1186/2191-219x-2-39. PubMed PMID: WOS:000209435700039
42. Kogan, M.J., Olmedo, I., Hosta, L., Guerrero, A.R., Cruz, L.J., Albericio, F.: Peptides and metallic nanoparticles for biomedical applications. Nanomedicine **2**(3), 287–306 (2007). https://doi.org/10.2217/17435889.2.3.287. PubMed PMID: WOS:000248250400008
43. Assadi, M., Afrasiabi, K., Nabipour, I., Seyedabadi, M.: Nanotechnology and nuclear medicine; research and preclinical applications. Hellenic J. Nucl. Med. **14**(2), 149–59 (2011). PubMed PMID: WOS:000292952700009
44. Ferro-Flores, G., Ocampo-Garcia, B.E., Santos-Cuevas, C.L., Morales-Avila, E., Azorin-Vega, E.: Multifunctional radiolabeled nanoparticles for targeted therapy. Curr. Med. Chem. **21**(1), 124–38 (2014). PubMed PMID: WOS:000327778900009
45. Barrefelt, Å.A., Brismar, T.B., Egri, G., Aspelin, P., Olsson, A., Oddo, L., et al.: Multimodality imaging using SPECT/CT and MRI and ligand functionalized ^{99m}Tc-labeled magnetic microbubbles. EJNMMI Res. **3**(1), 12 (2013)
46. Sandiford, L., Phinikaridou, A., Protti, A., Meszaros, L.K., Cui, X., Yan, Y., et al.: Bisphosphonate-anchored PEGylation and radiolabeling of superparamagnetic iron oxide: long-circulating nanoparticles for in vivo multimodal (T1 MRI-SPECT) imaging. ACS Nano. **7**(1), 500–512 (2012)
47. Zhao, Y., Yao, Q., Tan, H., Wu, B., Hu, P., Wu, P., et al.: Design and preliminary assessment of ^{99m}Tc-labeled ultrasmall superparamagnetic iron oxide-conjugated bevacizumab for single photon emission computed tomography/magnetic resonance imaging of hepatocellular carcinoma. J. Radioanal. Nucl. Chem. **299**(3), 1273–1280 (2014)
48. Madru, R., Kjellman, P., Olsson, F., Wingårdh, K., Ingvar, C., Ståhlberg, F., et al.: ^{99m}Tc-labeled superparamagnetic iron oxide nanoparticles for multimodality SPECT/MRI of sentinel lymph nodes. J. Nucl. Med. **53**(3), 459–463 (2012)
49. Misri, R., Meier, D., Yung, A.C., Kozlowski, P., Häfeli, U.O.: Development and evaluation of a dual-modality (MRI/SPECT) molecular imaging bioprobe. Nanomed. Nanotechnol. Biol. Med. **8**(6), 1007–1016 (2012). https://doi.org/10.1016/j.nano.2011.10.013
50. Nahrendorf, M., Zhang, H., Hembrador, S., Panizzi, P., Sosnovik, D.E., Aikawa, E., et al.: Nanoparticle PET-CT imaging of macrophages in inflammatory atherosclerosis. Circulation **117**(3), 379–387 (2008)
51. Stelter, L., Pinkernelle, J.G., Michel, R., Schwartländer, R., Raschzok, N., Morgul, M.H., et al.: Modification of aminosilanized superparamagnetic nanoparticles: feasibility of multimodal detection using 3T MRI, small animal PET, and fluorescence imaging. Mol. Imag. Biol. **12**(1), 25–34 (2010)

52. Glaus, C., Rossin, R., Welch, M.J., Bao, G.: In vivo evaluation of ^{64}Cu-labeled magnetic nanoparticles as a dual-modality PET/MR imaging agent. Bioconjug. Chem. **21**(4), 715–722 (2010)
53. Lee, H.-Y., Li, Z., Chen, K., Hsu, A.R., Xu, C., Xie, J., et al.: PET/MRI dual-modality tumor imaging using arginine-glycine-aspartic (RGD)—Conjugated radiolabeled iron oxide nanoparticles. J. Nucl. Med. **49**(8), 1371–1379 (2008)
54. Hoffman, D., Sun, M., Yang, L., McDonagh, P.R., Corwin, F., Sundaresan, G., et al.: Intrinsically radiolabelled [^{59}Fe]-SPIONs for dual MRI/radionuclide detection. Am. J. Nucl. Med. Mol. Imaging **4**(6), 548 (2014)
55. Pham, T.N., Lengkeek, N.A., Greguric, I., Kim, B.J., Pellegrini, P.A., Bickley, S.A., et al.: Tunable and noncytotoxic PeT/sPecT–MrI multimodality imaging probes using colloidally stable ligand-free superparamagnetic iron oxide nanoparticles. Int. J. Nanomed. **12**, 899 (2017)
56. Ichedef, C., Simonelli, F., Holzwarth, U., Bagaria, J.P., Puntes, V.F., Cotogno, G., et al.: Radiochemical synthesis of Ag-105 g-labelled silver nanoparticles. J. Nanopart. Res. **15**(11) (2013). https://doi.org/10.1007/s11051-013-2073-8. PubMed PMID: WOS:000326322200001
57. Chrastina, A., Schnitzer, J.E.: Iodine-125 radiolabeling of silver nanoparticles for in vivo SPECT imaging. Int. J. Nanomed. **5**, 653–9 (2010). PubMed PMID: WOS:000283715300068
58. Ashraf, A., Sharif, R., Ahmad, M., Masood, M., Shahid, A., Anjum, D.H., et al.: In vivo evaluation of the biodistribution of intravenously administered naked and functionalised silver nanoparticles in rabbit. IET Nanobiotechnol. **9**(6), 368–374 (2015). https://doi.org/10.1049/iet-nbt.2014.0075. PubMed PMID: WOS:000366254300007
59. Farrag, N.S., El-Sabagh, H.A., Al-Mahallawi, A.M., Amin, A.M., AbdEl-Bary, A., Mamdouh, W.: Comparative study on radiolabeling and biodistribution of core-shell silver/polymeric nanoparticles-based theranostics for tumor targeting. Int. J. Pharm. **529**(1–2), 123–133 (2017). https://doi.org/10.1016/j.ijpharm.2017.06.044. PubMed PMID: WOS:000408009200012
60. Zhou, M., Zhang, R., Huang, M.A., Lu, W., Song, S.L., Melancon, M.P., et al.: A chelator-free multifunctional Cu–^{64}CuS nanoparticle platform for simultaneous micro-PET/CT imaging and photothermal ablation therapy. J. Am. Chem. Soc. **132**(43), 15351–15358 (2010). https://doi.org/10.1021/ja106855m. PubMed PMID: WOS:000283621700049
61. Chakravarty, R., Chakraborty, S., Ningthoujam, R.S., Nair, K.V.V., Sharma, K.S., Ballal, A., et al.: Industrial-scale synthesis of intrinsically radiolabeled (CuS)–Cu–64 nanoparticles for use in positron emission tomography (PET) imaging of cancer. Ind. Eng. Chem. Res. **55**(48), 12407–12419 (2016). https://doi.org/10.1021/acs.iecr.6b03405. PubMed PMID: WOS:000389623500012
62. Peng, H., Liu, X., Wang, G., Li, M., Bratlie, K.M., Cochran, E., et al.: Polymeric multifunctional nanomaterials for theranostics. J. Mater. Chem. B **3**(34), 6856–6870 (2015)
63. Choi, K.Y., Liu, G., Lee, S., Chen, X.: Theranostic nanoplatforms for simultaneous cancer imaging and therapy: current approaches and future perspectives. Nanoscale. **4**(2), 330–342 (2012)
64. Reis, C.P., Neufeld, R.J., Ribeiro, A.J., Veiga, F.: Nanoencapsulation I. Methods for preparation of drug-loaded polymeric nanoparticles. Nanomed. Nanotechnol. Biol. Med. **2**(1), 8–21 (2006)
65. Srikar, R., Upendran, A., Kannan, R.: Polymeric nanoparticles for molecular imaging. Wiley Interdisc. Rev.: Nanomed. Nanobiotechnol. **6**(3), 245–267 (2014)
66. Subramanian, S., Dandekar, P., Jain, R., Pandey, U., Samuel, G., Hassan, P.A., et al.: Technetium-99m–labeled poly (dl-lactide-co-glycolide) nanoparticles as an alternative for sentinel lymph node imaging. Cancer Biotherapy Radiopharm. **25**(6), 637–644 (2010)
67. Allmeroth, M., Moderegger, D., Gündel, D., Koynov, K., Buchholz, H.-G., Mohr, K., et al.: HPMA-LMA copolymer drug carriers in oncology: an in vivo PET study to assess the tumor line-specific polymer uptake and body distribution. Biomacromol **14**(9), 3091–3101 (2013)
68. Allmeroth, M., Moderegger, D., Gündel, D., Buchholz, H.-G., Mohr, N., Koynov, K., et al.: PEGylation of HPMA-based block copolymers enhances tumor accumulation in vivo: a quantitative study using radiolabeling and positron emission tomography. J. Controlled Release **172**(1), 77–85 (2013)

69. Sun, X., Rossin, R., Turner, J.L., Becker, M.L., Joralemon, M.J., Welch, M.J., et al.: An assessment of the effects of shell cross-linked nanoparticle size, core composition, and surface PEGylation on in vivo biodistribution. Biomacromol **6**(5), 2541–2554 (2005)
70. Cartier, R., Kaufner, L., Paulke, B., Wüstneck, R., Pietschmann, S., Michel, R., et al.: Latex nanoparticles for multimodal imaging and detection in vivo. Nanotechnology **18**(19), 195102 (2007)
71. Zhang, R., Xiong, C., Huang, M., Zhou, M., Huang, Q., Wen, X., et al.: Peptide-conjugated polymeric micellar nanoparticles for dual SPECT and optical imaging of EphB4 receptors in prostate cancer xenografts. Biomaterials **32**(25), 5872–5879 (2011)
72. Simone, E.A., Zern, B.J., Chacko, A.-M., Mikitsh, J.L., Blankemeyer, E.R., Muro, S., et al.: Endothelial targeting of polymeric nanoparticles stably labeled with the PET imaging radioisotope iodine-124. Biomaterials **33**(21), 5406–5413 (2012)
73. Li, X., Xiong, Z., Xu, X., Luo, Y., Peng, C., Shen, M., et al.: ^{99m}Tc-labeled multifunctional low-generation dendrimer-entrapped gold nanoparticles for targeted SPECT/CT dual-mode imaging of tumors. ACS Appl. Mater. Interfaces **8**(31), 19883–19891 (2016)
74. Patil, R.R., Yu, J., Banerjee, S.R., Ren, Y., Leong, D., Jiang, X., et al.: Probing in vivo trafficking of polymer/DNA micellar nanoparticles using SPECT/CT imaging. Mol. Ther. **19**(9), 1626–1635 (2011)
75. Zhang, Y., Sun, Y., Xu, X., Zhang, X., Zhu, H., Huang, L., et al.: Synthesis, biodistribution, and microsingle photon emission computed tomography (SPECT) imaging study of technetium-99m labeled PEGylated dendrimer poly (amidoamine)(PAMAM)—Folic acid conjugates. J. Med. Chem. **53**(8), 3262–3272 (2010)
76. Lu, P.-L., Chen, Y.-C., Ou, T.-W., Chen, H.-H., Tsai, H.-C., Wen, C.-J., et al.: Multifunctional hollow nanoparticles based on graft-diblock copolymers for doxorubicin delivery. Biomaterials **32**(8), 2213–2221 (2011)
77. Majmudar, M.D., Yoo, J., Keliher, E.J., Truelove, J.J., Iwamoto, Y., Sena, B., et al.: Polymeric nanoparticle pet/mr imaging allows macrophage detection in atherosclerotic plaques novelty and significance. Circ. Res. **112**(5), 755–761 (2013)